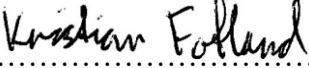




Universitetet  
i Stavanger

**FACULTY OF SCIENCE AND TECHNOLOGY**

**MASTER'S THESIS**

Study program/specialization: Offshore Technology, Marine and Subsea Technology	Spring semester 2018 Open/ <del>Confidential</del>
Author: Kristian Fotland	 ..... (signature of author)
Program coordinator: Prof. Muk Chen Ong, UiS.  Supervisor(s): Prof. Muk Chen Ong, UiS.  Dr. Yihan Xing.  Eirik Nilsen, IKM Technology.	
Title of master's thesis: Analysis of ROV thrusters and small marine propellers at specific rotational speeds.	
Credits: 30	
Keywords:  Shaft, rotary, marine propeller, hydrodynamics, excitation forces, vibration, bearing response.	Number of pages: 90  + supplementary material/other: 131  Stavanger, 13.06.2018 date/year

## Preface

The following study is my master's thesis, which is a mandatory part of the Master's degree program in Marine and Subsea Technology at the University of Stavanger. The thesis is carried out in the last semester of the Master's degree program and represents the end of the program. During the thesis, the knowledge gained throughout the study program becomes very useful. Furthermore, new challenges are met through the specific thesis topic, where new experiences and knowledge are achieved.

I would like to thank my program coordinator and supervisor Prof. Muk Chen Ong, and supervisor Dr. Yihan Xing, for their time devoted to me and this project. I am very grateful for their motivation, guidance, and constructive feedback.

I would also like to thank Eirik Nilsen and IKM Technology for the research topic that led to the subject of this thesis, and for their support throughout this project.

Stavanger, 13.06.2018

A handwritten signature in black ink that reads "Kristian Fotland". The signature is written in a cursive, slightly slanted style.

Kristian Fotland

# Table of Contents

Preface.....	i
Abstract.....	v
List of Figures.....	vi
List of Tables.....	viii
Abbreviations.....	x
Nomenclature.....	xi
Chapter 1 Introduction.....	1
1.1. Background and motivation.....	1
1.2. Previous work.....	3
1.3. Scope of work.....	5
1.4. Structure of report.....	7
Chapter 2 System description.....	8
2.1. ROV introduction.....	8
2.2. Thruster description.....	10
2.3. OpenModelica.....	14
Chapter 3 Theoretical background.....	16
3.1. Introduction.....	16
3.2. Shaft dynamics.....	16
3.3. The gyroscopic effect, whirling and critical speed.....	19

3.4.	Marine propeller dynamics.....	20
3.5.	The Wageningen B-screw series .....	25
3.6.	Open water test procedure.....	27
3.7.	Marine propeller forces and moments.....	27
Chapter 4	Estimation of propeller contributions .....	33
4.1.	Introduction .....	33
4.2.	Added mass and damping .....	34
4.3.	Propeller forces and moments.....	35
Chapter 5	Vibration analysis .....	39
5.1.	Introduction .....	39
5.2.	Signals and time data.....	39
5.3.	Frequency analysis .....	43
5.4.	Vibration displacement and bearing life .....	47
Chapter 6	OpenModelica modeling.....	49
6.1.	Introduction .....	49
6.2.	OM modeling and set-up.....	49
6.3.	Testing of OM model .....	54
Chapter 7	Numerical analysis and results.....	55
7.1.	Introduction .....	55
7.2.	Frequency spectrum .....	57

7.3. Bearing response for B4-71 propeller .....	65
7.4. Bearing response for different propellers.....	73
7.5. Bearing response to unbalanced propeller .....	79
Chapter 8 Conclusions and further work.....	82
8.1. Summary and conclusions.....	82
8.2. Recommendations for further work .....	84
References.....	86
Appendices.....	I

## Abstract

Thrusters are vital for the functionalities of remotely operated vehicles (ROVs). The development of thruster design is a trade-off between cost, thrust force, physical weight and size. Furthermore, it is known that problems with thrusters are a common fault in ROVs. As a result, this study is performed on different thruster configurations to highlight important aspects in the design of thruster systems. This includes the analysis of different marine propellers with 4 to 6 blades and with a diameter of 300 to 400 *mm*. A six degree of freedom model is created in OpenModelica to investigate vibrations and bearing responses in thruster systems. The model consists of a marine propeller, a shaft, and two bearings, and is applicable for simulating various steady-state cases. The results of the simulations return displacements in the axial, horizontal, and vertical directions, which are further used to investigate vibration amplitudes and bearing life. The marine propeller contributions to the OpenModelica model are based on propellers from the Wageningen B-screw propeller series and open water tests of this series. The hydrodynamic added mass and damping elements are calculated from different sets of regression equations depending on the number of blades on the propeller, blade area ratio, and pitch ratio. Meanwhile, the mean thrust and torque are obtained from open water test data of the relevant propeller. The mean thrust and torque are then further used to calculate the dynamic forces and moments from the marine propeller.

The bearing life of the bearings in the thruster is highly dependent on the axial load acting on the bearing, i.e., the thrust force. Moreover, if the propeller is not balanced then high centrifugal forces can occur, resulting in severe forces in the radial direction that can be of concern regarding the bearing life. Furthermore, the thruster and bearing design should be related to the maximum thrust force desired from the thruster. It is possible to use different propellers with the same design, to change the RPM-thrust force configuration, or to change the vibratory properties of the thruster system. However, the maximum thrust force for which the original thruster was designed should not be exceeded. Furthermore, the vibrations in the thruster system depend on the bearing configuration, stiffness, unbalance, and the propeller type.

# List of Figures

Figure 2.1: IKM Merlin UCV work class ROV (IKM Subsea AS, n.d.).

Figure 2.2: Cross-section of thruster (Courtesy of IKM Technology).

Figure 2.3: Pitch angle and diameter of propeller.

Figure 2.4: Thruster driveline (courtesy of IKM Technology).

Figure 2.5: OpenModelica Connection Editor, formulated from Ashghar and Tariq (2010).

Figure 3.1: Propeller global coordinate system.

Figure 3.2:  $K_t$ ,  $K_q$ , and efficiency curves for the B4-70 propeller (Bernitsas et al., 1981, p. 47).

Figure 4.1: B4 to B6 propellers.

Figure 4.2: Non-dimensionalized added mass coefficients.

Figure 4.3: Non-dimensionalized damping coefficients.

Figure 4.4: Thrust vs. speed of advance for B4-71 propeller.

Figure 4.5: Torque vs. speed of advance for B4-71 propeller.

Figure 4.6: Efficiency vs. speed of advance for B4-71 propeller.

Figure 5.1: The frequency response of a system (Meirovitch, 1986, p. 53).

Figure 6.1: 4 DOF vs. 6 DOF.

Figure 6.2: EM model.

Figure 6.3: 4 DOF model.

Figure 6.4: 6 DOF model.

Figure 7.1: Fresh new oil (left) vs. contaminated oil (right) from the thruster pedestal.

Figure 7.2: Thruster coordinate system.

Figure 7.3: Frequency response for the 4DOF thruster model in torsional direction at different speeds.

Figure 7.4: Frequency response for the 4DOF thruster model in axial direction at different speeds.

Figure 7.5: Frequency response for the 4DOF thruster model in horizontal direction at different speeds.

Figure 7.6: Frequency response for the 4DOF thruster model in vertical direction at different speeds.

Figure 7.7: Frequency response for the 4DOF vs. 6DOF thruster models in torsional direction.

Figure 7.8: Frequency response for the 4DOF vs. 6DOF thruster models in axial direction.

Figure 7.9: Frequency response for the 4DOF vs. 6DOF thruster models in horizontal direction.

Figure 7.10: Frequency response for the 4DOF vs. 6DOF thruster models in vertical direction.

Figure 7.11: Vibration amplitudes for the base case.

Figure 7.12: Vibration amplitudes for Cases 1-4.

Figure 7.13: Vibration amplitudes for Cases 1 and 5-7.

Figure 7.14: Vibration amplitudes for Cases 1, A, and B.

Figure 7.15: Vibration amplitudes for Cases C-E.

Figure 7.16: Vibration amplitudes for Cases C.1-E.1.

Figure 7.17: Vibration amplitudes for Cases 7, A.2, and B.2.

Figure 7.18: Vibration amplitudes for Cases C.2-E.2.



# List of Tables

Table 2.1: Electric motor.

Table 3.1: Non-dimensionalization of coefficients, assembled following Parsons and Vorus (1981).

Table 3.2: Models in the Wageningen B-screw series, assembled following van Lammeren et al. (1969).

Table 6.1: EM model inputs and outputs.

Table 7.1: Marine propeller B4-71 for different speeds.

Table 7.2: Marine propeller B4-71, shaft and bearings for 4 DOF vs. 6 DOF.

Table 7.3: Displacement RMS values for Case 1.

Table 7.4: Inputs for Cases 1-4.

Table 7.5: Displacement RMS values and bearing life for Cases 1-4.

Table 7.6: Inputs for Cases 1 and 5-7.

Table 7.7: Displacement RMS values and bearing life for Cases 1 and 5-7.

Table 7.8: Rating table.

Table 7.9: Summary of results for Cases 1-7.

Table 7.10: Cases A-E.

Table 7.11: Displacement RMS values and bearing life for Cases 1, A, and B.

Table 7.12: Displacement RMS values and bearing life for Cases C-E.

Table 7.13: Displacement RMS values and bearing life for Cases C.1-E.1.

Table 7.14: New bearing life for Cases C.1-E.1.

Table 7.15: Displacements RMS values and bearing life for Cases 7 and A.2-E.2.

## Abbreviations

ATM	-	Atmospheric
BAR	-	Blade area ratio
DASSL	-	Differential/algebraic system solver
DFT	-	Discrete Fourier transform
DNV	-	Det norske veritas
DOF	-	Degrees of freedom
DP	-	Dynamic positioning
EM	-	Equation of motion model
FFT	-	Fast Fourier transform
FRF	-	Frequency response function
GL	-	Germanischer Lloyd
IMR	-	Inspection maintenance repair
ISO	-	International organization for standardization
MARIN	-	Maritime research institute Netherlands
MIMO	-	Multiple input, multiple output
MSW	-	Meters sea water
NSMB	-	Netherlands ship model basin
OM	-	OpenModelica
PSD	-	Power spectral density
RMS	-	Root mean square
ROV	-	Remotely operated vehicle
UCV	-	Ultra-compact vehicle
WROV	-	Work class remotely operated vehicle

# Nomenclature

## Uppercase

$A$	-	Amplitude
$A_e$	-	Expanded area
$A_o$	-	Disc area
$C$	-	Damping matrix
$C_i$	-	Regression coefficients
$D$	-	Diameter
$F_i$	-	Forces
$G$	-	Shear modulus
$I_i$	-	Moment of inertia
$I_p$	-	Polar mass moment of inertia
$J$	-	Advance coefficient
$J$	-	Polar moment of inertia
$K$	-	Stiffness matrix
$K_Q$	-	Torque coefficient
$K_T$	-	Thrust coefficient
$L$	-	Angular momentum
$M$	-	Mass matrix
$M_{gyr}$	-	Gyroscopic moment
$P$	-	Propeller pitch
$P_{hyd}$	-	Hydrostatic pressure
$Q_i$	-	Torque
$R$	-	Radius
$R_n$	-	Reynolds number
$T$	-	Kinetic energy
$T_i$	-	Thrust
$T_p$	-	Period
$V_a$	-	Speed of advance
$V_{ex}$	-	Vessel speed

- W - Watt  
 $W_f$  - Wake factor

### Lowercase

- a - Acceleration  
c - Damping  
e - Vapor pressure  
 $e_T$  - Thrust eccentricity  
 $f$  - Frequency  
 $f_e$  - Excitation force  
 $f_H$  - Hydrodynamic force  
 $f_S$  - External excitation force  
g - Gravitational acceleration  
h - Hours  
j - Imaginary number  
k - Stiffness  
l - Length  
m - Mass  
n - Rotational speed  
 $p_{atm}$  - Atmospheric pressure  
 $p_0$  - Static pressure  
 $q_i$  - Hydrodynamic moment  
r - Radius local pitch  
t - Time  
v - Velocity  
x - Displacement vector  
z - Number of propeller blades  
 $z_{sw}$  - Water depth

## Greek letters and other symbols

- $\delta_i$  - Displacement
- $\eta_0$  - Open water efficiency
- $\theta_p$  - Pitch angle
- $\sigma_0$  - Cavitation number
- $\phi_k$  - Phase angle
- $\mathcal{F}$  - Fourier transform
- $\Omega$  - Whirling speed
- $\mu$  - Viscosity of fluid
- $\rho$  - Density of fluid
- $\tau$  - Average time
- $\omega$  - Angular velocity  
Angular frequency
- $\vartheta$  - Shaft slope
- $\phi$  - The angle of rotation in the propeller plane  
Shaft alignment angle relative to the flow

# Chapter 1

## Introduction

Marine propulsion is required for marine vessels and underwater vehicles to ensure maneuvering and station-keeping capabilities. The marine propulsion driveline investigated in this study originates from an electric thruster used on a work-class remotely operated vehicle (WROV). The thruster is of particular concern for any remotely operated vehicle (ROV) because the thruster system is the lowest control loop on the ROV system (Ait-Ahmed et al., 2007). Without proper thrust or with loss of thrust, the ROV cannot perform the intended operation, and thus a risk of damage or loss of assets arises (Christ & Wernli, 2014). The present study focuses on the development of a multibody simulation model that can be used for the design optimization and development of thruster systems. The simulation model includes a complete propulsion system, i.e., a motor, a shaft, bearings, and a propeller. From the model, it is possible to investigate the interactions between these components for various steady-state cases.

### 1.1. Background and motivation

The background of the present research topic originates from a case study provided by IKM Technology, who stated that their electric thruster sometimes fails in operations. This study aims to investigate the reason for the failure and provide corresponding preventive measures.

This led to further interest in the ROV thruster system and investigation of its components. According to Omerdic et al. (2003), thruster problems are one of the most common faults to occur on ROVs. After thorough literature research, the impression is that thruster development and design are mainly driven by achieving high efficiency from the thruster system, in as small and lightweight a package as practically possible. These design criteria are of course important in the ROV world, but should not be at the expense of the reliability of the system. The lack of detailed analysis of the thruster system might be because the dimensions of this type of thruster are smaller in size compared to the thrusters used on larger ships. Consequently, the placement

of bearings can be carried out in favor of the design without knowing if this has an impact on the overall performance of the thruster system. A comprehensive analysis of the system is difficult to perform, and to the author's knowledge no robust tools are available to aid such an analysis.

A continuous advancement in technology is occurring within the marine and subsea industry. For thruster systems this involves the introduction of lighter materials, new designs, and areas of use, such as deeper water and harsher climates and operating conditions (Carlton, 2012). An interesting consideration for propellers made of lighter materials is that these propellers are expected to move the same amount of water and provide the same amount of thrust as previous propellers made of conventional materials. This means that the hydrodynamic forces and corresponding added mass and damping terms are important to include in the design phases.

On the Norwegian continental shelf, where many subsea installations are in place, future trends predict new developments in subsea and deep waters (Norwegian Petroleum Directorate, u.d.). For example, inspection, maintenance, and repair (IMR) operations carried out by ROVs will increase as a result of new subsea developments and with the introduction of riser-less light well intervention (Keilen, 2005). Most ROVs undergo pre- and post-dive checks (IMCA, 2014), which is one of the reasons why ROVs can remain operative. However, resident or permanently deployed ROVs are now being introduced, where by the vehicle is intended to remain subsea for months. This is forcing ROV companies to increase the reliability of their ROV systems. Moreover, ROVs are the preferred tool for IMR operations since there is no risk of human injury. They can perform a wide range of tasks, and they are not restricted by water depth like regular manned diving, which is restricted to 180 meter depth on the Norwegian continental shelf (NORSOK U-100, 2015).

The present study aims to highlight the importance of including the hydrodynamic forces that act on the propeller in the design phase of the thruster. Furthermore, the aim is to demonstrate how these forces respond to changes in design properties and operating outputs. The marine propeller forces will be implemented in a model of a complete thruster system, which can be used for design analysis and optimization. This model can be very useful to the designers of such systems, in order to improve the reliability and robustness of the final product. The analysis of the rotating shaft performed in this study is valid for other shafts of common setup



and size and can therefore be used for similar shafts to those addressed in this study. Overall, clarifying the critical aspects in the design of thrusters can improve performance and reduce the maintenance time and cost associated with thruster systems.

## **1.2. Previous work**

The Netherlands Ship Model Basin (NSMB) was founded in 1929 and is now known as the Maritime Research Institute Netherlands (MARIN). Marine propeller series began to be designed systematically at MARIN, and the first results from an open water test of a propeller were presented in a publication in 1936 (Kuiper, 1992). Most previous research on marine propellers is typical of propellers used on large ships, and of propellers exposed to high loads or high speeds (Maritime Research Institute Netherlands, n.d.). Using the research carried out at MARIN, it is possible to use an empirical approach to calculate the hydrodynamic contributions of a marine propeller. The empirical approach is chosen to calculate propeller hydrodynamic contributions in the present study. Since it is considered the most applicable method if others use the model presented in this study. An empirical approach is also very computationally efficient compared to other numerical methods.

The empirical approach in this study is based on various propellers from the Wageningen B-screw series, which is a propeller type that has been thoroughly investigated and documented in contemporary studies (Kuiper, 1992). Generally, the series used for the calculation of propeller hydrodynamic contributions should preferably be of the same kind as the studied series. However, a study by Parsons and Vorus (1981) shows that use of the regression coefficients from the Wageningen B-screw series on a propeller without skew and rake results in only a 10-20% difference in the added mass and damping values, compared to the use of lifting surface or lifting line theory. These deviations are of some importance. However, the empirical approach provides a reasonable approximation of the added mass and damping values, which can be used for preliminary design purposes.

The resulting dynamic forces from the propeller are based on a study produced by Veritec (1985), based on an investigation performed on 20 ships by theoretical means of the dynamic

forces at the blade and at twice the blade rate frequency. This study resulted in a set of equations applicable for propellers with 4 to 6 blades. The dynamic forces used in this study are based on the mean thrust and mean torque. Which in turn are calculated by use of open water tests on the various propellers. These open water tests were taken from Bernitsas et al. (1981) and the propellers from these tests are from the Wageningen B-screw series.

Previous studies on the propulsion and bearing systems have mainly been conducted on large propulsion units. Where the bearing arrangement and propulsion components differ from the typical arrangement in ROV thrusters. One propulsion system that is similar to ROV thrusters is a dynamic positioning system on a small vessel, i.e., with a vessel length of about 25 meters. However, limited research is available on propulsion units of this size. Additionally, many of the standards covering marine engines and propulsion systems are specific for large propulsion units; for example, ISO-484 for ship screw propeller manufacturing tolerances is produced for propellers with a diameter of over 0.8 meters (ISO-484, 2015).

While DNV GL do have some technical requirements for an ROV to fulfill in order to obtain a class certificate in DNVGL-RU-UWT, this document does not cover calculations on the propulsion system. However, DNV GL does provide simplified guidelines for calculations on marine propellers and shafts in marine applications, in DNVGL-CG (DNV GL, 2015). These simplified calculations are not suitable for the OpenModelica model. Furthermore, the state of the art in marine propulsion design and analysis is Nauticus machinery software. This software considers strength, fatigue, and vibrations analyses of marine propulsion systems, and is able to analyze the shaft alignment, bearing load, and propeller design (DNV GL, 2014), among others. However, from the author's point of view Nauticus software is more suitable for heavy industry and large propulsion units, and is too comprehensive for smaller propulsion units and smaller companies.

### **1.3. Scope of work**

One of the main objectives of this study is to develop a six degree of freedom (DOF) model that includes a propeller, shaft, and bearings. The model can be used to simulate various steady-state cases of a thruster. The aim of this model is that it should be able to analyze a system and display the loads and possible weak points in the system being investigated. All of the main objectives of the study are listed below.

1. Develop a 6 DOF model of a thruster system in OpenModelica.
2. Investigate the bearing responses and suggest solutions to reduce vibrations in the system in order to extend the lifetime of the bearings.
3. Investigate the possibility to implement different propellers into the current design and identify possible changes that must be made if another propeller is to be used.

Furthermore, the model shall be validated and compared against previous studies. This includes the calculated added mass and damping values, in addition to thrust and torque values. Various excitation forces shall be compared against the frequency response of the system. Regarding the second objective, the driving parameters for the bearing life shall be investigated. If any changes are made to the design the associated pros and cons shall be discussed, and the accommodation of any necessary changes shall be addressed. The overall aim of the above objectives is to improve the reliability and robustness of thrusters and to reduce the maintenance time and cost associated with thruster systems.

In order to complete the work carried out in this study, some limitations and assumptions arise; these are listed below.

- Contributions from the duct around the propeller are not included in this study.

The duct is not included, since the effects of the duct vary with; the cross-sectional profile of the duct, the thrust, and the vessel speed. Moreover, a detailed analysis of the specific duct and its contributions would be required if the duct were to be included.

- Propeller hydrodynamic contributions are limited to an empirical approach with data from open water propeller tests, using propellers from the Wageningen B-screw series.

This approach is chosen since it is computationally efficient, and it is believed to be the most applicable method if others use the model developed in this study. Moreover, since this method is based on open water test results, the results from these calculations should have high accuracy.

- Undisturbed uniform inflow, incompressible flow, and inviscid flow are assumed through the marine propeller.

If this is not assumed then fluid dynamics must be included; however, the scope of the present study is not fluid dynamics, but vibrations and bearing loads.

- The study is limited to investigating propellers with 4 to 6 blades.

This study is limited to propellers with 4 to 6 blades, since the procedure used to calculate dynamic forces is limited to propellers with 4 to 6 blades. Moreover, the regression equation coefficients are only found for propellers with 4 to 7 blades.

## 1.4. Structure of report

The thesis is organized as follows:

- Chapter 2: Introduction to WROVs and the thruster system. An introduction to the modeling and simulation software OpenModelica is also provided.
- Chapter 3: Theoretical background on shaft dynamics, marine propeller added mass and damping, and marine propeller forces and moments.
- Chapter 4: The estimation of propeller hydrodynamic contributions is explained, and the effect of different propeller properties is shown.
- Chapter 5: Theoretical background on signal and vibration analysis. Moreover, theory on bearing life from vibration displacements is outlined.
- Chapter 6: Development and validation of the OpenModelica model.
- Chapter 7: Discussion of the various cases investigated, and presentation of results from the simulations.
- Chapter 8: Conclusion of the present study and recommendations for further work.

## Chapter 2

### System description

This chapter discusses ROVs in general and the thruster system on an IKM ROV along with its relevant components. In addition, OpenModelica software is introduced as the modeling and simulation environment selected for this study.



Figure 2.1: IKM Merlin UCV work class ROV (IKM Subsea AS, n.d.).

#### 2.1. ROV introduction

The thruster examined in this study is used on the IKM Merlin ultra-compact vehicle (UCV) work-class ROV, shown in Figure 2.1. The thrusters used on this ROV use a propeller with three blades, while the propellers investigated in this study have 4 to 6 blades. Work-class

ROVs are exposed to a high variety of loads both from the environment and the tasks performed by ROVs. Tasks related to the oil and gas industry can include pipeline inspections, operation of subsea valves, installation of subsea developments and the operation of tools for subsea maintenance (Ducan, 2014; Marine Technology Society, n.d.). A common depth rate requirement for work-class ROVs is 3000 meters in seawater (msw) (Christ & Wernli, 2014). At this depth, the ROV is exposed to severe pressures from its surroundings. The density of seawater can range from 1022 to 1030  $kg/m^3$  (Thurman, 1994), and in this study a seawater density of  $\rho = 1025 kg/m^3$  is used. The following formula can be applied to calculate the hydrostatic pressure assuming constant density:

$$P_{hyd} = p_{atm} - \rho g z_{sw} \quad (2.1)$$

where  $p_{atm}$  is the atmospheric pressure,  $\rho$  is the sea water density,  $g$  is the gravitational acceleration and  $z_{sw}$  is the water depth (Gudmestad, 2015). At 3000 meters depth, the hydrostatic pressure is approximately 300 times the atmospheric pressure. However, at depths of just a few hundred meters the hydrostatic pressure can be a challenge. To compensate for high hydrostatic pressure, most voids within an ROV must be filled with fluid. Alternatively, empty canisters must have a wall thickness that can handle the hydrostatic pressure.

Most ROVs are developed to be almost neutrally buoyant in water (Christ & Wernli, 2014), meaning they require propulsion to ascend and descend. The thrusters are the propulsion units on an ROV. Accordingly, ROVs are equipped with several thrusters which are oriented in different directions, allowing an ROV to maneuver in any DOF. A functional thruster system is essential for ROV operation and the failure of one or more thrusters results in an under-actuated system (Azis et al., 2012). The ROV can be overwhelmed by the environment (Christ & Wernli, 2014), or can be rendered incapable of performing its mission and must therefore cancel and return to the host for maintenance. A loss of all thrusters totally disables the ROV. Consequently, thrusters usually have a high priority in the ROV design and development phase (Christ & Wernli, 2014).

## 2.2. Thruster description

The thruster considered in this study is an electrical thruster. It is composed of the following main components: electric motor, motor shaft, thruster pedestal (housing), propeller, nozzle/duct, bearings, seals, couplings and propeller shaft (drive shaft). A cross-section of the complete thruster assembly is shown in Figure 2.2.

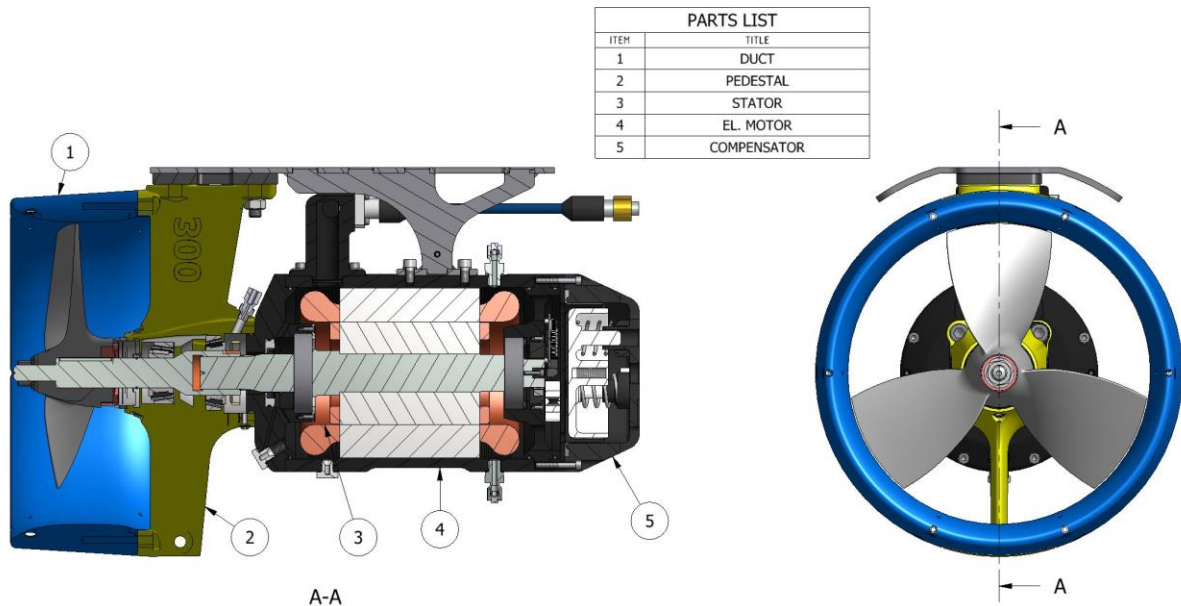


Figure 2.2: Cross-section of thruster (Courtesy of IKM Technology).

The complete thruster assembly is bolted to the ROV frame, so the thrusters cannot rotate. However, the thruster driveline can rotate at maximum output in the forward and reverse directions. The propeller has a fixed pitch and is built from a mono-block of aluminum. It has three blades with no skew and no rake to achieve similar operating conditions in both directions of rotation. The pitch angle and the diameter of the propeller are shown in Figure 2.3.



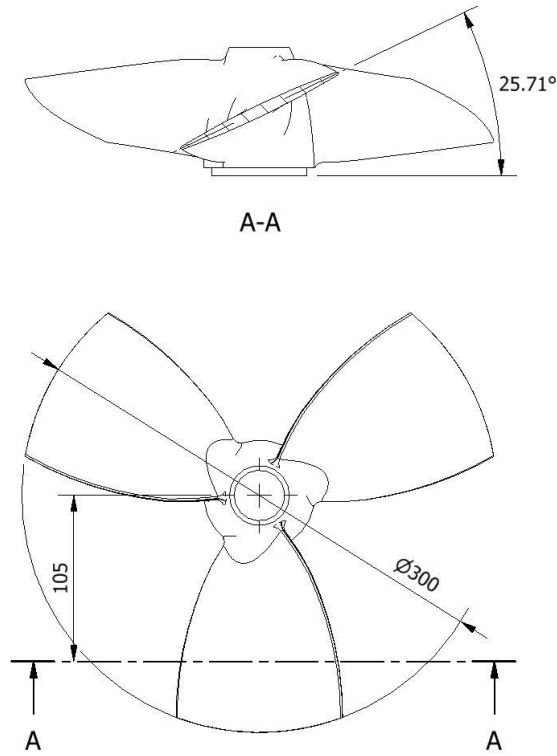


Figure 2.3: Pitch angle and diameter of propeller.

The pitch angle of the propeller is given by;  $\theta_p = \tan^{-1}\left(\frac{P}{2\pi r}\right)$  and the pitch is then;  $P = 2\pi r \tan(\theta_p)$ . The symbol  $r$  denotes the radius where the local pitch is measured. The propeller pitch used for calculation (local pitch) is generally taken at  $0.7R - 0.75R$  where  $R$  denotes the outermost radius of the propeller (Carlton, 2012). The pitch of the propeller in Figure 2.3 at  $0.7R$  is thus;  $P = 2\pi \times 105 \times \tan(25.71) = 317.65\text{mm}$ . The pitch ratio of a propeller is given by  $\frac{P}{D}$  and the pitch ratio of this propeller is then;  $\frac{P}{D} = 1.06$ .

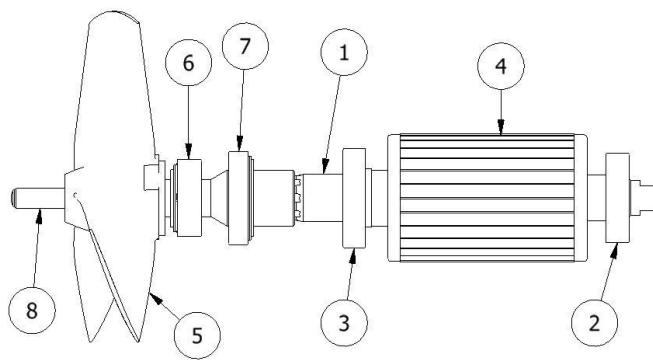
The blade area ratio (BAR) is given by;  $BAR = \frac{A_e}{A_o}$  where  $A_e$  is the expanded area of the propeller blades, i.e., when they are flattened out in the rotational plane of the propeller,  $A_o$  is the disc area created by the propeller when it is rotating, i.e., simply the area of a circle with the outermost diameter of the propeller. The expanded area of one blade is;  $A_e = 12511\text{mm}^2$ . The BAR of this propeller is then;  $BAR = \frac{3 \times 12511}{\pi \times 150^2} = 0.53$  (Carlton, 2012).

The duct is the blue component surrounding the propeller (item 1) shown in Figure 2.2 and here is of the “pull-push” type. This can be seen from the cross-section shape of the duct since the internal edges of the duct are nearly equal. Ducted propellers are typically used in applications where high thrust at low speed is needed. At zero vessel speed, the duct can contribute up to an additional 50% thrust. However, as the vessel speed increases the additional contribution from the duct drops (Carlton, 2012). The duct also reduces the number of vortices generated by the propeller when it rotates at high speeds. Since the duct surrounds the propeller, there is a lower risk of damage to the propeller from foreign objects (Christ & Wernli, 2014). In addition to the duct, grating covers can be installed in front of and behind the duct to further protect the propeller.

The electrical motor housing is fluid filled and features a compensator, which is shown to the right of the cross-section view in Figure 2.2 (item 5). The compensator enables fluid volume expansion and contraction in addition to compensating for hydrostatic pressure. As a result the external and internal pressure is equal, which permits a lower wall thickness of the motor housing, and provides favorable conditions concerning the seals for the motor housing. The electrical motor is a three-phase AC induction motor with a power of 14 kW. It develops torque when axial currents interact with the rotor and a radial magnetic field from the stator (Hughes & Drury, 2013). The stator windings are rigidly fixed in the motor housing and can be seen in Figure 2.2 (item 3). The rotor rotates along with the motor shaft and the connection between these two parts is a key coupling. A major advantage of the induction motor compared to other electrical motors is the absence of any mechanical contact between the stator and rotor (Hughes & Drury, 2013). The only mechanical contact in the motor are the two radial ball bearings which support the motor shaft; the motor bearings are shown in Figure 2.4 (item 2 and 3). Properties of the motor at maximum operating conditions are listed in Table 2.1. The thrust calculated using the inputs from Table 2.1 is 275.1 *kg*. However, the true thrust found from testing with these inputs is 250 *kg* in the reverse direction. The true thrust is lower in the reverse direction compared to the forwards direction, because in the reverse direction the outlet is facing towards the motor. Since the motor is on the outlet side in the reverse direction, it disturbs the flow and decreases the thrust efficiency in this direction.

Table 2.1: Electric motor.

Frequency	55 Hz
Power	14 kW
Speed	1655 rpm
Torque	81 Nm



PARTS LIST	
ITEM	TITLE
1	MOTOR SHAFT
2	RADIAL BALL BEARING
3	RADIAL BALL BEARING
4	ROTOR
5	PROPELLER Ø300
6	TAPERED ROLLER BEARING
7	TAPERED ROLLER BEARING
8	DRIVE SHAFT

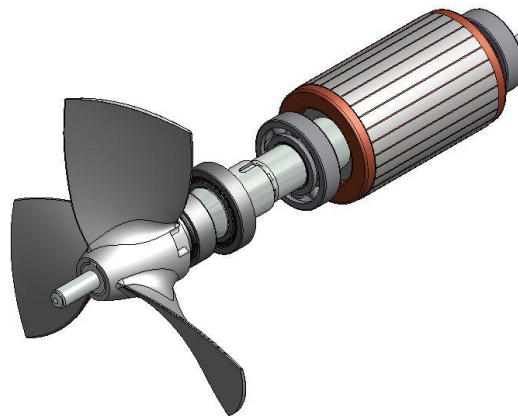


Figure 2.4: Thruster driveline (courtesy of IKM Technology).

Between the motor shaft and the drive shaft, a splined coupling transfers torque from the motor shaft to the drive shaft. The drive shaft is supported by two tapered roller bearings, as shown

in Figure 2.4 (items 6 and 7), which are arranged to handle axial forces in both directions, in addition to radial forces.

### **2.3. OpenModelica**

OpenModelica Connection Editor 1.12.0 is applied as the modeling and simulation environment in the present study. From here on OpenModelica Connection Editor will be referred to simply as OpenModelica (OM). OM is an open source software based on the Modelica language, but is also compatible with C and FORTRAN code. The Modelica language is used to model complex cyber-physical systems, which typically include robotics, automotive, aircraft, satellites, power plants, and systems biology. Some advantages of Modelica are its multi-domain modeling capability, dynamic optimization, visual acausal modeling, and typed declarative equation-based textual language (Fritzson, 2016). OM models can be both textual and graphical, which makes the modeling environment easy to read, build and expand. Moreover, electrics, mechanics, and control systems can be included in one model, and connection editing can be carried out through simple connections between model blocks. The method of building the OM model is similar to that of real systems are built; for example, appropriate standard components like a motor or pump can be found both in catalogs and in the standard Modelica library. If a component or function cannot be found in the Modelica library, then new self-defined components can be constructed based on standardized interfaces. Regarding results, OM enables 3D visualization of the model, numerical plotting, and graphical plotting of the results. One drawback of Modelica is that in some areas it lacks information and instructions on various blocks and functions. Furthermore, the support function for OM is limited as it is an open source software (Ashghar & Tariq, 2010; OpenModelica, 2018).

The first version of Modelica (1.0) was released in 1997 and was based on a differential algebraic equation system with some discrete features. The latest version, Modelica 3.4, came in 2017 and is version number 13 of all releases to date (Modelica Association, 2018). The first version of OM was released in 2005 and the current version, OM 1.12, in 2017; this is the eleventh version of OM (OpenModelica, 2018). A high-level of OM Connection Editor is presented in Figure 2.5, whereby CORBA (common object request broker architecture) is a



# Chapter 3

## Theoretical background

### 3.1. Introduction

Mathematical models for the analysis of rotating shafts and marine propellers are provided in this chapter. The method is based on Newton's second law and the equation of motion. These equations are then further implemented in the OM model as building blocks, which include the hydrodynamics, thrust, and torque from the marine propeller. Rigid bodies represent the propeller and shaft. Rigid body motion is chosen because the deformations of the bodies are small, since the sizes of the propeller and shaft are relatively small. Moreover, the areas of interest are associated with the vibrating amplitudes and forces acting on the bearings.

### 3.2. Shaft dynamics

According to (Meirovitch, 1970) rigid body motion is not so much a physical reality, but simply a mathematical idealization. However, for this system where the deformations of the body are believed to be small compared to the motion of the whole body, the rigid body concept is valid and represents a reasonable approximation of the real system. The concept describes the motion of the body in 6 DOF; three for rotational motion and three for translational motion. This differs from reality, where a body of finite dimensions has an infinite number of DOF since the body is composed of an infinite number of particles. However, the relations between force and linear momentum, torque, and angular momentum are equally valid for the rigid body principle. As a result, the principles of conservation of angular momentum and kinetic energy also apply to a rigid body. Moreover, the velocity and acceleration are the same as for particle motion, i.e., for any arbitrary point at a distance from the central axis.

With the origin at the center of mass, the velocity of any point in a rigid body can be obtained by (Meirovitch, 1970):

$$v_p = v_0 + \omega \times r \quad (3.1)$$

Moreover, the angular momentum can be obtained from:

$$L_0 = \int r \times (\omega \times r) dm \quad (3.2)$$

The moments and products of inertia can be displayed as a symmetric matrix referred to as the inertia matrix, which may be written as (Meirovitch, 1970):

$$[I] = \begin{bmatrix} I_{xx} & -I_{xy} & -I_{xz} \\ -I_{yx} & I_{yy} & -I_{yz} \\ -I_{zx} & -I_{zy} & I_{zz} \end{bmatrix} \quad (3.3)$$

Then the compact matrix form of the angular momentum, inertia tensor, and angular velocity is produced by (Meirovitch, 1970):

$$\{L\} = [I]\{\omega\} \quad (3.4)$$

Newton's second law is: "The time rate of change of the momentum of a mass  $m$  is equal to the net external force acting upon it" (Gross et al., 2011, p. 37). Here it is assumed that the mass is constant; Newton's second law is then written as:

$$F = ma \quad (3.5)$$

If the scalar product of Newton's second law is formed with  $dr$ , substituting  $dr = v dt$  and integrating between two points gives (Gross et al., 2011):

$$\frac{1}{2}mv_1^2 - \frac{1}{2}mv_0^2 = \int_{r_0}^{r_1} F \cdot dr \quad (3.6)$$

$$T = \frac{1}{2}mv^2 \quad (3.7)$$

$$T = \frac{1}{2}mv^2 + \frac{1}{2}I\omega^2 \quad (3.8)$$

The right-hand side of Equation (3.6) is the work  $U$  and the scalar quantity is the kinetic energy  $T$ , as shown in Equation (3.7). Equation (3.8) returns the combined kinetic energy for translational and rotational motion; a further description of this equation can be found in (Meirovitch, 1970). A well-known approach for describing a mechanical system is the use of the equations of motion, which are expressed by Lagrange's equations in scalar form as follows:

$$\frac{d}{dt} \left( \frac{\partial T}{\partial \dot{q}} \right) - \frac{\partial T}{\partial q} + \frac{\partial D}{\partial \dot{q}} + \frac{\partial V}{\partial q} = Q \quad (3.9)$$

$$\frac{d}{dt} \left( \frac{\partial L}{\partial \dot{q}_j} \right) - \frac{\partial L}{\partial q_j} = Q_j \quad (3.10)$$

where  $D$ ,  $V$ , and  $Q$  in Equation (3.9) represent the dissipation function, potential energy, and the vector of non-conservative forces obtained from the virtual work (Cheli & Diana, 2015), respectively. Meanwhile, Equation (3.10) is the more frequently generalized expression of the Lagrange equation and is commonly used when considering body deformation (Xing et al., 2011). By using Lagrange's equations, the final form of the equation of motion can be written as:

$$m\ddot{x}(t) + c\dot{x}(t) + kx(t) = f(t) \quad (3.11)$$

where  $m$  is the mass,  $c$  is the damping,  $k$  is the stiffness and  $f$  is the excitation force. Time is represented by  $t$  and  $x$  is the displacement of the mass from equilibrium. Accordingly, Equation (3.11) considers excitation forces depending on time. The forces can be constant, sinusoidal, random and periodic. For the solution of Equation (3.11), a general solution  $f(t) = 0$  and a particular solution  $f(t) \neq 0$  exist (Cheli & Diana, 2015; Krämer, 1993).



### 3.3. The gyroscopic effect, whirling and critical speed

Batrak (Lateral Vibration Prediction Issues, n.d.) describes whirling vibration as a change in position of a rotating body from the rotation axis. In classical mechanics whirling is known as precession motion, and can form various circular and elliptical orbits. The result of the shaft rotational speed and elliptical whirling speed is polyharmonic motion, caused by excitation forces in two planes. According to Batrak (Lateral Vibration Prediction Issues, n.d.) the vibration of a rotating propulsion shaft is considered as whirling under any circumstances. Vibrations can occur from hydrodynamic forces, unbalance, pulsating lubrication forces in bearings, and friction forces in material and couplings. Furthermore, the gyroscopic effect from the propeller can influence the whirling vibration. The gyroscopic effect arises from the larger mass and polar inertia moments of the propeller, and the gyroscopic moment can be obtained by (Batrak, Lateral Vibration Prediction Issues, n.d.):

$$M_{gyr} = AI_d\Omega^2\vartheta \quad (3.12)$$

where  $A = 1 - \frac{I_p}{I_d}S$ ,  $S = \text{whirling factor} = \frac{\omega}{\Omega}$ ,  $\Omega =$  whirling speed and  $\vartheta =$  shaft slope at propeller position. However, torsional vibrations are far more dangerous than whirling vibrations and are of greater concern for larger ships which use mechanical engines for ship propulsion (Batrak, Lateral Vibration Prediction Issues, n.d.; Batrak, Torsional Vibration Calculation Issues With Propulsion Systems, n.d.; Vizentin et al., 2017).

The critical speed of a rotating shaft is the speed where intense vibration occurs. This is reached when the shaft speed coincides with the natural frequencies of the shaft and the whirling vibration. When the bearings are included, many more critical speeds become possible; but in practice only a limited number of critical speeds occur, at the points where resonance curves intersect with each other (Veritec, 1985).

### **3.4. Marine propeller dynamics**

The marine propeller interacts with the vessel in several ways, either through coupling between the propulsion system and vessel, or alternatively, from pressure pulses generated by the propeller which hits the surface of the vessel. According to Carlton (2012) these forces and moments are considered to have a steady and a fluctuating component. For a thruster system, it is relevant to investigate the bearing forces, which can be categorized as follows (Carlton, 2012):

1. Propeller weight and center of gravity.
2. Dry propeller inertia.
3. Added mass, inertia, and moments.
4. Propeller forces and moments.
5. Out of balance forces and moments.

The bearing forces form a series of mechanical- and hydrodynamics-based forces and moments. The forces are transferred to the bearings, or contribute to changes in the vibratory properties of the shaft system. The propeller effective mass and inertia characteristics change when the propeller is immersed in water and vibrate as part of a rotating shaft system. For a propeller in water a damping term is also present, which has a vibratory behavior that differs from the individual vibration of the propeller blades. The vibration characteristics of a marine propeller are governed by hydrodynamic loading when operating in a non-uniform wake field, in addition to the vibration behavior of the marine propeller itself, which introduces variations in the section angle of attack. These two hydrodynamic effects result in variations in the hydrodynamic reaction loading. In order to derive these loads the marine propeller is considered as a rigid body in a homogeneous steady flow (Carlton, 2012).

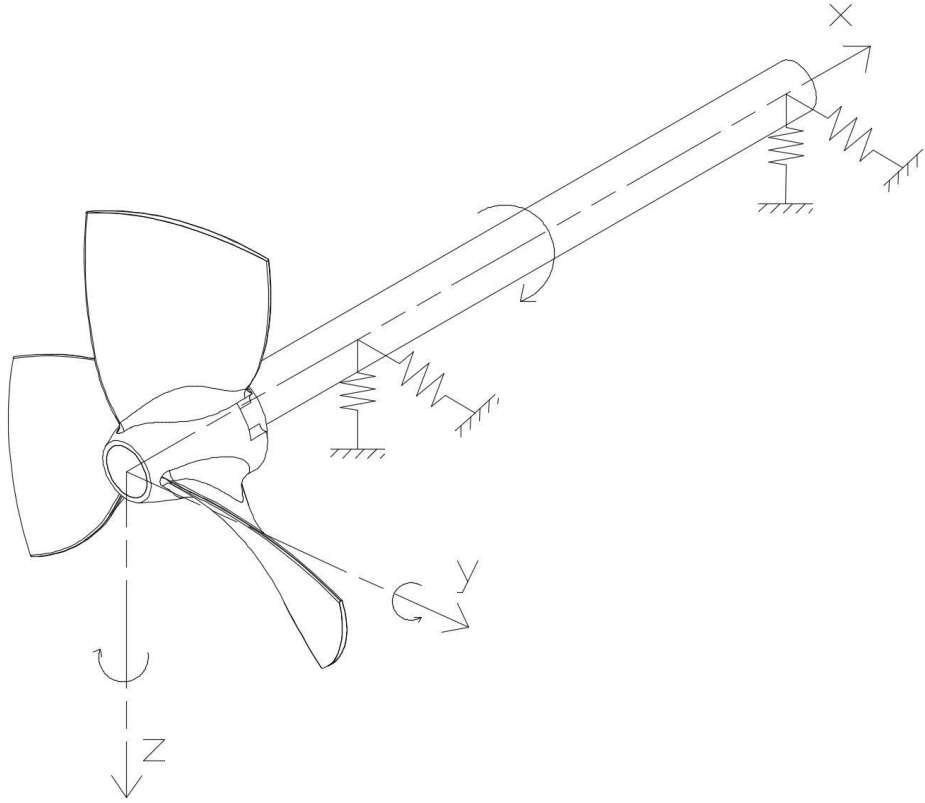


Figure 3.1: Propeller global coordinate system.

In this study, the propeller vibrates in six rigid body modes with orientations as defined in Figure 3.1. According to Carlton (2012) the equation of motion for the marine propeller can be written as:

$$M\ddot{x} = f_e + f_H + f_S \quad (3.13)$$

where  $x$  is the displacement,  $f_e$  is the excitation,  $f_H$  is the additional hydrodynamic, and  $f_S$  represents the external excitation forces and moment vectors. The mass and displacement can be written in matrix and vector form as follows (Carlton, 2012):

$$M\ddot{\mathbf{x}} = \begin{bmatrix} m & 0 & 0 & 0 & 0 & 0 \\ 0 & m & 0 & 0 & 0 & 0 \\ 0 & 0 & m & 0 & 0 & 0 \\ 0 & 0 & 0 & I_{xx} & 0 & 0 \\ 0 & 0 & 0 & 0 & I_{yy} & 0 \\ 0 & 0 & 0 & 0 & 0 & I_{zz} \end{bmatrix} \begin{bmatrix} \ddot{\delta}_x \\ \ddot{\delta}_y \\ \ddot{\delta}_z \\ \ddot{\phi}_x \\ \ddot{\phi}_y \\ \ddot{\phi}_z \end{bmatrix} \quad (3.14)$$

In the mass matrix,  $m$  is the mass of the propeller,  $I_{xx}$  is the polar mass moment, and  $I_{yy} = I_{zz}$  are the diametric mass moments of inertia. The hydrodynamic force vector for the marine propeller depends upon the displacements, velocities, and acceleration. The additional hydrodynamic force can then be represented by (Carlton, 2012):

$$f_H = -(M_a)\ddot{\mathbf{x}} - C_p\dot{\mathbf{x}} \quad (3.15)$$

In classical vibration theory, an additional stiffness matrix  $K_p$  is included in this expression. The stiffness matrix depends mainly on the immersion of the propeller. This matrix is excluded because the propeller is only considered when it is fully immersed. Rewriting the equation of motion by combining Equations (3.13) and (3.15) allows the following equation to be derived (Carlton, 2012):

$$[M + M_a]\ddot{\mathbf{x}} + C_p\dot{\mathbf{x}} - f_s = f_e \quad (3.16)$$

Furthermore, the added mass and damping matrices are needed. These matrices are of the same form, consisting of a full diagonal and some linear and rotational terms with a set of non-diagonal coupling terms, as seen in the two following equations (Carlton, 2012):

$$M_a = \begin{bmatrix} m_{11} & 0 & 0 & m_{41} & 0 & 0 \\ 0 & m_{22} & -m_{32} & 0 & m_{52} & -m_{62} \\ 0 & m_{32} & m_{22} & 0 & m_{62} & m_{52} \\ m_{41} & 0 & 0 & m_{44} & 0 & 0 \\ 0 & m_{52} & -m_{62} & 0 & m_{55} & -m_{65} \\ 0 & m_{62} & m_{52} & 0 & m_{65} & m_{55} \end{bmatrix} \quad (3.17)$$

$$C_p = \begin{bmatrix} c_{11} & 0 & 0 & c_{41} & 0 & 0 \\ 0 & c_{22} & -c_{32} & 0 & c_{52} & -c_{62} \\ 0 & c_{32} & c_{22} & 0 & c_{62} & c_{52} \\ c_{41} & 0 & 0 & c_{44} & 0 & 0 \\ 0 & c_{52} & -c_{62} & 0 & c_{55} & -c_{65} \\ 0 & c_{62} & c_{52} & 0 & c_{65} & c_{55} \end{bmatrix} \quad (3.18)$$

It can be seen from matrices (3.17) and (3.18) that there are terms that have identical values. These matrices represent the simplest form of interaction between orthogonal motions (Carlton, 2012). The hydrodynamic coefficients  $m_i$  and  $c_i$  can be calculated using the equations derived by Schwanecke (1963), which are:

$$\begin{aligned} m_{11} &= 0.2812 \frac{\pi \rho D^3}{Z} \left( \frac{A_e}{A_o} \right)^2 \\ m_{22} &= 0.6363 \frac{\rho D^3}{\pi Z} \left( \frac{P}{D} \right)^2 \left( \frac{A_e}{A_o} \right)^2 \\ m_{44} &= 0.0703 \frac{\rho D^5}{\pi Z} \left( \frac{P}{D} \right)^2 \left( \frac{A_e}{A_o} \right)^2 \\ m_{55} &= 0.0123 \frac{\pi \rho D^5}{Z} \left( \frac{A_e}{A_o} \right)^2 \\ m_{41} &= -0.1406 \frac{\rho D^4}{Z} \left( \frac{P}{D} \right) \left( \frac{A_e}{A_o} \right)^2 \\ m_{52} &= 0.0703 \frac{\rho D^4}{Z} \left( \frac{P}{D} \right) \left( \frac{A_e}{A_o} \right)^2 \\ m_{62} &= 0.0408 \frac{\rho D^4}{Z^2} \left( \frac{P}{D} \right) \left( \frac{A_e}{A_o} \right)^3 \\ m_{65} &= 0.0030 \frac{\pi \rho D^5}{Z^2} \left( \frac{A_e}{A_o} \right)^2 \end{aligned} \quad (3.19)$$

$$\begin{aligned}
c_{11} &= 0.0925\rho\omega D^3 \left(\frac{A_e}{A_o}\right) \\
c_{22} &= 0.1536 \frac{\rho\omega D^2}{\pi} \left(\frac{P}{D}\right)^2 \left(\frac{A_e}{A_o}\right) \\
c_{44} &= 0.0231 \frac{\rho\omega D^5}{\pi} \left(\frac{P}{D}\right)^2 \left(\frac{A_e}{A_o}\right) \\
c_{55} &= 0.0053\pi\rho\omega D^5 \left(\frac{A_e}{A_o}\right) \\
c_{41} &= -0.0463\rho\omega D^4 \left(\frac{P}{D}\right) \left(\frac{A_e}{A_o}\right) \\
c_{52} &= 0.0231\rho\omega D^4 \left(\frac{P}{D}\right) \left(\frac{A_e}{A_o}\right) \\
c_{62} &= 0.0981 \frac{\rho\omega D^4}{Z} \left(\frac{P}{D}\right) \left(\frac{A_e}{A_o}\right)^2 \\
c_{65} &= 0.0183 \frac{\pi\rho\omega D^5}{Z} \left(\frac{A_e}{A_o}\right)^2 \\
c_{35} &= 0.1128 \frac{\rho\omega D^4}{Z} \left(\frac{P}{D}\right) \left(\frac{A_e}{A_o}\right)^2
\end{aligned} \tag{3.20}$$

As seen from the damping coefficients Schwanecke distinguishes between the coefficients  $c_{26}$  and  $c_{35}$ , in contrast to other contemporary works. In this study, Equation (3.18) is used to calculate the damping coefficients. Schwanecke's equations relate specifically to fixed-pitch propellers. Another approach to find the hydrodynamic coefficients is to use the regression equation formulae from Parsons and Vorus (1981). These formulae are based on a lifting line formulation and are applicable for propellers with BAR ranging from 0.3 to 1.05 and pitch ratios from 0.5 to 1.4. The regression equations have the following form (Carlton, 2012):

$$\begin{Bmatrix} m_i \\ c_i \end{Bmatrix} = C_1 + C_2 \left(\frac{A_e}{A_o}\right) + C_3 \left(\frac{P}{D}\right) + C_4 \left(\frac{A_e}{A_o}\right)^2 + C_5 \left(\frac{P}{D}\right)^2 + C_6 \left(\frac{A_e}{A_o}\right) \left(\frac{P}{D}\right) \tag{3.21}$$

The regression Equations (3.21) result from the work done by Parsons and Vorus (1981), which in turn is based on the work of Hyllarides and van Gent (1974). Parsons and Vorus investigated the correlation by calculating the added mass and damping for a propeller from lifting surface and lifting line procedures. The regression equation formulae are based on the Wageningen B-screw series, and the equations are suitable for preliminary design purposes (Carlton, 2012). The regression equation coefficients ( $C_i$ ) are dimensionless values and vary only with the

number of blades on the propeller. In a literature search, regression equation coefficients are only identified for propellers with 4 to 7 blades; these can be found in Carlton (2012) or Parsons and Vorus (1981). Propellers with two or three blades are therefore not included in this study. The formulae produced by Parsons and Vorus (1981) are selected to calculate hydrodynamic coefficients in this study, because this approach covers the characteristics of the addressed propellers. Moreover, their study demonstrates that this method can be used for propellers outside the Wageningen B-screw series. For propellers without skew, the results of this approach are within 10-20% of the results for the Wageningen B-screw series.

The coefficients for Equation (3.21) are based on the following parameters from the Wageningen B-screw series; the number of blades, BAR, and pitch ratio. These parameters can easily be calculated for any type of marine propeller (Kuiper, 1992). When the regression equation results are calculated, they must be multiplied by a corresponding multiplier to obtain the final added mass and damping value. The appropriate multipliers for the various coefficients are listed in the following table.

Table 3.1: Non-dimensionalization of coefficients, assembled following Parsons and Vorus (1981).

Type of coefficient	Coefficients	Multipliers
Added mass moment of inertia	$m_{44}, m_{55}, m_{65}$	$\rho D^5$
Inertia coupling	$m_{41}, m_{52}, m_{62}$	$\rho D^4$
Added mass	$m_{11}, m_{22}, m_{32}$	$\rho D^3$
Rotational damping	$c_{44}, c_{55}, c_{65}$	$\rho n D^5$
Velocity coupling	$c_{41}, c_{52}, c_{62}$	$\rho n D^4$
Linear damping	$c_{11}, c_{22}, c_{32}$	$\rho n D^3$

### 3.5. The Wageningen B-screw series

The B-series originated following an investigation of G.S. Baker's A-series propellers performed in the NSMB, conducted because the A-series was known to be very efficient.

Testing revealed that the A-series was susceptible to cavitation. Subsequently, the B-series was developed with wider blade tips compared to the A-series. The development of the B-series continued and currently consists of 130 propellers with blade numbers ranging from 2 to 7 blades, with different pitches and BARs. The B-series has a small skew and a positive rake, and was given the name Wageningen after the city in which it was developed.

The Wageningen B-screw series has since been thoroughly investigated, documented, and tested regarding various propeller characteristics. For instance, propeller tests have been performed in open water with a uniform flow over the propellers. Typical propeller models from the Wageningen B-screw series are presented in Table 3.2 (van Lammeren et al., 1969).

Table 3.2: Models in the Wageningen B-screw series, assembled following van Lammeren et al. (1969).

Z	P/D	Ae/Ao													
2	0.5 to 1.40	0.30													
3			0.35			0.50			0.65			0.80			
4				0.40			0.55			0.70			0.85	1.00	
5					0.45			0.60			0.75				1.05
6						0.50			0.65			0.80			
7							0.55			0.70			0.85		

As shown in Table 3.2, only a few BARs are presented for each number of blades on the propeller. However, for other propeller series many other BARs exist for the number of blades indicated in Table 3.2. The notation used to describe the different propellers in the Wageningen B-screw series has the following form; for example, B4-70-100, which indicates a B-screw series propeller with four blades, a BAR of 0.7, and a pitch ratio equal to 1.0 (van Lammeren et al., 1969). The same notation is used to describe the characteristics of the propellers addressed in this study.



### 3.6. Open water test procedure

Open water testing is carried out to derive the open water characteristics of marine propellers. Testing is preferably carried out on a full-scale model of the propeller. The basin used for open water testing should be sufficiently large to avoid blockage, and the propeller should be positioned in such a way that pressure build-up does not occur. A dynamometer is used to measure thrust and torque, and a current meter is used to measure the speed of advance of the propeller. Recording devices should be placed such that they do not influence the propeller in any way. Immersion of the propeller is arranged so that air from the surface is not drawn into the propeller. The shaft speed should be kept constant throughout the test, and the revolution rate should be high to obtain a high Reynolds number, according to recommended guidelines (ITTC, 2002; Molland, 2008).

### 3.7. Marine propeller forces and moments

The forces and moments produced by the propeller react on the bearings, contributing to a significant increase in the bearing forces, and are calculated from open water test data of the various propellers. The effective thrust force from a propeller is rarely directed along the shaft axis. This is a result of the effects from the wake field and a possible shaft inclination relative to the flow. The line of action of the effective thrust is typically raised above the shaft axis as a result of slower water velocities in the upper part of the propeller. Furthermore, tangential velocity components can also result in deviations of the effective thrust force in the plane of symmetry of the axial wake field. This produces variable forces and moments in both the vertical and horizontal directions. The distance from where the effective thrust force acts on the shaft centerline is termed the thrust eccentricity, and can be expressed by the following equation (Carlton, 2012):

$$e_T^2(t) = e_{Ty}^2(t) + e_{Tz}^2(t) \quad (3.22)$$

The equation is time dependent because of the differences in the flow field due to the rotating propeller. The resulting forces and moments can be expressed as the sum of a Fourier expansion series, containing one constant and one fluctuating component (Carlton, 2012):

$$F(t) = F_0 + \sum_{k=1}^n F_k \cos(\omega t + \phi_k) \quad (3.23)$$

$$M(t) = M_0 + \sum_{k=1}^n M_k \cos(\omega t + \phi_k) \quad (3.24)$$

If the shaft inclination angle is high then the effective thrust force is high in the x-direction. However, in the absence of a high shaft inclination angle the bearing forces depend on the wake field characteristics, vessel speed, propeller RPM, skew, and blade number (Carlton, 2012). Nevertheless, the dynamic forces in this study are calculated using the work by Veritec (1985). Veritec (1985) performed an investigation of the dynamic forces at the blade and at twice the blade rate frequency on 20 different ships. The number of blades on the propellers considered in this investigation are between 4-6. The results of Veritec (1985)'s work are presented in Equation (3.25)-(3.26) and Appendix A, and indicate that propellers with an odd number of blades generally induce smaller thrust fluctuations and larger bending moments than propellers with an even number of blades.

Equations (3.25) and (3.26) only apply to 4 bladed propellers, and the relevant equations for 5- and 6-bladed propellers can be found in Appendix A. Since the equations for dynamic forces are restricted to propellers with 4 to 6 blades, the propellers investigated in this study are thus restricted to those with blade numbers in this range.

$$F_{x(1)} = 0.084T_0 \pm 0.031T_0, F_{x(2)} = 0.022 \pm 0.004T_0 - \text{Thrust}$$

$$F_{z(1)} = 0.008T_0 \pm 0.004T_0, F_{z(2)} = 0.008T_0 \pm 0.004T_0 - \text{Vertical force} \quad (3.25)$$

$$F_{y(1)} = 0.012T_0 \pm 0.011T_0, F_{y(2)} = 0.00T_0 \pm 0.001T_0 - \text{Horizontal force}$$

$$M_{x(1)} = 0.062Q_0 \pm 0.025Q_0, M_{x(2)} = 0.016Q_0 \pm 0.010Q_0 - \text{Torque}$$

$$M_{z(1)} = 0.075Q_0 \pm 0.05Q_0, M_{z(2)} = 0.019Q_0 \pm 0.013Q_0 - \text{Vertical torque} \quad (3.26)$$

$$M_{y(1)} = 0.138Q_0 \pm 0.09Q_0, M_{y(2)} = 0.040Q_0 \pm 0.036Q_0 - \text{Horizontal torque}$$

As seen from Equations (3.25) and (3.26), the dynamic components are expressed by the mean thrust  $T_0$  and the mean torque  $Q_0$ . The mean thrust and mean torque are both obtained from open water propeller characteristics plots produced by Bernitsas et al. (1981). An example of a plot is shown in Figure 3.2 for the Wageningen B4-70 propeller. The plots are expressed through the torque and thrust coefficients, in terms of the number of blades, BAR and pitch ratio, and the advance coefficient. The Reynolds number used in the open water characteristics plots of Bernitsas et al. is  $2.0 \times 10^6$ . The non-dimensionalized Reynolds number is:

$$R_n = \frac{\rho n D^2}{\mu} = \frac{\rho V D}{\mu} \quad (3.27)$$

FIGURE 41. WAGENINGEN B-SERIES PROPELLERS  
 FOR 4 BLADES  $AE/AO = 0.700$   
 $P/D = 0.50$  TO  $1.40$

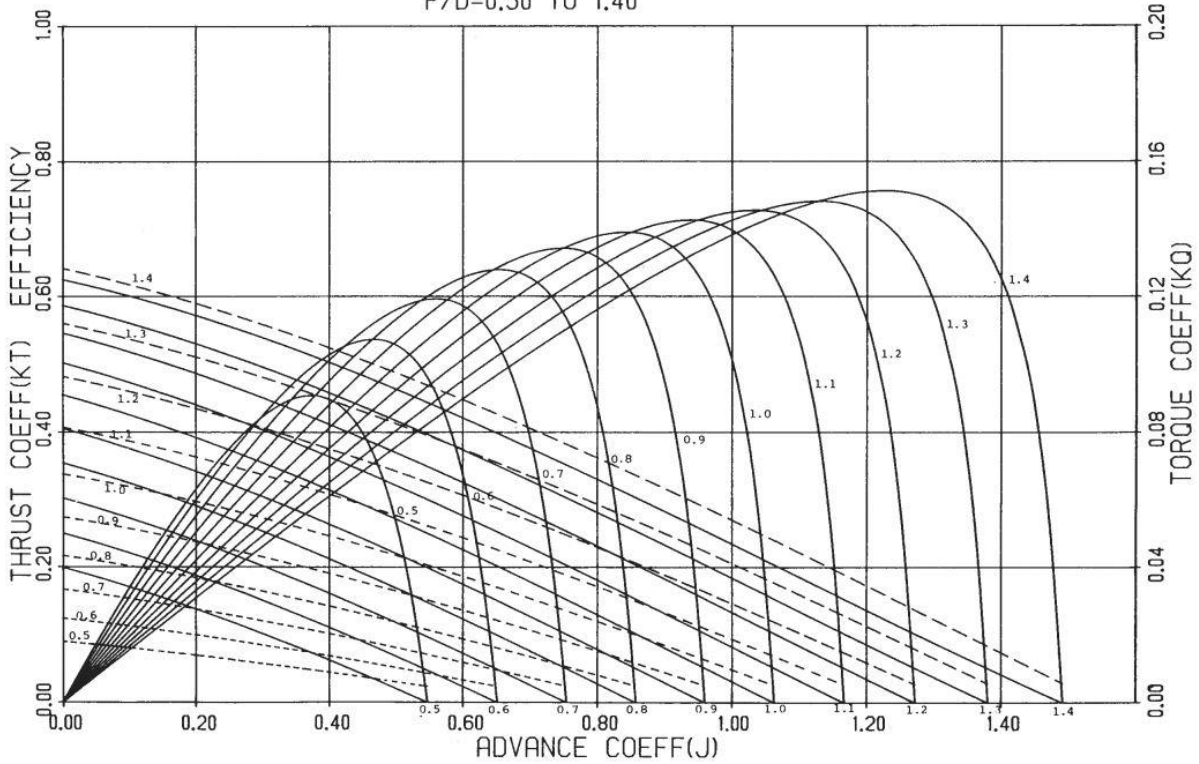


Figure 3.2:  $K_t$ ,  $K_q$ , and efficiency curves for the B4-70 propeller (Bernitsas et al., 1981, p. 47).

The declining lines in Figure 3.2 are the thrust (solid lines) and torque (dotted lines) coefficient curves, while the polynomial curves are the efficiency curves. The optimal point for each pitch ratio is found at the top of the efficiency curve. An interesting aspect of the propeller force and torque is to analyze how these vary with different propeller characteristics. The non-dimensional terms taken from Figure 3.2 and the cavitation number used to express general open water characteristics are shown in Equation (3.28) (Carlton, 2012).

$$\text{Thrust coefficient; } K_T = \frac{T}{\rho n^2 D^4}$$

$$\text{Torque coefficient; } K_Q = \frac{Q}{\rho n^2 D^5}$$

(3.28)

$$\text{Advance coefficient; } J = \frac{V_a}{nD}$$

$$\text{Cavitation number; } \sigma = \frac{\text{static head}}{\text{dynamic head}} = \frac{p_0 - e}{\frac{1}{2}\rho V^2}$$

The thrust and torque of marine propellers working sufficiently below the free surface depend upon the following parameters: propeller diameter  $D$ , the speed of advance  $V_a$ , the rotational speed  $n$ , the density of the fluid  $\rho$ , the viscosity of the fluid  $\mu$ , and the static pressure of the fluid at the propeller station ( $p_0 - e$ ), where  $p_0$  is the static pressure and  $e$  is the vapor pressure at ambient temperature. For calculation of the cavitation number,  $V$  is a representative velocity and can be expressed as;  $V = nD$ . High cavitation effects can have a negative impact on thrust and torque performance. Other problems related to cavitation include vibration issues and erosion on the propeller blades. Cavitation is usually a greater concern when the propeller is subjected to high speeds or high load. The number of blades on the propeller can be a convenient parameter to change in order to handle cavitation problems; for example, a greater number of blades results in a higher area upon which the load can act. The open water efficiency can also be affected by cavitation, since this parameter is expressed in terms of the thrust, torque, and advance coefficients as shown in Equation (3.29) (Carlton, 2012; Molland, 2008).

$$n_o = \frac{J}{2\pi} \frac{K_T}{K_Q} \quad (3.29)$$

For calculation of the advance coefficient as presented in Equation (3.28),  $V_a$  is the speed of advance, which is equal to the vessel speed  $V_{ex}$ , modified by a wake factor  $W_f$ , as shown in the following equation (Gerr, 1989; Ong et al., 2007):

$$V_a = V_{ex} W_f \quad (3.30)$$

The required thrust power can be calculated by the simplified expression;  $P_T = T \times V_A$ . Propeller efficiency is typically in the range from 0.35 to 0.75; the highest efficiency is usually reached by propellers with the lowest number of blades and declines with increasing number of blades (MAN Diesel & Turbo, 2011).

## Chapter 4

### Estimation of propeller contributions

#### 4.1. Introduction

The estimation of propeller contributions as discussed in Chapter 3 are limited to propellers with blade numbers ranging from 4 to 6. The differences in geometry for the investigated propeller and the Wageningen B-screw series are as follows. First, the B-series has a small skew and rake, while the propellers addressed in this study have no skew and rake. According to Parsons and Vorus (1981) and Kuiper (1992) a small difference in skew and rake does have a small impact on the performance of the propellers. Another difference in geometry is the blade tips; the B-series has rounded smooth edges, while the investigated propellers have blade tips of finite length, which are common for propellers used with a duct (Kuiper, 1992). The investigated propellers are the B4-71, B5-88, and B6-106, with pitch ratios ranging from 0.5 to 1.4. The propellers are shown in the figure below.

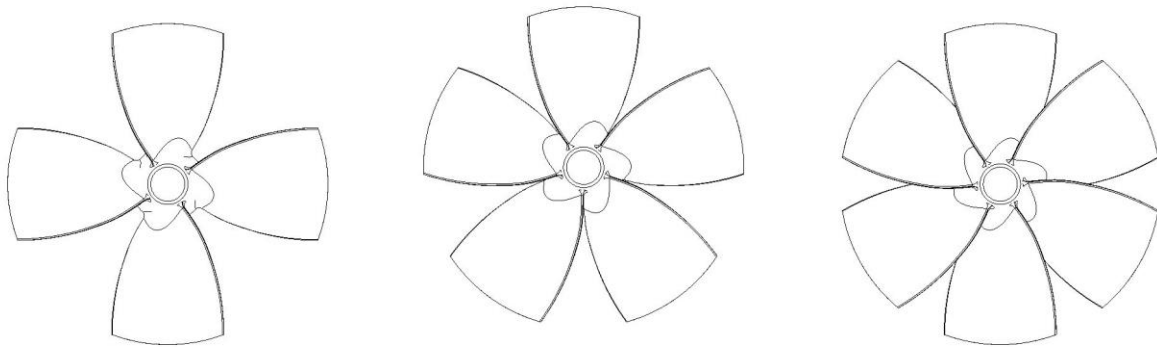


Figure 4.1: B4 to B6 propellers.

The hydrodynamic damping, forces, and moments depend on the rotational rate. Furthermore, the hydrodynamic forces and moments depend on the blade rate frequency component, while the blade rate frequency depends on the number of blades and the angular velocity. Thus, the

calculation method presented in this study is only applicable for the investigation of steady-state cases. This is because the propeller contributions can only be calculated for one specific speed at a time.

## 4.2. Added mass and damping

To demonstrate the estimation of the added mass and damping, the non-dimensionalized regression results produced using Equation (3.21) for the B4-71 propeller are presented in Figures 4.2 and 4.3, for pitch ratios ranging from 0.5 to 1.4. The coefficients listed on the right y-axis use this axis, while the remaining coefficients belong to the left y-axis. The final added mass and damping values are obtained when the non-dimensionalized results are multiplied with the appropriate multiplier from Table 3.1.

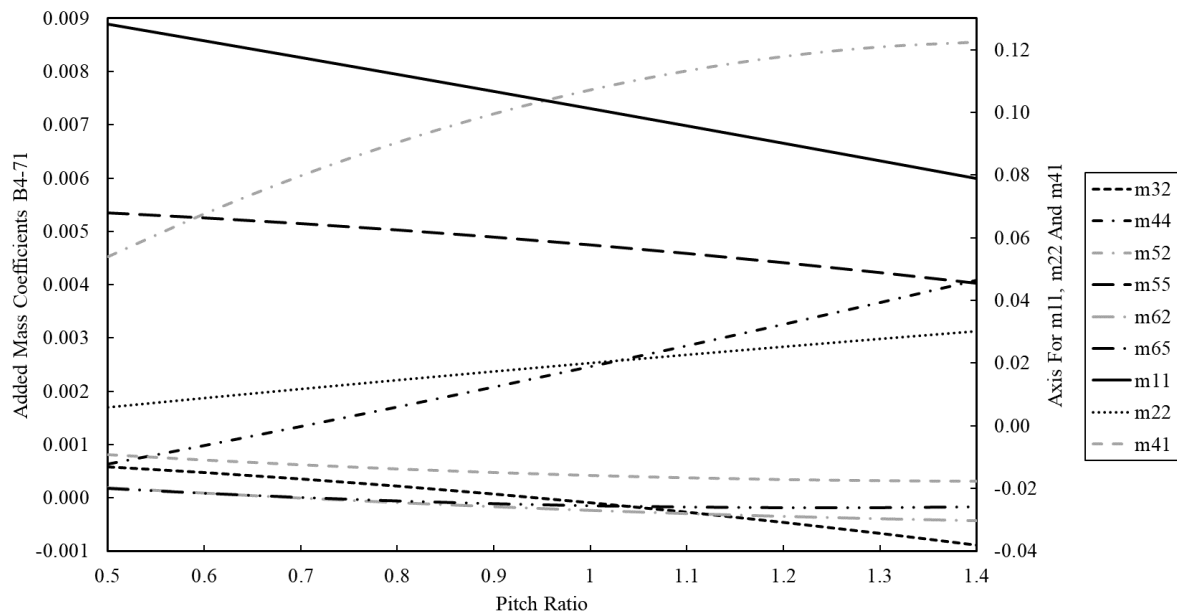


Figure 4.2: Non-dimensionalized added mass coefficients.



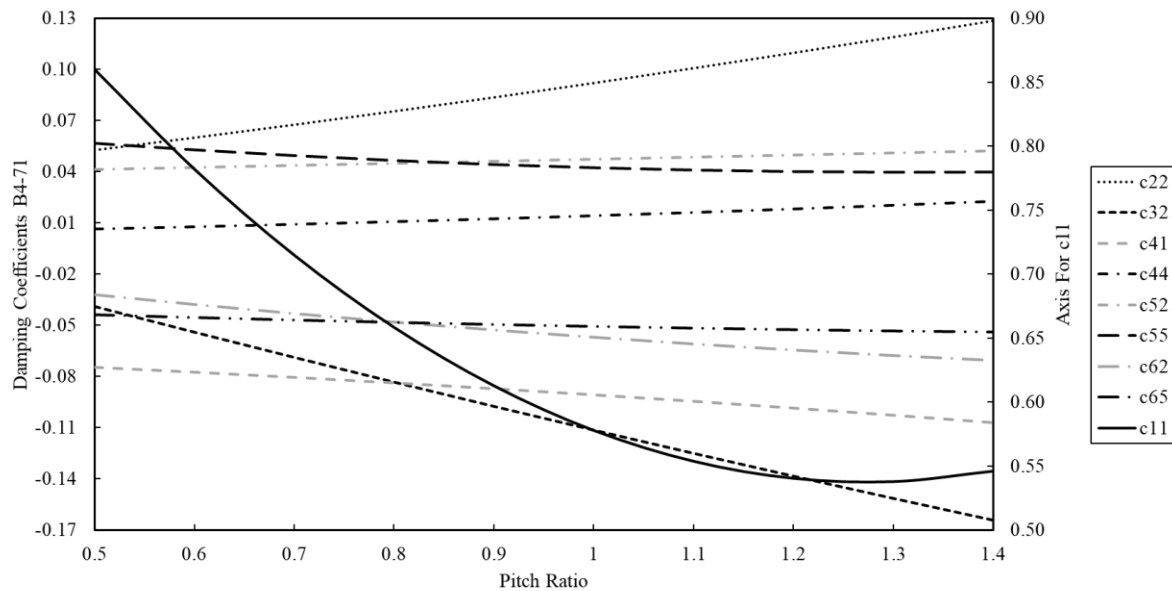


Figure 4.3: Non-dimensionalized damping coefficients.

As shown in Figures 4.2 and 4.3, the damping coefficients are of a higher magnitude than the added mass coefficients. This implies that the propeller damping terms are important to include in propeller calculations. The magnitude of the different terms also varies; the highest terms and therefore the most important to include for the added mass and damping terms are 11, 41, 22, and 32.

### 4.3. Propeller forces and moments

As explained in Section 3.7, marine propeller forces and moments can be calculated with the use of open water test data from Bernitsas et al. (1981). These data are not available for all BARs, so test data for the BAR that is nearest to the investigated propeller is used. For instance, the B4-71 propeller uses B4-70 open water test data to estimate marine propeller forces and moments. Accordingly, the thrust, torque, and efficiency can be calculated using Figure 3.2

and Equation (3.28) for the B4-71 propeller at different speeds, as shown in the Figures 4.4, 4.5, and 4.6.

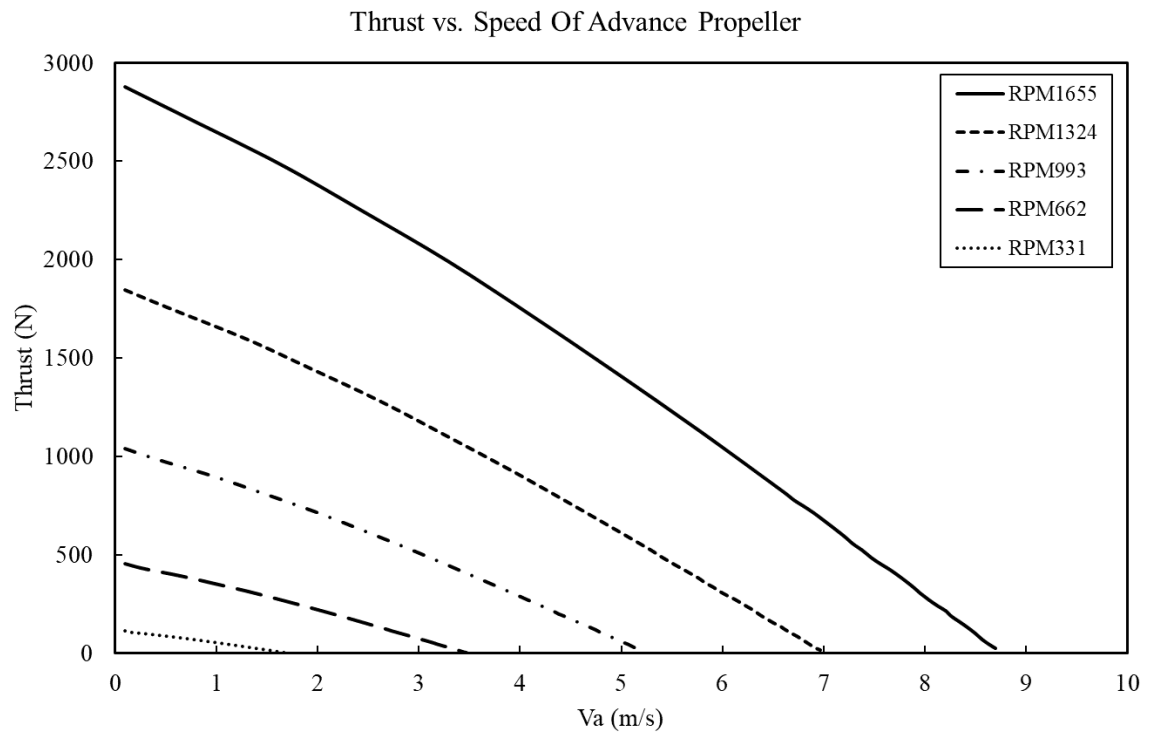


Figure 4.4: Thrust vs. speed of advance for B4-71 propeller.

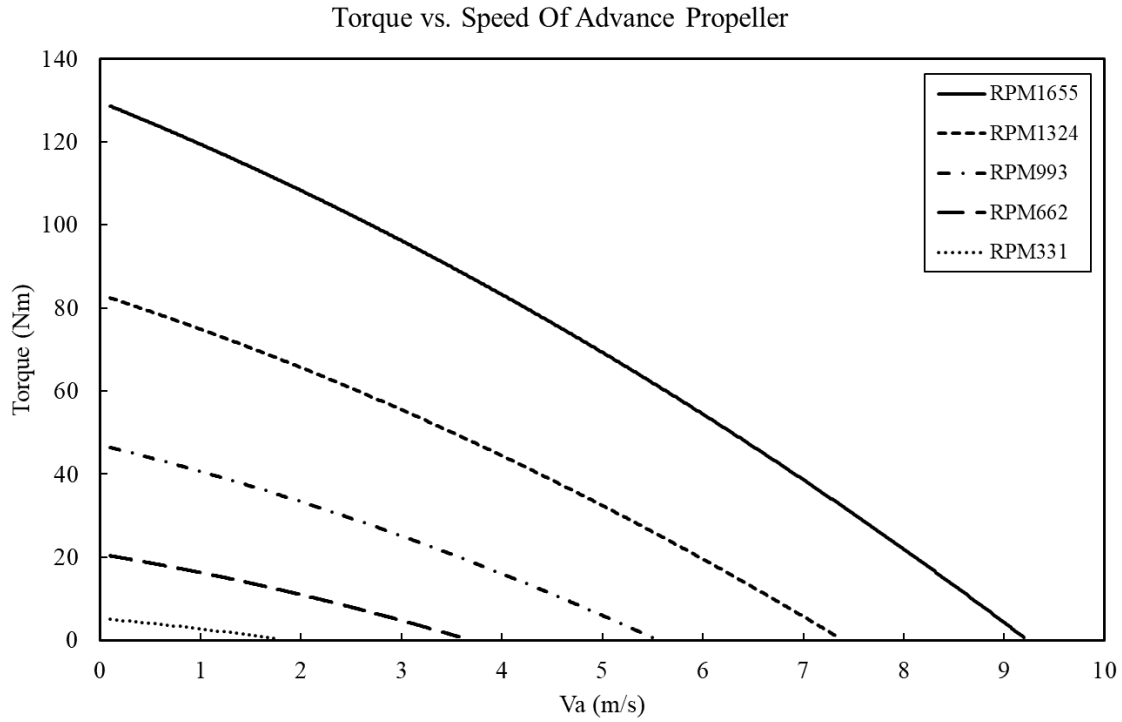


Figure 4.5: Torque vs. speed of advance for B4-71 propeller.

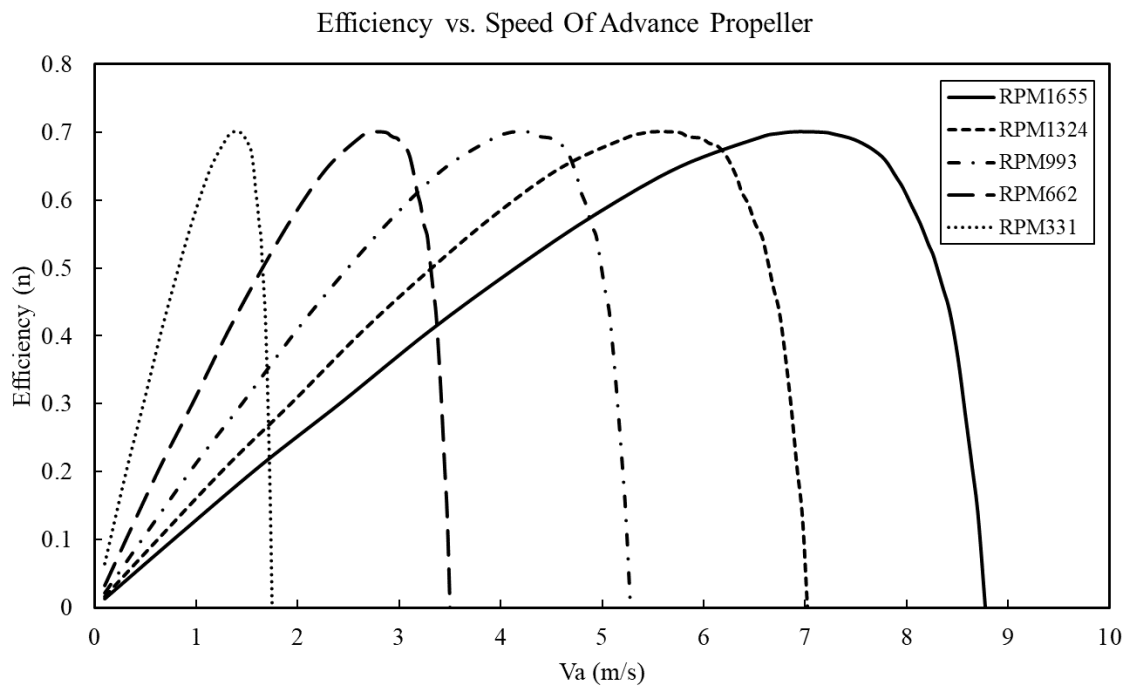


Figure 4.6: Efficiency vs. speed of advance for B4-71 propeller.

The accuracy of the results presented in Figures 4.4-4.6 is not optimal since the thrust, torque, and advance coefficients are taken directly from the open water test plots. However, if the results from Figures 4.4-4.6 are back-calculated to find the coefficients, the results are satisfying and applicable for preliminary calculations, which is appropriate for this study. The coefficients from the open water test plots are found using a plot digitizer.

The “efficiency vs. speed of advance” plot illustrates that an optimal rotational speed exists for a specific speed of advance. The optimal speed is found at the top of the curves, and the effective region for a given rotational speed is situated within (below) the curve.

# Chapter 5

## Vibration analysis

### 5.1. Introduction

This chapter provides an introduction to vibration analysis and time signals. This includes how a continuous time signal is processed for further investigation of the frequencies in the system. Moreover, the method of obtaining the frequency response from a Fourier series is also explained, in addition to a method to describe the level of a dynamic signal, which can further be used for bearing life calculation.

### 5.2. Signals and time data

Vibrations can originate from the power source, an unbalanced shaft, and misalignment between rotating elements. In addition, vibrations are generated by the marine propeller from the displaced water. From the OM simulations, various vibratory motions can be extracted from a given time domain and sampling time frequency. This continuous time signal can subsequently be used for further investigation of the system frequency, amplitude, and phase.

According to Boashash (1992) in mechanics the frequency of vibratory motion can be defined as the number of oscillations per unit of time, where vibrations are any to-and-fro motion and one oscillation is defined as a complete to-and-fro motion. Referring to Newton's equation of motion, Equation (3.11), the harmonic motion of such systems has a displacement, velocity, and acceleration which can be expressed by the following equations (Boashash, 1992):

$$x = A \cos \omega t \quad (5.1)$$

$$\dot{x} = -\omega A \sin \omega t \quad (5.2)$$

$$\ddot{x} = -\omega^2 A \cos \omega t \quad (5.3)$$

$$(-\omega^2 m - \omega c + k)A = f \quad (5.4)$$

where  $A$  is the amplitude and  $\omega$  is the angular frequency, and Equation (5.4) is the rewritten equation of motion and represents the mixture of harmonic vibrations in the system. As demonstrated by Equations (5.1-5.3) the harmonic response from the system is composed of a sum of sinusoidal signals. Hence, the signals can be expressed by Fourier series which can further be used in a discrete Fourier transform (DFT) and computed by fast Fourier transform (FFT). The frequency response can then be obtained and used for experimental studies and comparisons. The continuous Fourier transform, and the time signal are defined in the following equations (Brandt, 2011):

$$\mathcal{F}[x(t)] = X(f) = \int_{-\infty}^{\infty} x(t)e^{-j2\pi ft} dt \quad (5.5)$$

$$\mathcal{F}^{-1}[X(f)] = x(t) = \int_{-\infty}^{\infty} X(f)e^{j2\pi ft} df \quad (5.6)$$

where  $f = \frac{\omega}{2\pi}$ ,  $j$  is an imaginary number, and Equation (5.6) is the inverse Fourier transform. Different signals have different spectra and therefore must be treated according to the type of signal, e.g., periodic, random, or transient. According to the mathematical theory of Fourier series, a periodic signal  $x_p(t)$  can be written as (Brandt, 2011):

$$x_p(t) = \frac{a_0}{2} + \sum_{k=1}^{\infty} a_k \cos\left(\frac{2\pi k}{T_p} t\right) + \sum_{k=1}^{\infty} b_k \sin\left(\frac{2\pi k}{T_p} t\right) \quad (5.7)$$

Periodic signals can, in theory, be a sum of infinite sinusoids as in Equation (5.7), each with their own amplitude and phase. The sinusoids of a periodic signal contain only discrete frequencies, and these frequencies are integer harmonics of the fundamental frequency  $\frac{1}{T_p}$ , where  $T_p$  is the period of the signal. The coefficients  $a_k$  and  $b_k$  from Equation (5.7) can be calculated from the following equations (Brandt, 2011):

$$a_k = \frac{2}{T_p} \int_{t_1}^{t_1+T_p} x_p(t) \cos\left(\frac{2\pi k}{T_p} t\right) dt, \text{ for } k = 0, 1, 2, \dots$$

$$b_k = \frac{2}{T_p} \int_{t_1}^{t_1+T_p} x_p(t) \sin\left(\frac{2\pi k}{T_p} t\right) dt, \text{ for } k = 1, 2, 3, \dots \quad (5.8)$$

The integration of Equation (5.8) occurs over an arbitrary period of the periodic signal. Equation (5.7) can be rewritten as one sinusoid for each frequency with an individual phase angle,  $\phi_k$ , for easier physical interpretation (Brandt, 2011):

$$x_p(t) = \frac{a_0}{2} + \sum_{k=1}^{\infty} a'_k \cos\left(\frac{2\pi k}{T_p} t + \phi_k\right) \quad (5.9)$$

where  $a'_k$  and  $\phi_k$  are defined as:

$$a'_k = \sqrt{a_k^2 + b_k^2} \quad (5.10)$$

$$\phi_k = \arctan\left(\frac{b_k}{a_k}\right) \quad (5.11)$$

According to Brandt (2011) the Fourier series can also be written with complex coefficients instead of real coefficients. The following equations provide the complex coefficients:

$$c_0 = \frac{a_0}{2} \quad (5.12)$$

$$c_k = \frac{1}{2}(a_k - jb_k) = \frac{1}{T_p} \int_{t_1}^{t_1+T_p} x_p(t) e^{-\frac{j2\pi k}{T_p} t} dt, \text{ for } k > 0$$

Furthermore, the Fourier series can be written as follows:

$$x_p(t) = \sum_{k=-\infty}^{\infty} c_k e^{-\frac{j2\pi k}{T_p} t} \quad (5.13)$$

The summation of Equation (5.13) occurs over both positive and negative frequencies. It is assumed that if the left-hand side of the equation is real, then the right-hand side must also be real. Moreover, it is known that the cosine function is an even function and the sine is an odd function. The complex coefficients must then comply with the following equations (Brandt, 2011):

$$\begin{aligned}
\operatorname{Re}[c_{-k}] &= \operatorname{Re}[c_k] \\
\operatorname{Im}[c_{-k}] &= -\operatorname{Im}[c_k] \\
\therefore c_{-k} &= c_k^* \\
&\text{for all } k \neq 0
\end{aligned}
\tag{5.14}$$

where “\*” represents the complex conjugate with one real and one imaginary part. Thus, the physical frequency content is split symmetrically and the true amplitudes are the positive components. This is similar to the continuous Fourier transform properties from Equation (5.5) (Brandt, 2011).

A measure used to describe the level of a dynamic signal is the root mean square (RMS) value, which is simply the square root of the mean square of the signal. The RMS value can be calculated from the average time,  $\tau$ , and the signal,  $x(t)$ . Alternatively, for any type of signal the RMS value can be calculated from the summed area under the graph from a power spectral density (PSD) plot for a specific frequency range, as shown in the following equations (Brandt, 2011):

$$\begin{aligned}
x_{RMS} &= \sqrt{\frac{1}{\tau} \int_0^{\tau} x^2(t) dt} \\
x_{RMS} &= \sqrt{\text{area under graph}}
\end{aligned}
\tag{5.15}$$

The impulse response of a system is the dynamic output from the system for a given input as a function of time. For a linear system, the impulse response is obtained from the inverse transfer function, whereby the transfer function is obtained from a Laplace transform. From the transfer function, each output value is calculated from a given input value. Furthermore, the convolution result relates the input time signal to the impulse response. The Fourier transform can be used to transform the impulse response into the frequency domain to obtain the frequency response function (FRF), which is discussed in more detail in the following section (Brandt, 2011).



### 5.3. Frequency analysis

To transform the measured signal into a spectrum the DFT method is used in this study. The finite DFT and the time signal (inverse DFT) can be defined with the following equations (Brandt, 2011):

$$X(k) = \sum_{n=0}^{N-1} x(n)e^{-j2\pi kn/N}, \text{ for } k = 0, 1, \dots, N-1 \quad (5.16)$$

$$x(n) = \frac{1}{N} \sum_{k=0}^{N-1} X(k)e^{j2\pi kn/N}, \text{ for } n = 0, 1, \dots, N-1 \quad (5.17)$$

where  $x(n) = x(n\Delta t)$  is the sampled signal and  $N$  is the number of samples. Since the DFT does not include the differentiator,  $dt$ , is Equation (5.16) divided by  $N$  in order to obtain physically interpretable results. One major difference between the DFT and the continuous Fourier transform from Equation (5.5) is that the DFT is a discrete sum of the samples and the other is a continuous integral (Brandt, 2011).

A direct calculation of Equation (5.16) would result in a number of computations  $N^2$ , where one computation consists of a complex multiplication and a complex addition. With the use of an algorithm (FFT) to calculate the DFT, the computations can be reduced to less than  $2N \log_2 N$  without using more data storage for a given array (Cooley & Tukey, 1965).

According to Proakis and Manolakis (2007) the radix-2 FFT algorithm is a commonly used algorithm. It splits the sample into even- and odd-numbered samples, and by using the FFT algorithm the number of complex multiplications is reduced to  $\frac{N}{2} \log_2 N$  while complex additions are reduced to  $N \log_2 N$ . The speed improvement factor can be used as an example, with a value of 204.8 for complex multiplications with a data sample of  $N = 1024$ . This is obtained by using the radix-2 FFT algorithm, compared to calculating the DFT complex multiplications. Further explanation of FFT algorithms can be found in Proakis and Manolakis (2007).

The FRF for complex exponential and sinusoidal signals is a function of the frequency variable and the Fourier transform of the unit sample response; the FRF is expressed by the following equation (Proakis & Manolakis, 2007):

$$H(\omega_e) = \sum_{k=-\infty}^{\infty} h(k) e^{-j\omega k} \quad (5.18)$$

where  $H(\omega)$  is the FRF and  $h(k)$  is the unit impulse. The FRF describes the characteristics of the system, i.e., the spectrum, magnitude and phase (Proakis & Manolakis, 2007). The FRF is useful when comparing the input frequency and natural frequency vs. the resonant frequency.

From the equation of motion of a mass-damper-spring system, Equation (3.11), the forced response from harmonic excitations can be obtained. The equation of motion concerning both real and complex computations is expressed by (Meirovitch, 1986):

$$\ddot{x}(t) + 2\zeta\omega_n\dot{x}(t) + \omega_n^2x(t) = \frac{k}{m}f(t) = \omega_n^2A\cos\omega t \quad (5.19)$$

where  $\zeta$  is the relative damping factor and  $\omega_n$  is the natural frequency of un-damped oscillations. The natural frequency is then obtained by the following equation:

$$\omega_n = \sqrt{\frac{k_i}{m_i + m_{A,i}}} \quad (5.20)$$

The harmonic response for such systems in compact form is expressed by (Meirovitch, 1986):

$$x(t) = X(\omega_e)\cos(\omega_e t - \phi_k) \quad (5.21)$$

where the amplitude and the phase angle are obtained by:

$$X(\omega_e) = \frac{A}{\sqrt{\left(1 - \left(\frac{\omega_e}{\omega_n}\right)^2\right)^2 + \left(2\zeta\frac{\omega_e}{\omega_n}\right)^2}} \quad (5.22)$$

$$\phi_k = \tan^{-1} \frac{2\zeta \frac{\omega_e}{\omega_n}}{1 - \left(\frac{\omega_e}{\omega_n}\right)^2} \quad (5.23)$$

where  $\omega_e$  is the excitation frequency. The above results can also be obtained using complex vectors; the solution for the complex solution is as follows (Meirovitch, 1986):

$$\ddot{x}(t) + 2\zeta\omega_n\dot{x}(t) + \omega_n^2x(t) = \omega_n^2Ae^{j\omega_e t} \quad (5.24)$$

$$x(t) = A|H(j\omega_e)|e^{j(\omega_e t - \phi_k)} \quad (5.25)$$

$$|H(j\omega_e)| = \frac{1}{\sqrt{\left(1 - \left(\frac{\omega_e}{\omega_n}\right)^2\right)^2 + \left(2\zeta \frac{\omega_e}{\omega_n}\right)^2}} \quad (5.26)$$

where  $|H(j\omega_e)|$  is the magnitude of the frequency, which is known as the magnification factor, and the phase angle is as in Equation (5.23). Significant insight about the behavior of a system can be gained by studying how the magnitude of the FRF changes with the excitation frequency. Figure 5.1 illustrates how a system responds to different relative damping factors, with the FRF on the y-axis and the excitation frequency/natural frequency ratio (the relative frequency ratio) on the x-axis. The non-dimensional relative damping factor can be obtained from the following equation (Meirovitch, 1986):

$$\zeta = \frac{c}{2\sqrt{mk}} \text{ or } \frac{c}{2m\omega_n} \quad (5.27)$$

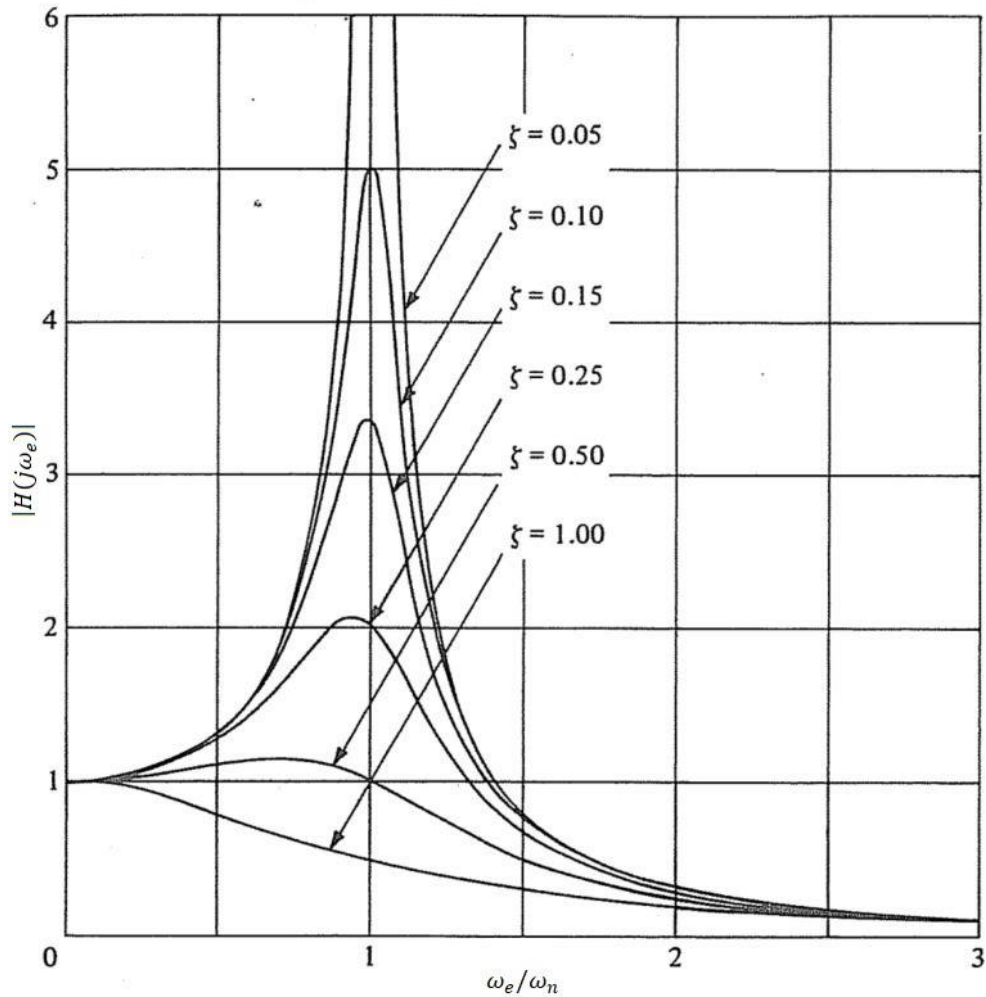


Figure 5.1: The frequency response of a system (Meirovitch, 1986, p. 53).

As seen from Figure 5.1, the amplitudes decrease and the peaks tend to shift to the left for  $\omega_e/\omega_n = 1$  as damping increases. For a relative damping factor of larger than  $1/\sqrt{2}$  the response has no peaks, and for the un-damped case, the peak extends towards infinity. So, for the un-damped case when the excitation frequency approaches the natural frequency, resonance exists for the harmonic oscillator, and severe vibrations can occur. Differentiating Equation (5.26) with respect to  $\omega_e$  and setting the result equal to zero leads to the following expression, which can be used to identify the location where the peaks occur (Meirovitch, 1986):

$$\omega_e = \omega_n \sqrt{1 - 2\zeta^2} \quad (5.28)$$

Equation (5.28) indicates that the maximum response occurs at  $\omega_e/\omega_n < 1$  for damped systems, as previously explained with Figure 5.1. Note that the solution of Equation (5.25) is not valid at resonant conditions corresponding to  $\omega_e = \omega_n$  (Meirovitch, 1986). However, the solution for this case is not included, since damping is included in all of the systems investigated in this study.

#### 5.4. Vibration displacement and bearing life

The bearing life depends on the total bearing force, i.e., the thrust, vertical, and horizontal hydrodynamic forces and moments from the propeller (Amini & Steen, 2011). The bearing forces are obtained from the vibration displacements and the stiffness of the system, i.e.,  $F_i = \delta_i \times k_i$ . Since the vibration forces fluctuate with time, the RMS values of the displacements are used in the bearing life calculations. The fluctuations are due to propeller operation in the wake field (Carlton, 2012) and unbalance in the rotating system. The basic equation for calculating bearing life with 90% reliability according to ISO-281 (2007) is obtained by the following equations in revolutions and hours:

$$L_{10} = \left(\frac{C}{P}\right)^a \quad (5.29)$$

$$L_{10h} = \frac{10^6}{60 \times RPM} L_{10} \quad (5.30)$$

where  $P = XF_r + YF_a$  is the equivalent dynamic bearing load, with  $F_r$  and  $F_a$  as the actual radial and axial loads, and  $X$  and  $Y$  are respectively the radial and axial load factors according to the bearing type.  $C$  is the basic dynamic load for the specific bearing and  $a$  is the exponent of the life equation, according to the bearing type. For tapered roller bearings  $a = 10/3$ . Furthermore, the following apply for tapered roller bearings according to SKF Group (2016):

- $\frac{F_a}{F_r} \leq e \rightarrow P = F_r$ .
- $\frac{F_a}{F_r} > e \rightarrow P = 0.4F_r + YF_a$ .

where  $e$  is the calculation factor for the specific bearing. The RMS values of the displacements used for bearing life calculations are; in the axial direction,  $\delta_x = RMS\ of\ \delta_x(t)$ , horizontal  $\delta_y = RMS\ of\ \delta_y(t)$ , and vertical  $\delta_z = RMS\ of\ \delta_z(t)$ . According to Amini and Steen (2011) the total radial force acting on the bearing can be calculated from the following equation:

$$F_r = \sqrt{F_z^2 + F_y^2} \quad (5.29)$$

As seen from Equation (5.29) the radial forces include both the horizontal and the vertical force component. Thus, all of the loading components are accounted for.

# Chapter 6

## OpenModelica modeling

### 6.1. Introduction

This chapter explains the OM model, and the functionality and testing of the model is briefly introduced. Discussions of the various components used in the OM model follows, in addition to the primary models used for later simulations. Moreover, the created self-defined blocks are presented and explained.

### 6.2. OM modeling and set-up

The modeling began by considering only the marine propeller. This was done to limit the model and to have full control of the model and the propeller contributions. Once this model was built, tested, and verified, it could then be expanded to include a drive shaft and two bearings. The propeller is represented by a multibody block from the standard OM library, which acts as a rigid body and can be modified with physical dimensions and an inertia tensor. This block is then connected to a self-defined directional block, named DOF-block. The DOF-block contains revolute and prismatic blocks from the OM library which enable rotational and translational motion. The model supports motion up to 6 DOF. However, the model can be constrained to only allow motion in selected DOF. Figure 6.1 illustrates the difference between a 4 DOF-block and a 6 DOF-block, where “frame\_a” and “frame\_b” are the connection points for the DOF-block. The revolute blocks are shown in column 1 and the prismatic blocks in column 2. The vectors under the revolute and the prismatic blocks determine which DOF is “open”, i.e.,  $n = \{x, y, z\}$ . Moreover, a value of “1” in one of these directions indicates that motion is allowed in this direction, while “0” means that it is locked in this direction.

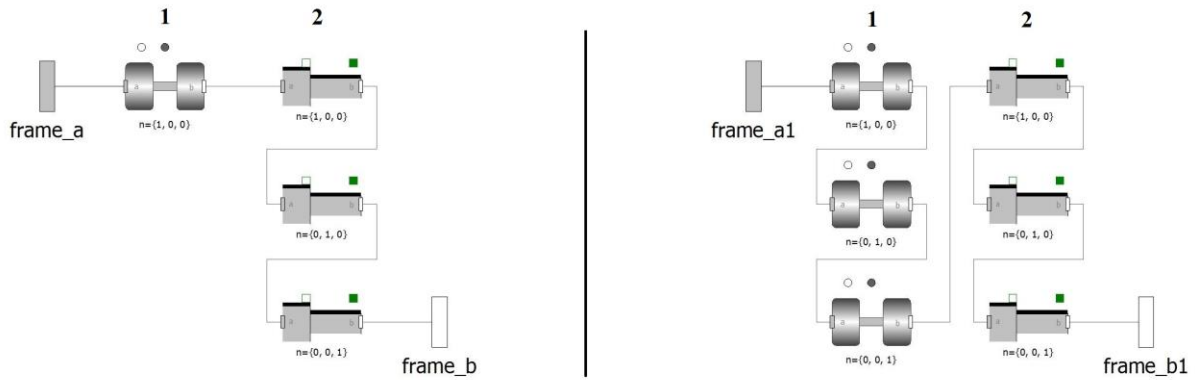


Figure 6.1: 4 DOF vs. 6 DOF.

Furthermore, a separate model is created which contains the equation of motion, i.e., the added mass, damping, stiffness, and dynamic force and torque contributions. This model is further referred to as the equation of motion model (EM). The EM contributions are coded into separate self-defined blocks according to the theory presented in previous chapters. In addition, a relative sensor from the OM library measures translational and rotational motion, i.e., the position, velocity, and acceleration of the body to which the sensor is connected. The EM is created as a separate model to ease the expansion and streamline the primary models. Since the EM model consists of the added mass, damping, stiffness, and the force and torque contributions, the EM model can be used to represent both the marine propeller and the bearings in the system. However, the inputs to the EM models must be different. When the EM model is connected to the marine propeller the added mass, damping, and the force and torque matrices are active. In contrast, when the EM model represents a bearing then only the stiffness matrix is active. The appearance of the EM model when opened in OM is shown in Figure 6.2. The added mass, damping, bearing and force-torque blocks are built from multiple input – multiple output (MIMO) blocks, and the inputs and outputs for the various blocks are shown in Table 6.1.



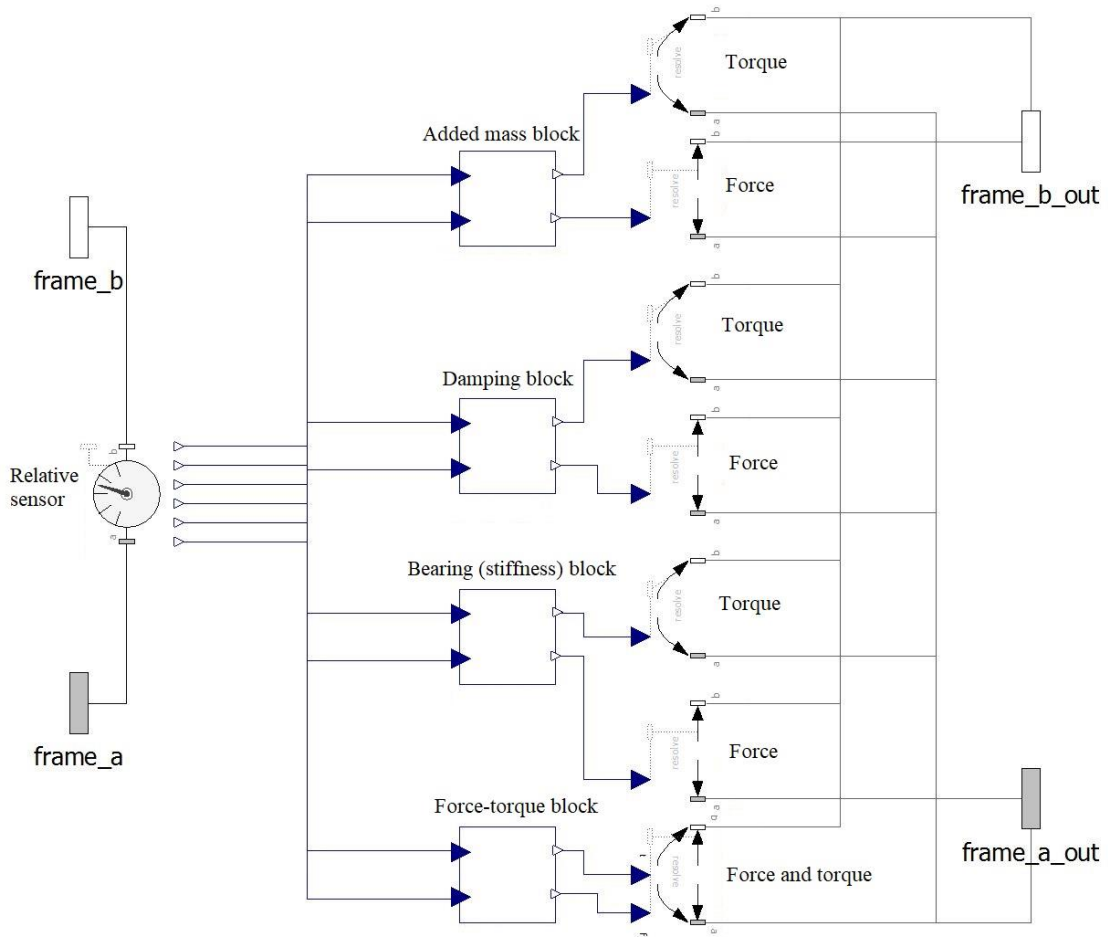


Figure 6.2: EM model.

Table 6.1: EM model inputs and outputs.

Block:	Input 1:	Input 2:	Output 1:	Output 2:
Added mass	Relative acceleration	Relative angular acceleration	Force	Torque
Damping	Relative velocity	Relative angular velocity	Force	Torque
Bearing	Relative position	Relative angles	Force	Torque
Force-torque	Relative velocity	Relative angular velocity	Force	Torque

The relative sensor, force, torque, and the “force and torque” blocks must have a reference connection and a connection to the relevant body. This is done by connecting the blocks “frame\_a” and “frame\_a\_out” to a fixed point, and the blocks “frame\_b” and “frame\_b\_out” are connected to the relevant body, as shown in Figures 6.3 and 6.4. The coding for the various blocks in the EM model is shown in Appendix C. Meanwhile, the inputs for the added mass and damping blocks are calculated for the relevant rotational speed and propeller in the Appendix “regression equations” (Appendix H), while the inputs for the force-torque block are calculated in the Appendix “thrust and torque” (Appendix H). The latter represents the dynamic force and moment contribution from the propeller. The inputs for the added mass, damping, and force-torque block must be re-calculated when the propeller and/or the rotational speed are changed.

Figures 6.3 and 6.4 are the two primary models used for simulations in this study. The figures show the appearance of the models when they are opened in OM. The first model (Figure 6.3) only includes 4 DOF and a marine propeller, while the second model (Figure 6.4) uses 6 DOF and contains a marine propeller, a drive shaft, and two bearings.

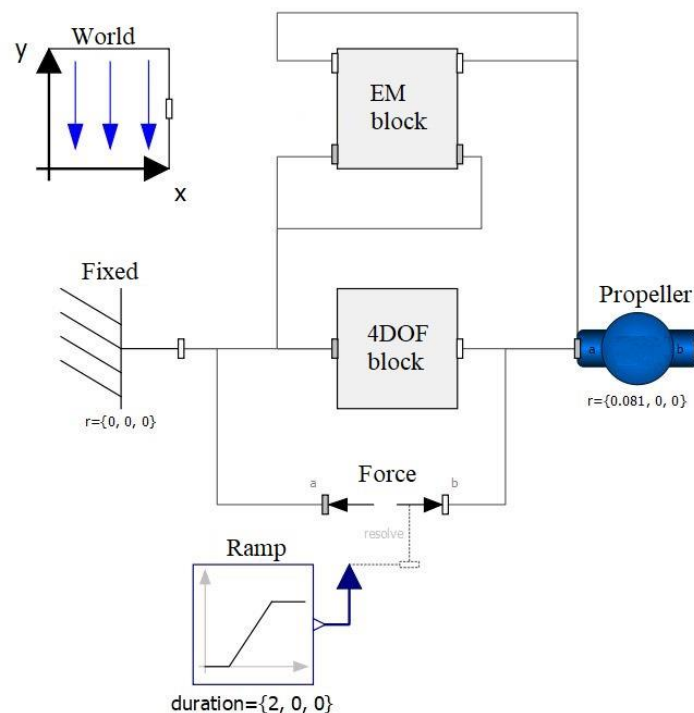


Figure 6.3: 4 DOF model.

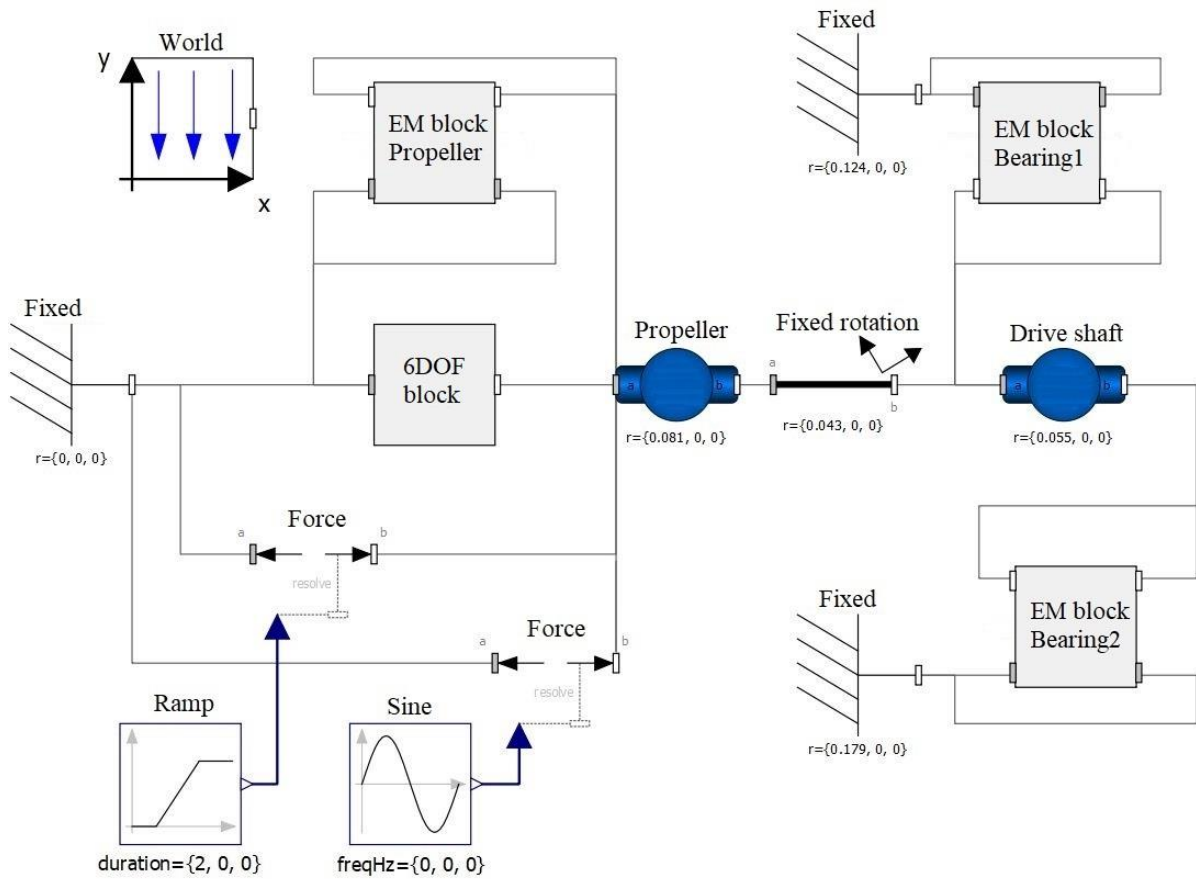


Figure 6.4: 6 DOF model.

The world block in Figures 6.3 and 6.4 defines the coordinate system and the gravity field. Since the force-torque block from the EM model only considers the dynamic forces, the mean thrust is represented in the model by the ramp and a force block. The mean thrust in Newtons is the input to the ramp block, while the duration vector below the ramp block defines the length in seconds until the input (mean thrust) is reached. The fixed blocks are fixed points in the model, and the vector below these blocks defines the locations of these points in the coordinate system (x, y, z). Meanwhile, for the vectors below the propeller, drive shaft, and fixed rotation blocks define the length in meters between points “a” and “b” on these blocks. The fixed rotation block is only applicable for the 6 DOF model and serves as a fixed translation and rotation block; hence it is used to define the length between the propeller and the first bearing. Note that the length of the drive shaft is not the actual length, but the distance between the first

and second bearings. However, the actual weight, inertia, and center of gravity (COG) are used as inputs in the drive shaft block.

The remaining force and sine blocks in Figure 6.4 are only active if an unbalanced propeller is being investigated. The centrifugal force resulting from this unbalanced must then be calculated in Newtons and is then the amplitude of the sine function. Moreover, the frequency is the angular velocity and is applied in the “y” and “-z” directions.

### **6.3. Testing of OM model**

Testing starts with the 4 DOF model and is carried out by constraining the body to only allow for translational and rotational motion in 2 DOF. Each component is then tested separately to verify that they are correctly implemented. For example, the added mass parameters  $m_{44}$  and  $m_{41}$  can be tested simultaneously in one simulation. The components are then further verified by evaluating the results from the simulation. This is performed for all parameters to verify that all outputs from the model are correct. When the 4 DOF model has been fully checked and the results are verified, a few cases are run using the full 6 DOF model to check that the results are reasonable. The models are further validated in Section 7.2 when the frequency response is analyzed. In this section the excitation and natural frequencies are controlled and verified.

# Chapter 7

## Numerical analysis and results

### 7.1. Introduction

The two bearings in the pedestal, i.e., the two bearings closest to the propeller, are the bearings that experience the highest loads. This is because these two bearings support the drive shaft both axially and radially. The following study is therefore carried out on the propeller, the drive shaft, and the two bearings associated with the drive shaft. This setup is also applicable for hydraulic thrusters because they typically require a similar setup for the propeller and drive shaft. A significant difference between the electric thruster in Figure 2.2 and a typical hydraulic thruster is that the electric motor is replaced by a hydraulic motor (Forum Energy Technologies, 2018). One challenge regarding the thruster is the lifetime of the bearings. Figure 7.1 shows an oil sample from the thruster pedestal after just a few hundred operating hours. As seen in the figure, the oil is severely contaminated. This contamination can only result from the two bearings associated with the drive shaft, because the pedestal is a closed area containing only these two bearings and the drive shaft.



Figure 7.1: Fresh new oil (left) vs. contaminated oil (right) from the thruster pedestal.

The bearings associated with the drive shaft are of the tapered roller type (bearing type: 33206 and 32009X). The bearings are mounted in opposite directions, meaning that they can accommodate radial loads and axial loads in both directions. However, only one bearing can accommodate axial loads in each direction. With this in mind, when the thruster is operating in pushing mode the axial load is carried by the bearing closest to the propeller (bearing 1), and in pulling mode the load is carried by the next bearing (bearing 2). The following case studies focus on the propeller in pushing mode, hence the bearing located closest to the propeller. A reminder of study objectives two and three which apply to this chapter is listed below.

- The second objective of this study is to investigate the bearing responses and suggest solutions to reduce vibrations in the system, in order to extend the lifetime of the bearings. This includes studying the bearing and shaft design.
- The third objective includes studying the possibility to implement different propellers to the current design and possible changes that must be made if another propeller is to be used.

Furthermore, the results from the bearing response and bearing life will be rated according to the following criteria:

1. Torsional vibration amplitudes.
2. Axial vibration amplitudes.
3. Horizontal vibration amplitudes.
4. Vertical vibration amplitudes.
5. Bearing lifetime.
6. Impact on design.
7. Benefit vs. performance.

The vibration amplitude criteria will then be compared to a base case and, likewise, bearing life criteria will be compared to the bearing life of the base case. Criteria 6 and 7 demand a subjective assessment of the relevant measure. The bearing lifetime criteria can be linked to the design lifetime of the ROV, which is typically 20 years. However, the sum of operation hours after 20 years is difficult to estimate and differs for each ROV.

## 7.2. Frequency spectrum

Before studying the bearing response, the OM model is controlled against inputs to the system and natural frequencies. This is done by studying the frequency spectrum of the 4 DOF and 6 DOF models. The frequency spectrum should show peaks at the excitation frequency and the natural frequency of the system.

The sampling frequency for the frequency spectrum analysis is set to  $\Delta t = 0.0001s$  and the sampling length is 10s. The Nyquist theorem for sampling rate states that the sample rate should be at least twice the highest frequency component of interest (Scheffer & Girdhar, 2004). The chosen sampling frequency is higher than this statement to ensure that all responses are included in the results, and that the accuracy of results is sufficiently high. The results are displayed in log-log plots with amplitudes shown in  $\mu m$  on the y-axis and frequency in  $Hz$  on the x-axis.

The frequency spectrum of the 4 DOF model is produced for a B4-71 propeller with a pitch ratio of 1.0. The frequency spectrum is plotted for a propeller with speed equal to the maximum output from the motor (Table 2.1) and then for 80, 60, and 40 percent of this speed, as shown in Table 7.1. The OM model of the 4 DOF model is shown in Figure 6.3. Calculations of the various inputs for the matrices in the EM block are shown in the “regression equations” and “thrust and torque” Appendices. Note that the inputs to OM matrices vary with rotational speed.

Table 7.1: Marine propeller B4-71 for different speeds.

No. and color	Frequency ( $f_e$ ) (Hz)	Speed (RPM)	Mean thrust T (N)	Mean torque Q (Nm)	Stiffness $k_{11}, k_{22}, k_{33}$ (N/m)	Stiffness $k_{44}$ (Nm/rad)
1. Gray	110.3	1655	1708	82	$1.0 \times 10^8$	$2.4 \times 10^4$
2. Magenta	88.3	1324	1095	52	$1.0 \times 10^8$	$2.4 \times 10^4$
3. Cyan	66.2	993	618	30	$1.0 \times 10^8$	$2.4 \times 10^4$
4. Black	44.1	662	271	13	$1.0 \times 10^8$	$2.4 \times 10^4$

The primary differences between the 4 DOF and 6 DOF models, except for the degrees of freedom, are that the 6 DOF model includes a shaft and two bearings in addition to the propeller. Moreover, for the 4 DOF model only one EM block is used, as both the propeller contributions and the stiffness are represented by this one block. In contrast, for the 6 DOF model three EM blocks are used; one EM block represents the propeller, with the stiffness matrix set to zero, while the other two EM blocks represent the bearings, and only the stiffness matrices are active at these blocks. The OM model of the 6 DOF model is shown in Figure 6.4. The distances between the components are based on the thruster from Figures 2.2 and 2.4. The frequency spectrum of the 6 DOF model is compared to the 4 DOF model with the inputs from Table 7.2.

Table 7.2: Marine propeller B4-71, shaft and bearings for 4 DOF vs. 6 DOF.

Color	Speed (RPM)	Mean thrust T (N)	Mean torque Q (Nm)	Stiffness $k_{11}, k_{22}, k_{33}$ (N/m)	Stiffness $k_{44}$ (Nm/rad)	Stiffness $k_{55}, k_{66}$ (Nm/rad)
1. Black	1655	1708	82	$1.0 \times 10^8$	$2.4 \times 10^4$	
2. Cyan	1655	1708	82	$1.0 \times 10^8$	$2.4 \times 10^4$	$4.0 \times 10^4$

The stiffness values  $k_{11}, k_{22}, k_{33}, k_{55}$  and  $k_{66}$  represent the stiffness of the bearings. However, these values are only approximate values based on bearing stiffness values from Tong and Hong (2014) and Knaapen (1997). This is done since the bearing stiffness can be altered by varying the axial and radial preload on the bearings, and because this preload is not known. Furthermore, the stiffness value  $k_{44}$  is based on the torsional stiffness of the drive shaft, which is obtained from the following formula:

$$k_{44} = \frac{G J}{l} \quad (7.1)$$

where  $G$  is the shear modulus,  $J = \pi \frac{d^4}{32}$  is the polar moment of inertia, and  $l$  is the length of the shaft. The length of the drive shaft  $l = 228mm$  and the diameter  $d = 30mm$ , where the latter



is the diameter on the shaft where the propeller is located; this diameter is chosen to represent the diameter of the whole shaft. Note that the axial stiffness is only applied at one block, since only one bearing is active in each direction. Furthermore, the torsional stiffness is applied in one block, because this is applicable for the whole shaft. The inputs to bearing one and bearing two for the 6 DOF model are shown in Appendix C, while the frequency spectra of the cases according to Tables 7.1 and 7.2 are shown in the Figures 7.3-7.10. The frequency spectra are obtained from the vibration displacements, i.e.,  $\phi_x$ ,  $\delta_x$ ,  $\delta_y$  and  $\delta_z$ .

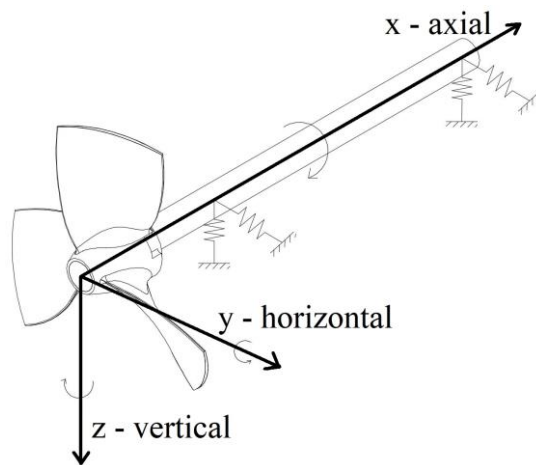


Figure 7.2: Thruster coordinate system.

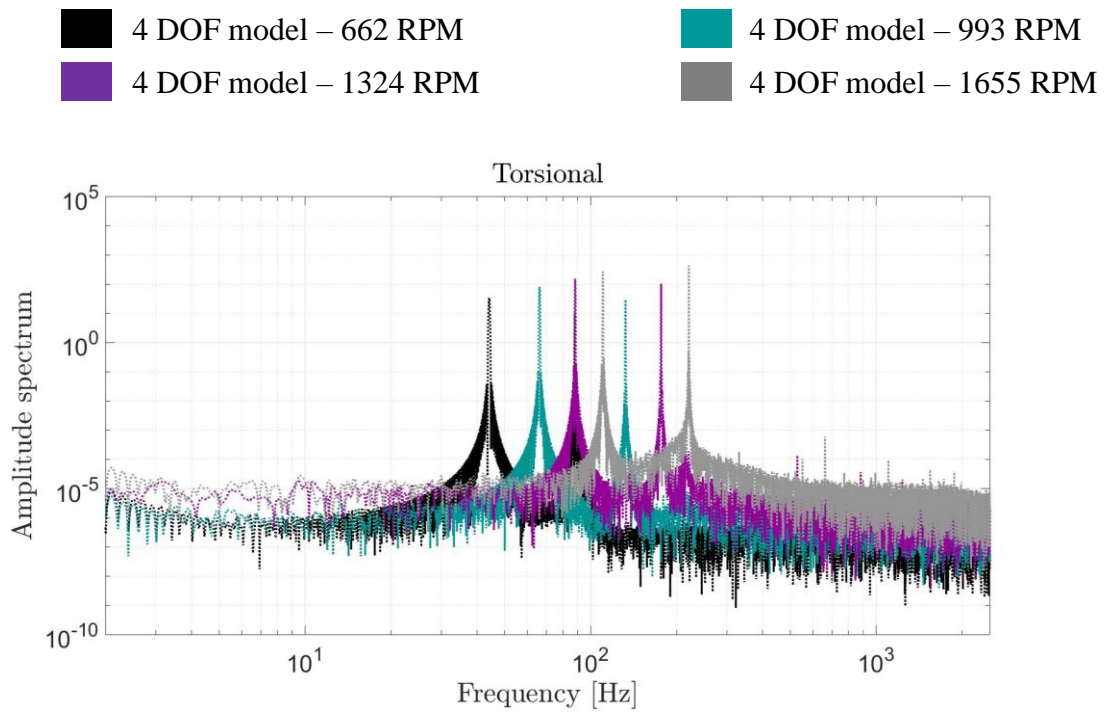


Figure 7.3: Frequency response for the 4DOF thruster model in torsional direction at different speeds.

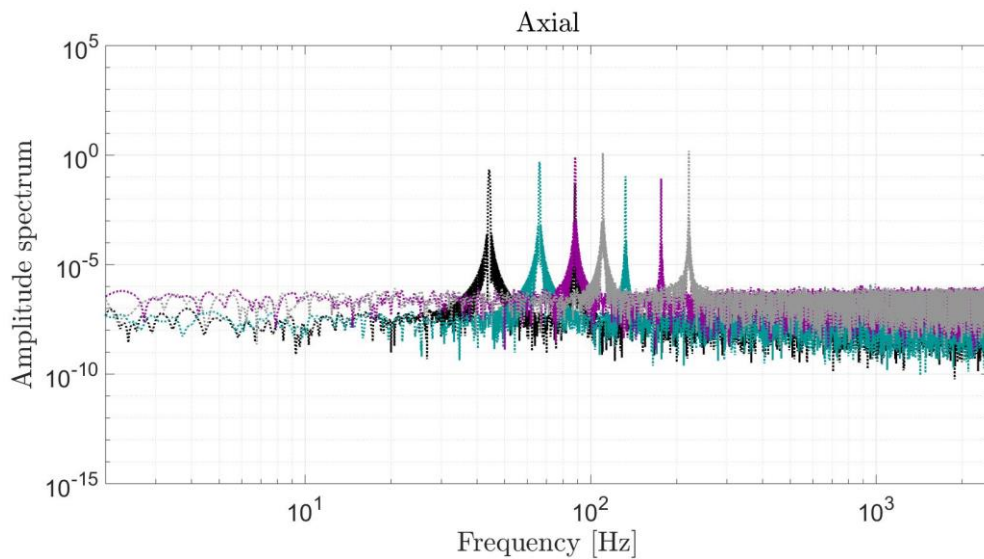


Figure 7.4: Frequency response for the 4DOF thruster model in axial direction at different speeds.

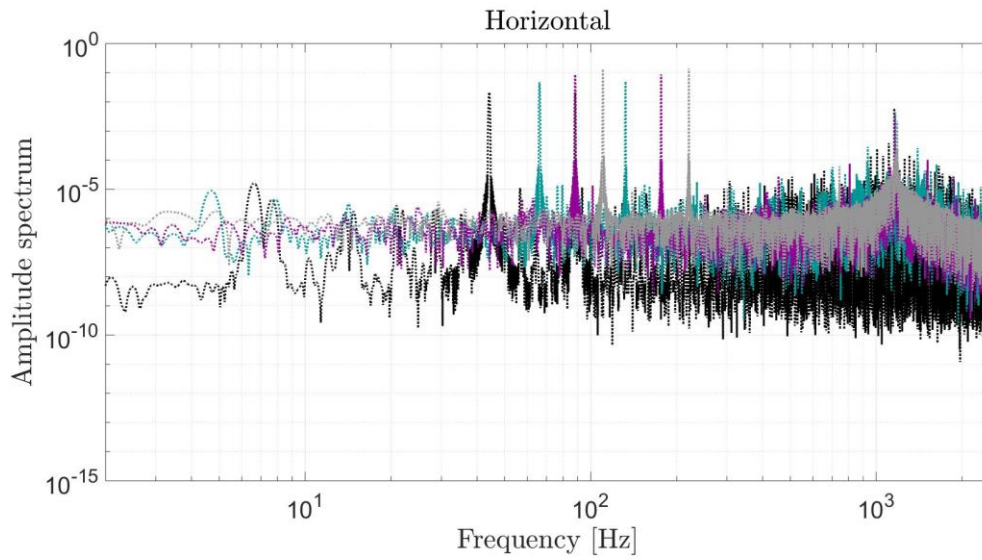


Figure 7.5: Frequency response for the 4DOF thruster model in horizontal direction at different speeds.

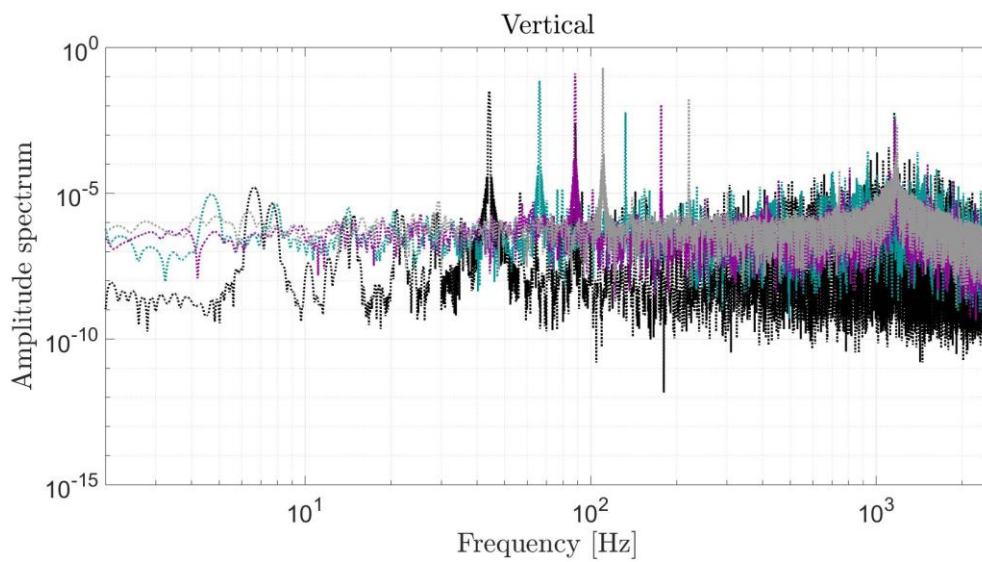


Figure 7.6: Frequency response for the 4DOF thruster model in vertical direction at different speeds.

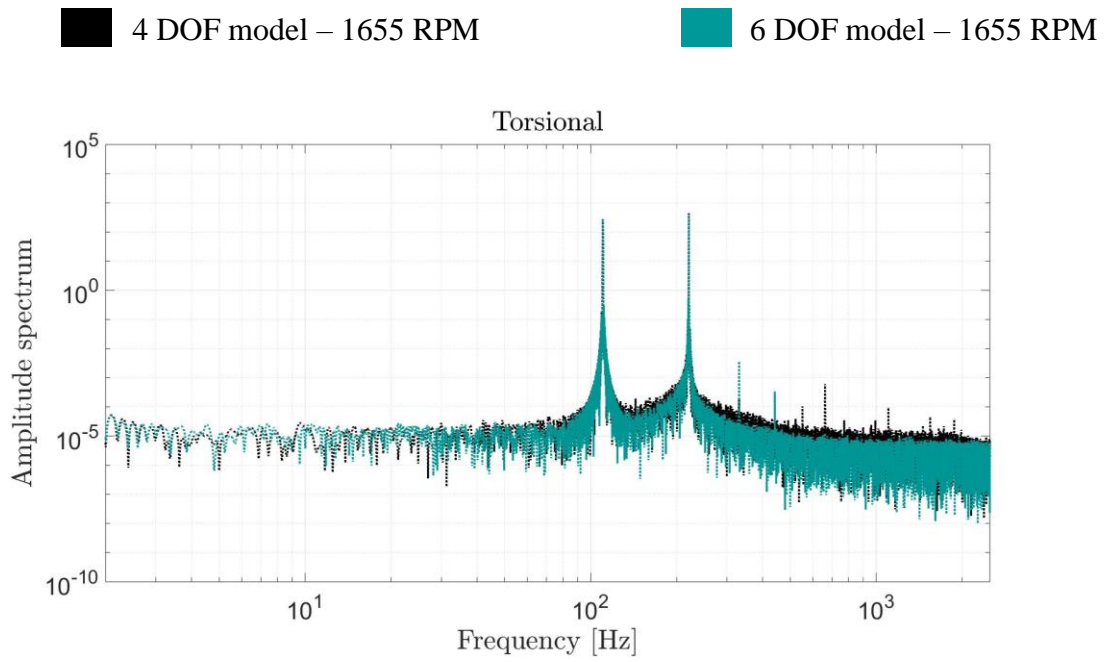


Figure 7.7: Frequency response for the 4DOF vs. 6DOF thruster models in torsional direction.

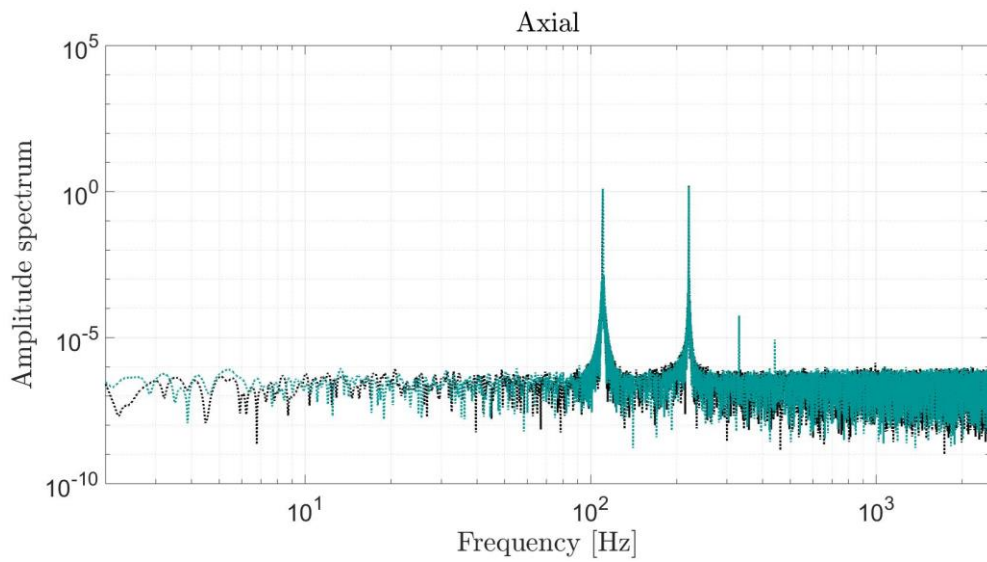


Figure 7.8: Frequency response for the 4DOF vs. 6DOF thruster models in axial direction.

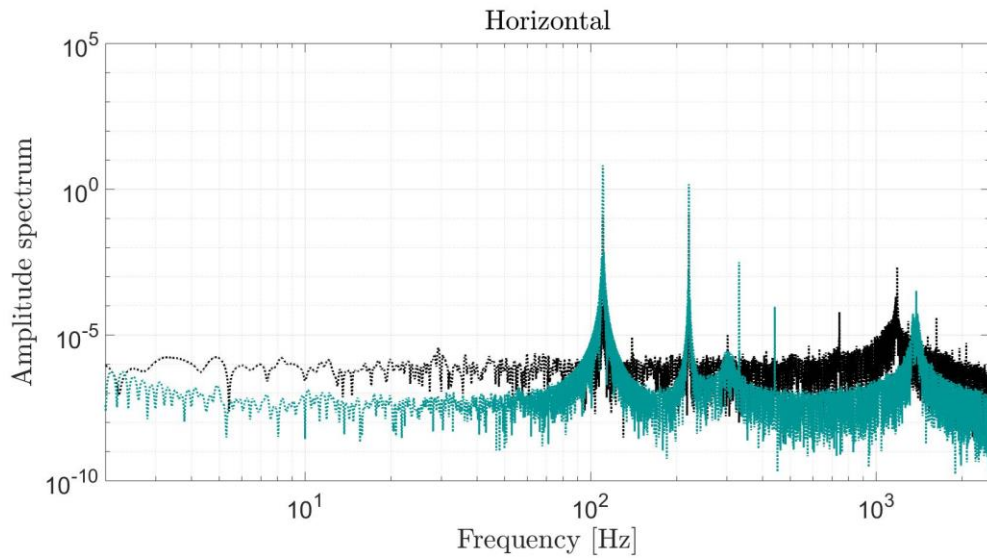


Figure 7.9: Frequency response for the 4DOF vs. 6DOF thruster models in horizontal direction.

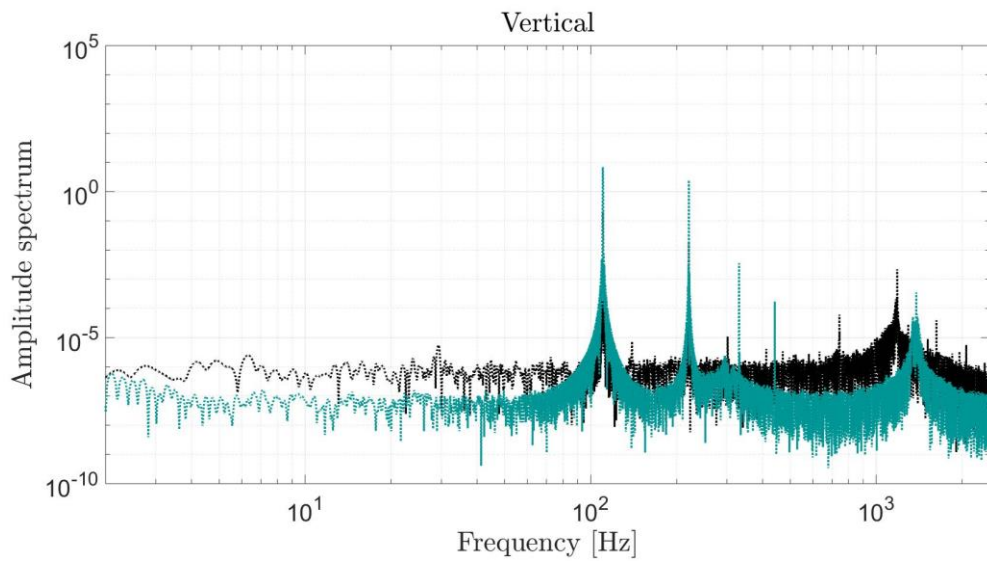


Figure 7.10: Frequency response for the 4DOF vs. 6DOF thruster models in vertical direction.

The small difference in the y- and z-directions indicates that the model vibrates in a non-circular orbit. Regarding the excitation frequency, this depends on the rotational speed and the number of blades on the propeller. As seen from the results from the Figures 7.3-7.10, significant peaks occur at the first and second blade rate frequency, which correspond to the input frequency; hence the input frequency corresponds to the OM model. At 1655 RPM the first and second blade frequencies are 110.3 Hz and 220.6 Hz.

The Figures 7.3 and 7.7 are the torsional vibrations about the rotating axis (x-axis), while the Figures 7.4-7.6 and 7.8-7.10 are the translational vibrations, i.e., the vibrations in the axial, horizontal, and vertical directions. As seen in the Figures 7.7-7.10 are the peaks (highest values) higher for the 6 DOF model in comparison to the 4 DOF model; this is due to the free vibration of the propeller and the distances between the propeller and the supports. However, the amplitude spectrum in the horizontal and vertical directions is generally lower for the 6 DOF model. This is because the 6 DOF model has two bearings providing support in the radial direction, while only one bearing supports the 4 DOF model. Consequently, the 6 DOF model receives twice the support of the 4 DOF model in the radial direction. However, the axial stiffness is the same since only one bearing is active in each direction for the 6 DOF model. The torsional stiffness is also the same for both models.

Furthermore, some of the natural frequencies of the system can be calculated and checked against the frequency response. First, the natural frequency of the 4 DOF model at 1655 RPM is calculated in the axial direction:

$$f_{n,11} = \frac{1}{2\pi} \sqrt{\frac{k}{m+m_A}} = \frac{1}{2\pi} \sqrt{\frac{1 \times 10^8}{2.7987+1.45}} = 772.1 \text{ Hz.}$$

From the frequency response in the axial direction, it is not possible to determine any significant peaks except for the excitation frequencies, possibly due to high damping or stiffness values. Furthermore, the natural frequencies in the horizontal and vertical directions are approximately the same and can be calculated as follows:

$$f_{n,22} \approx f_{n,33} = \frac{1}{2\pi} \sqrt{\frac{1 \times 10^8}{0.5545+1.45}} = 1124.1 \text{ Hz.}$$

This value corresponds with the frequency response in the horizontal and vertical directions, as a clear peak just above  $10^3$  Hz. Overall,

the responses from the system versus the inputs are considered to be reasonable, and further analysis can continue.

### 7.3. Bearing response for B4-71 propeller

Further investigations continue on the B4-71-100 propeller, but with a focus on the 6 DOF system and a rotational speed of 1655 RPM. Concerning the first objective, the bearing responses at the first bearing closest to the propeller are investigated for various cases to study how this influences the vibration amplitudes on the bearing, and hence the life of the bearing. The 6 DOF system from Table 7.2 is used as the base case, and other investigations are compared to this case. The amplitudes shown in the following figures are the half of the highest peak-to-peak values, while the amplitudes for the base case are shown in Figure 7.11, where various values at the propeller and the two bearings are shown.

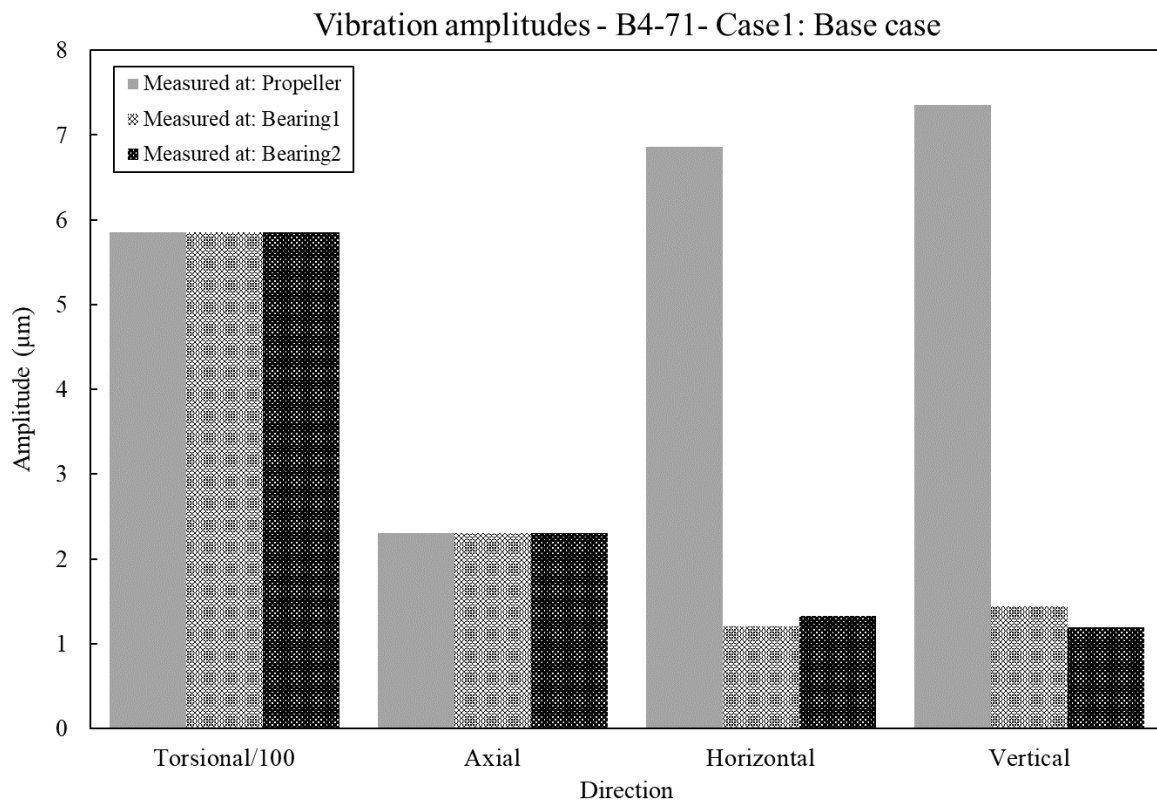


Figure 7.11: Vibration amplitudes for the base case.

The torsional and axial vibrations are the same at each point, as seen in Figure 7.11, since there is only one shaft in place and the propeller is rigidly connected to the shaft. The vibration amplitudes are naturally lower at bearings one and two than at the propeller because the bearings are supported, while the propeller is not. Furthermore, bearing life calculations require the RMS values of displacements in the axial, horizontal, and vertical directions. Since the propeller is operating in pushing mode the axial force acts upon bearing one. The bearing life is therefore calculated for this bearing (bearing one), since it experiences the highest load and has the shortest lifetime. As a result, only the RMS values at bearing one are needed; these values are shown in Table 7.3.

Table 7.3: Displacement RMS values for Case 1.

Direction:	Axial	Horizontal	Vertical
RMS $\delta_i$ ( $\mu m$ ):	17.14	0.88	1.04

Bearing one is a tapered roller bearing (33206) with the following properties:

$$C = 79.7 \text{ kN}, e = 0.35 \text{ and } Y = 1.7.$$

$$\text{When } \frac{F_a}{F_r} > e, \text{ then } P = 0.4F_r + YF_a.$$

The bearing life is then calculated as follows:

$$RMS \delta_r = \sqrt{0.88^2 + 1.04^2} = 1.3624 \mu m.$$

$$0.4F_r = 1.3624 \times 10^{-6} m \times 10^8 N/m = 136.24 N.$$

$$1.7F_a = 17.14 \times 10^{-6} m \times 10^8 N/m = 1714.00 N.$$

$$L_{10h} = \frac{10^6}{60 \times 1655 RPM} \times \left( \frac{79700 N}{0.4 \times 136.24 + 1.7 \times 1714.00} \right)^{10/3} = 58.37 \times 10^4 h.$$



The bearing life for same setup at 993 RPM is as follows:

$$L_{10h} = \frac{10^6}{60 \times 993 \text{ RPM}} \times \left( \frac{79700N}{0.4 \times 46.39 + 1.7 \times 619.10} \right)^{10/3} = 29.09 \times 10^6 \text{ h.}$$

The bearing life is calculated at 993 RPM to determine the effect of the rotational rate on the bearing life. Typical ROV thrusters are mostly run at half of their maximum output (or lower). At this point, the bearing life seems to be satisfactory. However, these calculations apply to a perfectly balanced system, which is unlikely. Despite the fact that a perfectly balanced system is uncommon, further studies follow on this system to investigate the effects of different stiffness values.

As discussed earlier, the properties of the bearing stiffness can be altered by changing the axial and radial preloads. Further information about bearing preloads can be found in Tong and Hong (2014) and Knaapen (1997). The consequences of an altered preload on the bearings will therefore be investigated. A change in the preload could be an assembly blunder, or it could occur following some time in operation. However, the preload on the bearings can also work as a tool to adjust the stiffness of the system to the desired value. A higher and lower stiffness of the bearings will therefore be investigated in Cases 2 and 3, to establish how this affects the system with respect to vibration amplitudes and bearing life.

The torsional stiffness can also be varied by changing the diameter of the drive shaft. An increase in diameter from 30mm to 40mm is assumed to be realistic and doable. This will be studied further in Case 4 to investigate if this is beneficial for the system. Note that only the torsional stiffness is changed in this case, and the mass of the shaft is kept constant. The various inputs for Cases 1 to 4 are shown in Table 7.4; for these case studies it is only necessary to consider the resulting amplitudes at bearing one, which are presented in Figure 7.12.

Table 7.4: Inputs for Cases 1-4.

Case	Speed (RPM)	Mean thrust T (N)	Mean torque Q (Nm)	Stiffness $k_{11}, k_{22}, k_{33}$ (N/m)	Stiffness $k_{44}$ (Nm/rad)	Stiffness $k_{55}, k_{66}$ (Nm/rad)
1. Base case	1655	1708	82	$1.0 \times 10^8$	$2.4 \times 10^4$	$4.0 \times 10^4$
2. Higher stiffness	1655	1708	82	$2.5 \times 10^8$	$2.4 \times 10^4$	$1.0 \times 10^5$
3. Lower stiffness	1655	1708	82	$5.0 \times 10^7$	$2.4 \times 10^4$	$2.0 \times 10^4$
4. Larger shaft	1655	1708	82	$1.0 \times 10^8$	$7.7 \times 10^4$	$4.0 \times 10^4$

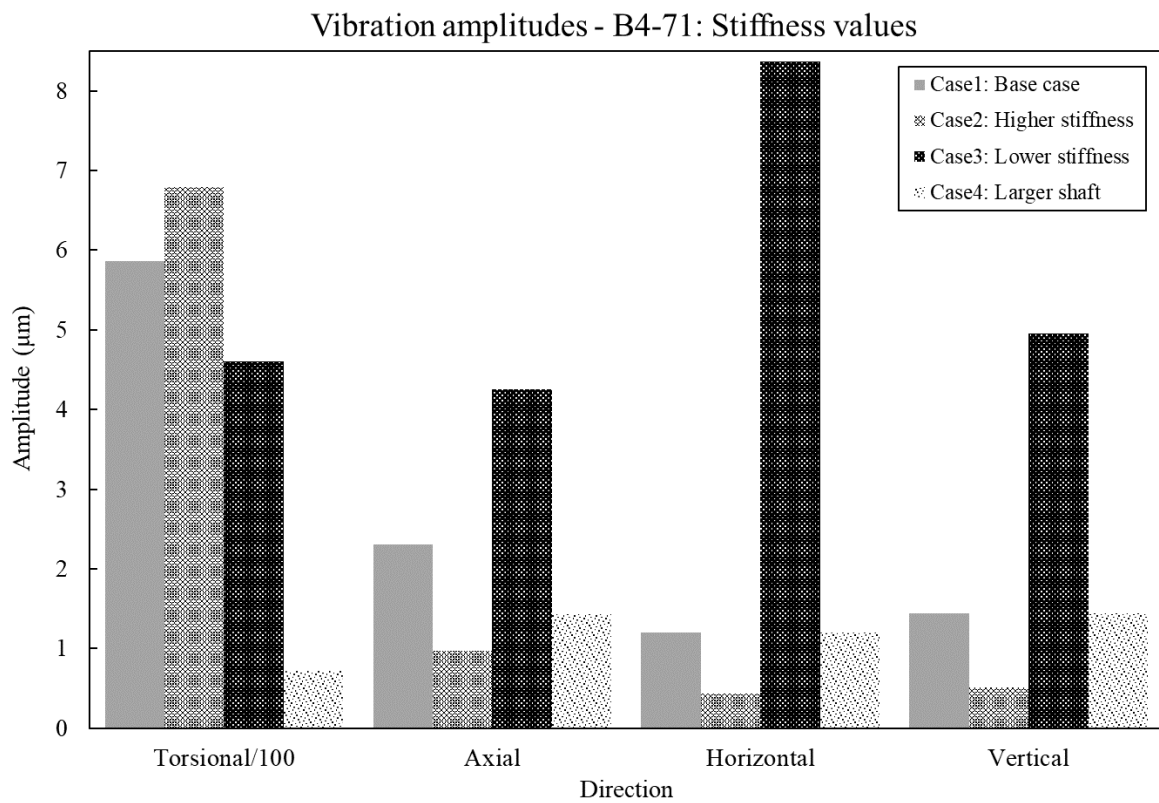


Figure 7.12: Vibration amplitudes for Cases 1-4.

Table 7.5: Displacement RMS values and bearing life for Cases 1-4.

Case	RMS-axial $\mu m$	RMS-horizontal $\mu m$	RMS-vertical $\mu m$	$L_{10h}(h)$
1. Base case	17.14	0.88	1.04	$58.37 \times 10^4$
2. Higher stiffness	6.86	0.32	0.37	$58.63 \times 10^4$
3. Lower stiffness	34.26	4.93	2.91	$54.71 \times 10^4$
4. Larger shaft	17.11	0.88	1.04	$58.71 \times 10^4$

Since the thrust is high and is the same for Cases 1 to 4, it can be seen in Table 7.5 that the bearing life does not significantly fluctuate. This is because the bearing life is mainly driven by the axial load, i.e., the propeller thrust.

The following case studies investigate the effects of changing the distance between the two bearings, and of an unbalanced rotor. The speed, mean thrust, and mean torque will be as in the base case, in addition to the stiffness values. For the base case, the distance between the two bearings on the drive shaft is  $55mm$ . This distance plus half of this distance is the distance between the bearings in Case 5. For Case 6 the distance is only half of the distance from the base case. Accordingly, for Case 5 the distance between the bearings is  $82.5mm$  and for Case 6 it is  $27.5mm$ .

For the unbalanced rotor, it is assumed that the center of mass for the propeller is located at a radial distance  $r_c$  from the center of the propeller. This distance is chosen as 5% of the diameter of the propeller, i.e., for a propeller with a diameter equal to  $300mm$ ,  $r_c = 15mm$ . The centrifugal force from the change in the center of mass is then;  $F_c = mr_c\omega^2$  where  $m$  is the mass of the propeller and  $\omega$  is the angular velocity, i.e.,  $\omega = 1655RPM \times \frac{2\pi}{60} = 173.32 \frac{rad}{s}$ .

Table 7.6: Inputs for Cases 1 and 5-7.

Case	Bearing distance (mm)	Centrifugal force, $F_c$ (N)
1. Base case	55	-
5. Longer bearing distance	82.5	-
6. Shorter bearing distance	27.5	-
7. Unbalanced rotor	55	653.3

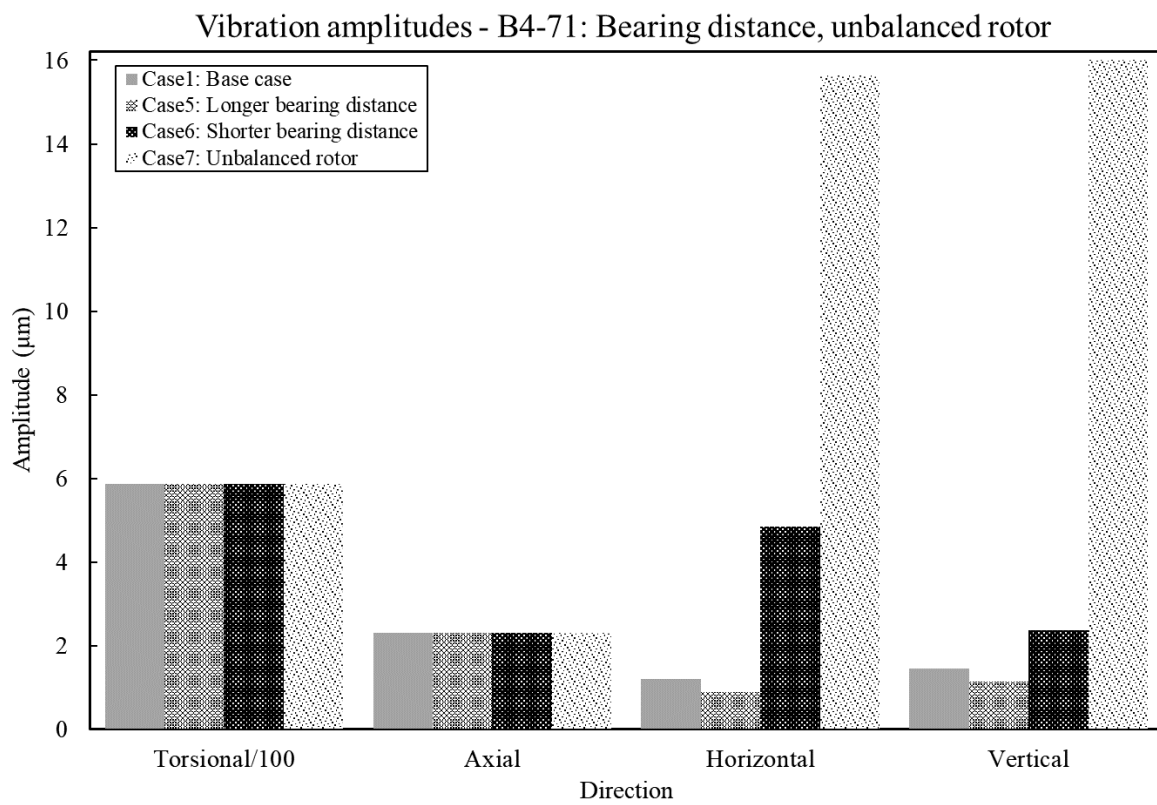


Figure 7.13: Vibration amplitudes for Cases 1 and 5-7.

Table 7.7: Displacement RMS values and bearing life for Cases 1 and 5-7.

Case	RMS-axial $\mu m$	RMS-horizontal $\mu m$	RMS-vertical $\mu m$	$L_{10h}(h)$
1. Base case	17.14	0.88	1.04	$58.37 \times 10^4$
5. Longer bearing distance	17.14	0.66	0.82	$59.19 \times 10^4$
6. Shorter bearing distance	17.14	2.88	1.41	$53.79 \times 10^4$
7. Unbalanced rotor	17.14	10.75	10.77	$32.99 \times 10^4$

As seen from the bearing life results in Table 7.7, the bearing life does not considerably differ with the distance between bearings. However, an unbalanced propeller can significantly impact the bearing life. For the unbalanced propeller case the velocity and acceleration in the vertical and horizontal directions increases. Subsequently, this affects the added mass, damping, and the dynamic force and torque contributions. A summary of cases studies 1 to 7 follows in Table 7.9. The various cases are rated according to the criteria established in Table 7.8.

Table 7.8: Rating table.

Criteria	Rating				
	Bad (-2)	Worse (-1)	~Equal base case (-)	Better (+1)	Good (+2)
1. Torsional vibration	$> +300.0\mu m$	$< +300.0\mu m$	$\pm 50.0\mu m$	$< -300.0\mu m$	$> -300.0\mu m$
2. Axial vibration	$> +3.0\mu m$	$< +3.0\mu m$	$\pm 0.5\mu m$	$< -3.0\mu m$	$> -3.0\mu m$
3. Horizontal vibration	$> +3.0\mu m$	$< +3.0\mu m$	$\pm 0.5\mu m$	$< -3.0\mu m$	$> -3.0\mu m$
4. Vertical vibration	$> +3.0\mu m$	$< +3.0\mu m$	$\pm 0.5\mu m$	$< -3.0\mu m$	$> -3.0\mu m$
5. Bearing life	$> -50 \times 10^3 h$	$< -50 \times 10^3 h$	$\pm 5000 h$	$< +50 \times 10^3 h$	$> +50 \times 10^3 h$
6. Impact on design	Large impact	Small impact	No impact	-	-
7. Benefit vs. performance	Bad	Worse	-	Better	Good

Table 7.9: Summary of results for Cases 1-7.

Case study	Criteria						Score
	1	2	3	4	5	6	
1. Base case	-	-	-	-	-	-	-
2. Higher stiffness	-1	+1	+1	+1	-	-	+2
3. Lower stiffness	+1	-1	-2	-2	-1	-	-5
4. Larger shaft	+2	+1	-	-	-	-1	+2
5. Longer bearing distance	-	-	-	-	+1	-1	0
6. Shorter bearing distance	-	-	-2	-1	-1	-1	-5
7. Unbalanced rotor	-	-	-2	-2	-2	-	-6

As seen from the summary of cases presented in Table 7.9, with a higher bearing stiffness or a larger drive shaft the system exhibits beneficial properties with respect to vibrations. However, it is not certain that a higher bearing stiffness can be obtained by changing the preload on the bearing. The bearing does have limitations on how much preload that can be applied, and the bearing might have to be replaced to obtain the desired stiffness values, as in Case 2. Different bearings will affect the design, as will a larger shaft diameter. Furthermore, if the achievement of a specific bearing stiffness depends on a preload and this preload is somehow lost, the consequences can be fatal; thus special care must be taken to prevent this from happening.

The bearing life for the considered cases varies less than expected. This is mainly due to the high thrust load from the propeller, which is the same in all cases. The thrust is an axial force, which is significantly greater than the radial forces, and the bearing life is highly dependent on the axial force acting on the bearing. However, for the unbalanced propeller the radial forces become considerably high. This is the least desirable case of those tested thus far. It is therefore strongly recommended to avoid or restrict unbalance in the thruster system as far as possible to prevent problems with the thruster.

## 7.4. Bearing response for different propellers

In this section the second objective is considered; whether it is possible to implement different propellers in the configuration, either larger in size or with more blades, as in the base case. If this is not possible, then necessary measures are implemented to achieve similar results as in the base case. The reason for choosing a larger propeller is usually to obtain a higher thrust or a different torque and RPM configuration. However, propellers with a different number of blades exhibit different vibratory properties when operating in the wake field. Accordingly, the number of blades on the propeller can be varied to alter the vibration properties of the thruster system. To have some consistency between the various cases, all of the thrust and torque values are taken at the advance ratio of  $J = 0.5$ , pitch ratio of  $\frac{P}{D} = 1.0$ , and speed of 1655 RPM.

The first two cases studied in this section are propellers with diameter of 300mm as in the base case (Case 1). Case A is a B5-88 propeller and Case B is a B6-106 propeller; these propellers are selected to investigate the impact on vibration displacements and bearing life of a different number of blades on the propeller. For Cases C, D, and E the diameters of the studied propellers are increased to  $D = 400\text{mm}$ ; here the investigated propellers are of the types B4-71, B5-88, and B6-106 respectively. The various cases studied in this section are presented in Table 7.10.

Table 7.10: Cases A-E.

Case and propeller type	Diameter (mm)	Speed (RPM)	Mean thrust T (N)	Mean torque Q (Nm)
A. B5-88	300	1655	1833	89
B. B6-106	300	1655	1895	93
C. B4-71	400	1655	5397	344
D. B5-88	400	1655	5794	374
E. B6-106	400	1655	5988	392

As shown in Table 7.10, the mean thrust and mean torque increase with an increased number of blades for the same speed of advance ( $J = 0.5$ ) and the same diameter. For diameter  $D = 400\text{mm}$  the mean thrust and mean torque values increase significantly compared to the smaller propeller. These values are most likely too high for the current bearing arrangement. However, Cases C, D, and E will be tested in the current system to evaluate their performance. Countermeasures can then be selected according to the results. The various stiffness values in the Cases A-E are as in the base case (Case 1) in the previous section, while the vibration amplitudes for Cases A and B are compared with the base case as shown in Figure 7.14. Finally, the vibration amplitudes for Cases C to E are shown in Figure 7.15.

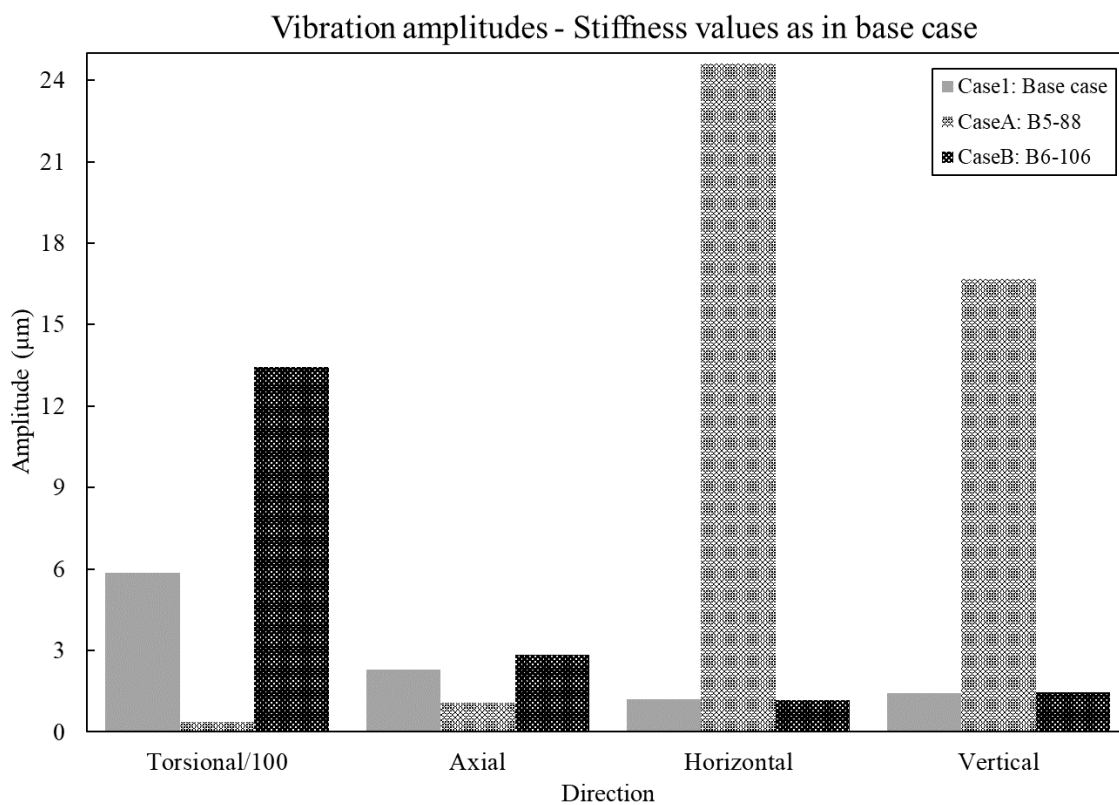


Figure 7.14: Vibration amplitudes for Cases 1, A, and B.



Table 7.11: Displacement RMS values and bearing life for Cases 1, A, and B.

Case	RMS-axial $\mu m$	RMS-horizontal $\mu m$	RMS-vertical $\mu m$	$L_{10h}(h)$
1. Base case	17.14	0.88	1.04	$58.37 \times 10^4$
A. B5-88	18.34	16.88	11.08	$22.99 \times 10^4$
B. B6-106	19.05	0.88	1.02	$41.32 \times 10^4$

As mentioned in Section 3.7, propellers with an odd number of blades have different characteristics concerning thrust fluctuations and bending moments to propellers with an even number of blades. This is clearly shown in the results shown in Figures 7.14 and 7.15, where 5-bladed propellers exhibit amplitudes of smaller magnitude in the torsional and axial directions, and amplitudes of higher magnitude in the horizontal and vertical directions, than propellers with 4 and 6 blades. This is because of the changes in the dynamic forces, which can be directly seen from the dynamic force and moment equations for the various propellers in Appendix A. Moreover, the velocity and acceleration of the 5-bladed propeller behaves quite differently from that of the 4- and 6-bladed propellers; this affect the added mass, damping, and the dynamic forces and moments of the propeller.

As seen from the results of Cases A and B in Table 7.11, high forces in the horizontal and vertical directions for the 5-bladed propeller result in a more than halving of the bearing lifetime compared to the 4-bladed propeller. A significant decrease in bearing life also occurs for the 6-bladed propeller, but less critically than for the 5-bladed propeller. It should be noted that the thrust is higher for Cases A and B, and this force is the main contribution to the change in bearing life. However, if the 6-bladed propeller is operated with the same thrust as the 4-bladed propeller, then its bearing life would be approximately the same as in the base case (Case 1). Also note that the torsional vibration amplitudes for Case C in Figure 7.15 are multiplied by  $\frac{1}{200}$ , and not  $\frac{1}{100}$  as for Cases D and E.

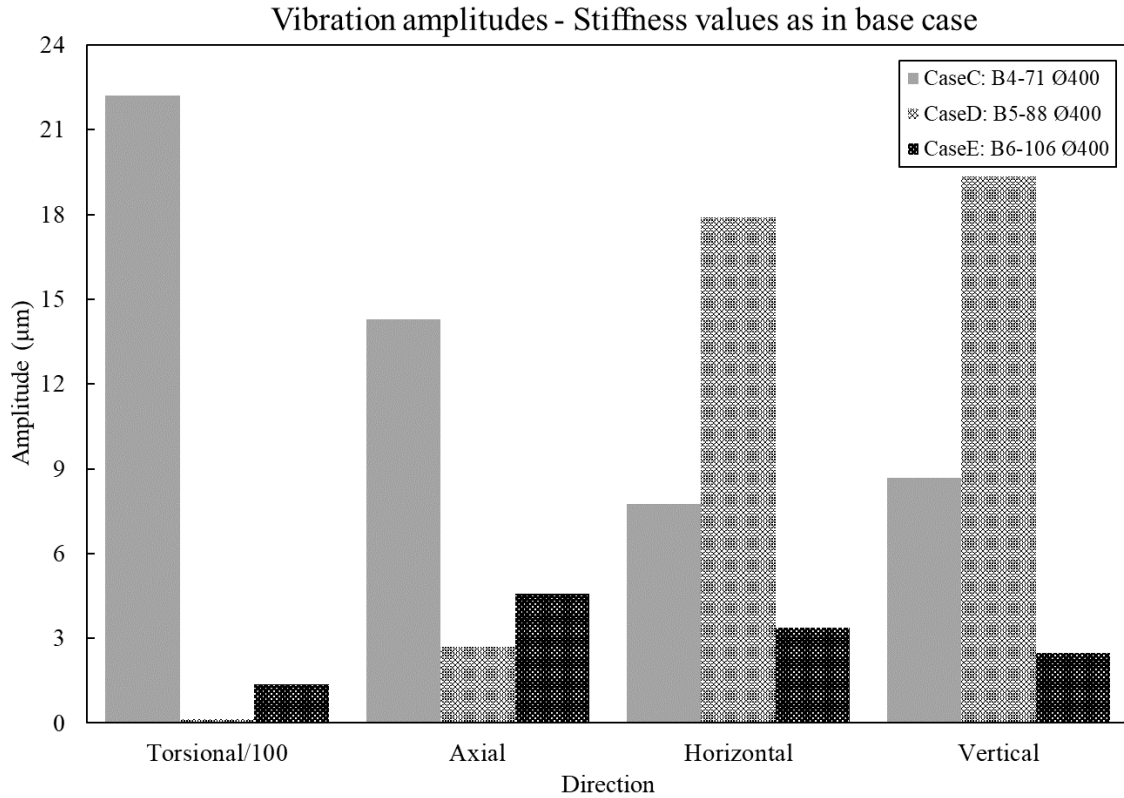


Figure 7.15: Vibration amplitudes for Cases C-E.

Table 7.12: Displacement RMS values and bearing life for Cases C-E.

Case	RMS-axial $\mu m$	RMS-horizontal $\mu m$	RMS-vertical $\mu m$	$L_{10h}(h)$
C. B4-71	54.90	5.67	5.87	$1.14 \times 10^4$
D. B5-88	57.96	12.73	13.56	$8.39 \times 10^3$
E. B6-106	59.96	2.54	1.71	$9.18 \times 10^3$

As expected, the bearing life results of Cases C to E are very low, as seen in Table 7.12. The primary reason for this low lifetime is the high thrust resulting from larger propellers, meaning that the bearing type or configuration must be changed. Since the propeller diameter is increased by  $\frac{4}{3}$ , the shaft will also be increased by  $\frac{4}{3}$ . The new mean diameter of the shaft will

then be  $\varnothing 40mm$ , and the new torsional stiffness for this shaft will be as in Case 4 (see Section 7.3). A new tapered roller bearing corresponding to this diameter is therefore used in the following simulations. New simulations of Cases C to E will be performed with the same setup as previously, except for the shaft and bearings. The stiffness values  $k_{55}$  and  $k_{66}$  will be changed to the values used in Case 2 from Section 7.3; it is assumed that these values are more appropriate because of the larger bearing. The new simulations of Cases C to E are named C.1, D.1, and E.1. The bearing chosen for these simulations has the designation 33208, and has the following new property;  $C = 128kN$ . The vibration amplitudes, displacements, and bearing life for Cases C.1-E.1 are presented in Figure 7.16 and Table 7.13.

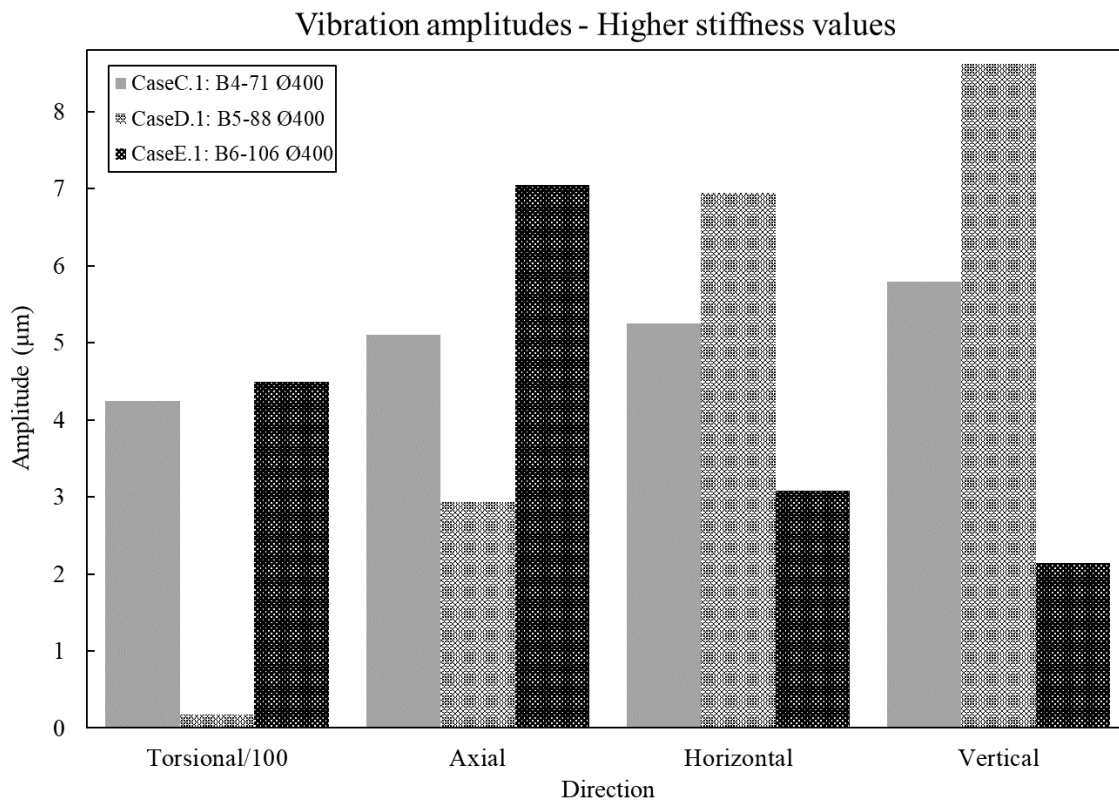


Figure 7.16: Vibration amplitudes for Cases C.1-E.1.

Table 7.13: Displacement RMS values and bearing life for Cases C.1-E.1.

Case	RMS-axial $\mu m$	RMS-horizontal $\mu m$	RMS-vertical $\mu m$	$L_{10h}(h)$
C.1. B4-71	54.08	3.48	3.77	$6.07 \times 10^4$
D.1. B5-88	57.97	5.04	6.08	$4.67 \times 10^4$
E.1. B6-106	60.08	2.25	1.50	$4.41 \times 10^4$

As seen from the new vibration amplitudes shown in Figure 7.16, the magnitude of the amplitudes has decreased. However, the bearing life is still low, which implies that the bearing cannot handle the high load it is experiencing. As a consequence, the bearing configuration must be altered; this could either involve adding thrust bearings or situating two bearings in each direction of the current bearing. The latter option is chosen so that the axial load is distributed over two bearings. The new bearing life for this configuration is shown in Table 7.14.

Table 7.14: New bearing life for Cases C.1-E.1.

Case	$L_{10h}(h)$
C.1. B4-71	$61.23 \times 10^4$
D.1. B5-88	$47.06 \times 10^4$
E.1. B6-106	$44.42 \times 10^4$

The bearing life with two active bearings in each direction yields a bearing life similar to the base case, and this setup is therefore considered acceptable. As seen from Figure 7.16 of the larger propellers, the vibration amplitudes for the 4-blade propeller are no longer the most advantageous. The 4-blade propeller also delivers the lowest thrust. For propellers with  $D = 400mm$ , the use of a propeller with 5 or 6 blades should therefore be considered. However, this decision depends on the required thrust and whether the torsional and axial vibrations or the radial vibrations are considered the most important.

## 7.5. Bearing response to unbalanced propeller

For the case studies in this section an unbalance is applied to the system, i.e., the center of mass for the propeller is set off-center in the radial direction. The radial distance to the new center of mass for the propellers is chosen to be the same as in Case 7, i.e.,  $r_c = 15mm$ . The unbalanced propeller is applied to the Cases A, B, and C.1-E.1. The various unbalanced inputs for the OM models are shown in Appendix G. The case studies in this section are named A.2-E.2. Cases 7, A.2, and B.2, where the propellers are of the same diameter, will be compared in Figure 7.17, while the Cases C.2-E.2 are presented in Figure 7.18.

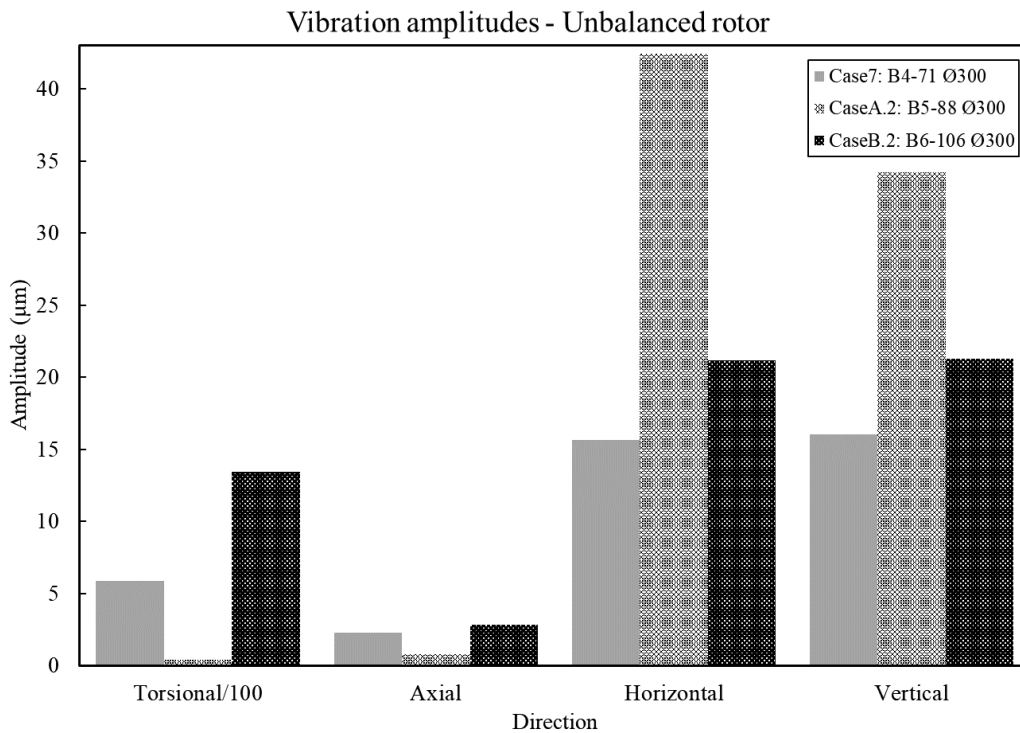


Figure 7.17: Vibration amplitudes for Cases 7, A.2, and B.2.

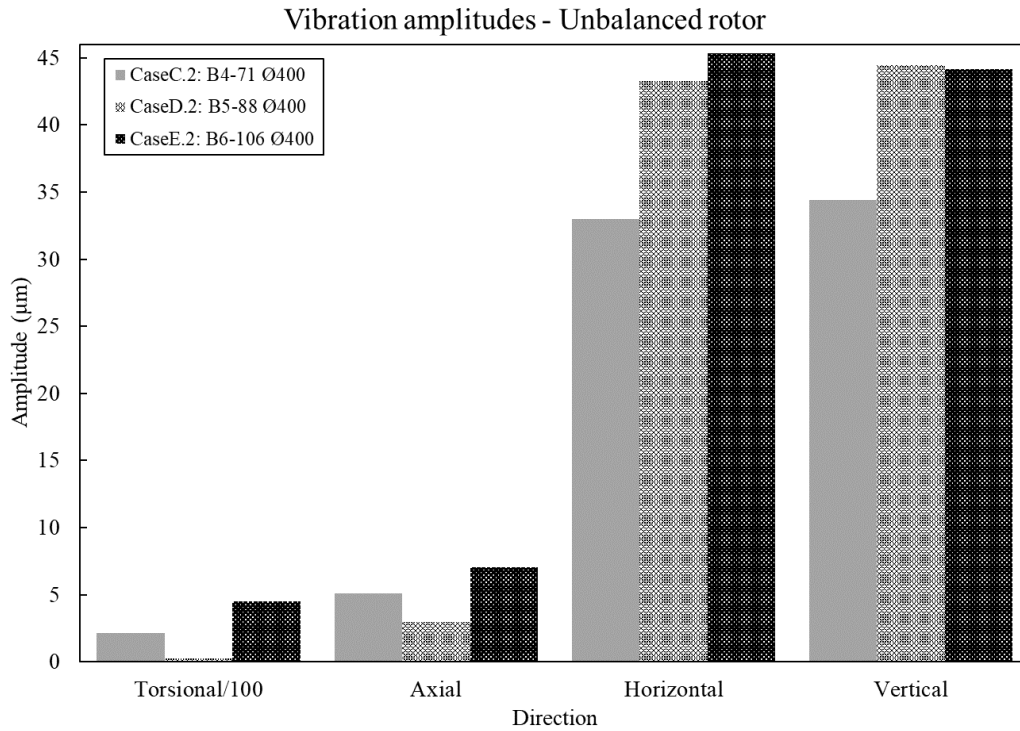


Figure 7.18: Vibration amplitudes for Cases C.2-E.2.

Table 7.15: Displacements RMS values and bearing life for Cases 7 and A.2-E.2.

Case	RMS-axial $\mu m$	RMS-horizontal $\mu m$	RMS-vertical $\mu m$	$L_{10h}(h)$
7. B4-71	17.14	10.75	10.77	$32.99 \times 10^4$
A.2. B5-88	18.34	21.31	16.91	$18.27 \times 10^4$
B.2. B6-106	19.05	14.47	14.49	$20.59 \times 10^4$
C.2. B4-71	54.08	22.49	22.58	$42.75 \times 10^4$
D.2. B5-88	57.97	26.47	26.74	$32.55 \times 10^4$
E.2. B6-106	60.08	30.52	30.41	$27.60 \times 10^4$

As seen from the results shown in Figures 7.17, 7.18, and Table 7.15, the radial components are considerably increased; this affects the bearing life significantly. An interesting observation arising from the unbalanced cases is that unbalance seems to have a greater impact upon 4- and 6-bladed propellers, which are the propellers with the most beneficial vibratory properties when thruster systems are balanced. As seen from Figure 7.18 showing results for the larger propellers, the 5-bladed propeller is no longer the propeller with the least desirable performance. The increase of radial vibrations from balanced cases to unbalanced cases of the 400mm diameter propellers is highest for the 6-bladed propeller, followed the 4-bladed, and finally the 5-bladed propeller, as this value is approximately 15 times higher for the B6, 6 times higher for the B4, and 5.8 times higher for the B5 propeller, respectively.

Furthermore, it is clear that even a small unbalance affects the vibrations in the thruster system and the bearing life. However, achieving a perfectly balanced system might be unrealistic. Balancing issues related to the thruster investigated in this study can result from different materials of its various components. For instance, if the propeller is made of aluminum and the shaft of stainless steel the key coupling between these two parts can be a source of unbalance. Moreover, inaccuracy in production and assembly can lead to unbalance, in addition to changes in shape or damage to the propeller after some time in operation. Essentially, unbalance in the thruster system should be avoided or constrained as far as possible.

## Chapter 8

### Conclusions and further work

#### 8.1. Summary and conclusions

A 6 DOF model is created in OM that consists of a marine propeller, a shaft, and two bearings. The model can be used to study various steady-state cases, whereby the resulting forces and vibration properties can be obtained from the simulation. The various inputs to the marine propeller in OM are obtained by use of an empirical approach. This approach is used to calculate the marine propeller hydrodynamic contributions, i.e., the added mass and damping elements. The equations used to calculate the added mass and damping are based on sets of regression coefficients, which in turn are based on the Wageningen B-screw series. The marine propellers investigated in this study are not from the Wageningen B-screw series. However, Parsons and Vorus (1981) demonstrate that this method is applicable for propellers outside the Wageningen B-screw series, i.e., for propellers without skew and rake, such as the propellers investigated here. Furthermore, the thrust and torque of the marine propellers are obtained from open water tests of the relevant propellers from the Wageningen B-screw series. The tests chosen to represent the propellers investigated in this study are those with the most similar BAR. The characteristics acquired from the open water tests are the thrust and torque coefficients and the propeller efficiency versus the advance coefficient. From this the mean thrust and mean torque can be obtained, and these values are further used in a set of equations produced by Veritec (1985). These equations are used to calculate the dynamic forces and moments from the marine propeller. Note that hydrodynamic contributions from the marine propeller are simplified calculations and should only be used for preliminary design calculations and studies. In this way, the first objective of developing a 6 DOF model in OM was achieved. A challenge that arose when developing the OM model was to include the propeller added mass, damping, and the dynamic forces and moments in the model. The various contributions had to be calculated for the specific rotational speed before the results could be entered into the OM model. This also explains why only steady-state cases can be investigated with the current model.



Concerning the second objective regarding vibrations in the thruster system, vibration amplitudes are dependent on the stiffness and bearing location, and above all if unbalance is present in the rotating system. A higher stiffness resulting from the bearing configuration and bearing pre-load has beneficial effects on the vibration amplitudes in the axial, horizontal, and vertical directions. However, the torsional vibrations are higher, which may affect the fatigue life of the shaft. Furthermore, a shaft with larger diameter produces favorable vibrational results in the axial and torsional directions, so the life of the shaft could be extended by increasing its size. As for the bearing location, a larger distance between bearings has beneficial effects on horizontal and vertical vibrations, while a shorter distance produces the opposite effect. It should be noted that the bearing distance of the base case is considered to be small initially. However, the situation that results in the greatest radial vibrations is an unbalanced propeller, where the worst case was a 6-bladed propeller with diameter  $400\text{mm}$ . The radial vibrations of this propeller were increased by about 15 times compared to the balanced case.

The difference in vibratory characteristics between propellers with varying numbers of blades results from the different velocities and accelerations produced, i.e., angular and linear motion. As seen from the comparison of the selected added mass and damping terms in Appendix E, the added mass and damping results do not vary considerably between propellers with a different number of blades and with the same pitch ratio. An exception is the damping term  $c_{22}$  for the 6-bladed propeller, which is much higher than for the other two investigated propellers. This indicates that the accelerations affecting the added mass vary with the number of blades on the propeller, as do the velocities, which affect the damping, and the dynamic forces and moments. The B4 and B6 propellers follow the same pattern; however, the magnitudes of the motions are higher for the B6 propeller. These propellers have high values in the axial direction and small values in the horizontal and vertical directions. Conversely, the B5 propeller exhibits small values in the axial direction, and high values in the horizontal and vertical directions. Furthermore, the equations used to calculate dynamic forces and moments vary with the number of blades on the propeller. This also affects the results of the simulations. Accordingly, the dynamic force and moment equations are listed in Appendix A for B4-B6 propellers.

The thruster investigated in this study has two tapered roller bearings which accept the axial and radial load from the marine propeller. However, only one bearing takes the axial load at any one time, depending on the rotational direction. Consequently, it is sufficient to investigate the bearing life of one bearing. The bearing life is highly dependent on the axial load, i.e., the thrust from the propeller and this force is usually much higher than the radial force. The bearing load is calculated from the RMS values of displacements in the axial, horizontal, and vertical directions. From the investigated cases the radial forces are only a concern for the 5-bladed propeller, or an unbalanced propeller. In the worst investigated case a small unbalance more than halves the bearing life of the balanced case. Unbalance causes large centrifugal forces; this is of great concern and should be avoided or constrained as far as possible. Careful consideration should also be taken if the bearing depends on a pre-load for normal operation, since a loss of bearing pre-load can lead to large and destructive forces on the bearing. Furthermore, actions to prolong the bearing life follow the same principles as reducing the vibrations in the system, as previously discussed. The thruster and bearing design should be related to the maximum thrust force. Regarding the third objective of using different propellers in the same design, this can be done. However, the maximum thrust force must not exceed the thrust force of the original propeller. Another propeller can be used to change the RPM-thrust force configuration or to change the vibratory properties of the thruster system.

## **8.2. Recommendations for further work**

A significant part of the scope of this study was to develop a functional model in OM. Further work on marine propeller hydrodynamic contributions and the implementation of these contributions into OM is recommended. Moreover, detailed further investigation of the bearings and their natural frequencies is also advised. Additional topics for further work are presented below:

- Examine the possibility to include two and three-bladed propellers. To do this, it might be necessary to use a different approach to calculate the marine propeller hydrodynamic contributions, i.e., the added mass, damping, thrust, and torque. A possible approach is lifting line theory. If a lifting line approach is selected, then it is possible to implement

this calculation directly into OM. If the marine propeller hydrodynamic contributions are calculated directly in OM, this enables the analysis of transient cases.

- Conduct a thorough analysis of the bearings in the thruster, with a focus on the bearing stiffness and the natural frequencies of the bearing. Investigate whether the natural frequencies of the bearings affect the other rotating components in the thruster system.
- Consider the duct around the propeller and the possibility of including contributions from the duct in the OM model.
- Investigate shaft analysis, torsional vibrations, and shaft fatigue.

## References

- Ait-Ahmed, N., Vonnet, M., Loron, L., & Guibert, C. (2007). On Modeling of Marine Thrusters for Underwater Vehicles. *7th IFAC Conference on Control Applications in Marine Systems*, 211-216.
- Amini, H., & Steen, S. (2011). Experimental and Theoretical Analysis of Propeller Shaft Loads in Oblique Inflow. *Journal of Ship Research*, Vol. 55, 1-21.
- Ashghar, S., & Tariq, S. (2010). *Design and Implementation of a User Friendly OpenModelica Graphical Connection Editor*. (Master's thesis). Linköpings universitet, Linköpings.
- Azis, F., Aras, M., Rashid, M., & Othman, M. (2012). Problem Identification for Underwater Remotely Operated Vehicle (ROV) : A Case Study. *International Symposium on Robotics and Intelligent Sensor, Procedia Engineering 41*, 554-560.
- Batrak, Y. (n.d.). *Lateral Vibration Prediction Issues*. (ShaftDesigner - SKF Solution Factory) Retrieved 01 16, 2018, from <http://www.shaftdesigner.com/downloads/PAPER%20LATERAL%20VIBRATION%20PREDICTION%20ISSUES.pdf>
- Batrak, Y. (n.d.). *Torsional Vibration Calculation Issues With Propulsion Systems*. (ShaftDesigner - SKF Solution Factory) Retrieved 01 16, 2018, from <http://www.shaftdesigner.com/downloads/PAPER%20TORSIONAL%20VIBRATION%20CALCULATION%20ISSUES%20WITH%20PROPULSION%20SYSTEMS.pdf>
- Bernitsas, M., Ray, D., & Kinley, P. (1981). *Kt, Kq and Efficiency Curves for the Wageningen B-series Propellers*. University of Michigan. Retrieved 01 24, 2018, from [http://teacher.buet.ac.bd/mmkarim/diag\\_kt\\_kq\\_B-series.pdf](http://teacher.buet.ac.bd/mmkarim/diag_kt_kq_B-series.pdf)
- Boashash, B. (1992). Estimating and Interpreting The Instantaneous Frequency of a Signal - Part 1 : Fundamentals. *Proceedings of the IEEE*, Vol. 80, Issue 4, 520-538.
- Brandt, A. (2011). *Noise and Vibration Analysis : Signal Analysis and Experimental Procedures*. Wiley.

- Carlton, J. S. (2012). *Marine Propellers and Propulsion*. Butterworth-Heinemann, Elsevier Ltd.
- Cheli, F., & Diana, G. (2015). *Advanced Dynamics of Mechanical Systems*. Springer.
- Christ, R. D., & Wernli, R. L. (2014). *ROV Manual : A User Guide for Remotely Operated Vehicles*. Butterworth-Heinemann, Elsevier Ltd.
- Cooley, J., & Tukey, J. (1965). An Algorithm for the Machine Calculation of Complex Fourier Series. *Mathematics of Computation*, Vol. 19, 297-301.
- DNV GL. (2014). *Nauticus Machinery : For marine propulsion design and analysis*. Retrieved 04 30, 2018, from [https://www.dnvgl.com/Images/Nauticus-Machinery-brochure\\_tcm8-56706.pdf](https://www.dnvgl.com/Images/Nauticus-Machinery-brochure_tcm8-56706.pdf)
- DNV GL. (2015). *DNV GL - Class Guideline : 0038-0039*. DNV GL. Retrieved 04 30, 2018, from <https://rules.dnvgl.com/servicedocuments/dnvgl/#!/industry/1/Maritime>
- Ducan, F. (2014). *ROV Motion Control Systems*. (Ph.D, dissertation). NTNU, Trondheim.
- Forum Energy Technologies. (2018). *f-e-t.com*. Retrieved 03 13, 2018, from <http://www.f-e-t.com/products/drilling-and-subsea/subsea-technologies/components-and-tooling/thrusters/hydraulic-thrusters>
- Fritzson, P. (2016). *Introduction to Object-Oriented Modeling, Simulation, Debugging and Dynamic Optimization with Modelica using OpenModelica*. Retrieved 01 15, 2018, from <https://openmodelica.org/doc/ModelicaShortCourse/ModelicaTutorial-slides-PeterFritzson-160202-BT.pdf>
- Gerr, D. (1989). *Propeller Handbook - The Complete Reference for Choosing, Installation, and Understadning Boat Propellers*. International Marine, McGraw-Hill .
- Gross, D., Hauger, W., Schröder, J., Wall, W. A., & Govindjee, S. (2011). *Engineering Mechanics 3 : Dynamics*. Springer.
- Gudmestad, O. T. (2015). *Marine Technology and Operations : Theory and Practice*. WIT Press.
- Hughes, A., & Drury, W. (2013). *Electric Motors and Drives : Fundamentals, Types and Applications*. Elsevier Science.

- Hylarides, S., & Gent, W. van. (1974). *Propeller Hydrodynamics and Shaft Dynamics. Symposium on High Powered Propulsion of Large Ships, Part 1*. NSMB.
- IKM Subsea AS. (n.d.). *www.ikm.com*. Retrieved 01 12, 2018, from IKM Group:  
<http://www.ikm.com/ikm-subsea-norway/merlin-ucv>
- IMCA. (2014). *Code of Practice for : The Safe & Efficient Operation of Remotely Operated Vehicles*. International Marine Contractors Association.
- ISO-281. (2007). *Rolling Bearings - Dynamic load ratings and rating life*. International Organization for Standardization.
- ISO-484. (2015). *Shipbuilding - Ship screw propellers - Manufacturing tolerances*. International Organization for Standardization.
- ITTC. (2002). ITTC - Recommended Procedures and Guidelines: Testing and Extrapolation Methods Propulsion, Propulsor Open Water Test. *23rd International Towing Tank Conference*. Venice.
- Keilen, H. (2005). *Norwegian Petroleum Technology, A success story*. Norwegian Academy of Technology Sciences.
- Knaapen, R. (1997). *Experimental Determination of Rolling Element Bearing Stiffness*. Eindhoven University of Technology.
- Krämer, E. (1993). *Dynamics of Rotors and Foundations*. Springer-Verlag Berlin Heidelberg.
- Kuiper, G. (1992). *The Wageningen Propeller Series*. MARIN Publication.
- Lammeren, W.P.A. van., Manen, J. D. van, & Oosterveld, M.W.C. (1969). The Wageningen B-screw Series. *Transactions of SNAME, Vol. 77*, 296-317.
- MAN Diesel & Turbo. (2011). *Basic Principles of Ship Propulsion*. Retrieved 01 24, 2018, from <https://marine.man.eu/docs/librariesprovider6/propeller-aftship/basic-principles-of-propulsion.pdf?sfvrsn=0>
- Marine Technology Society. (n.d.). *www.rov.org*. Retrieved 01 12, 2018, from [http://www.rov.org/rov\\_history.cfm](http://www.rov.org/rov_history.cfm)
- Maritime Research Institute Netherlands. (n.d.). *marin.nl*. Retrieved 04 29, 2018, from <http://www.marin.nl/web/Organisation/History.htm>

- Meirovitch, L. (1970). *Methods of Analytical Dynamics*. McGraw-Hill.
- Meirovitch, L. (1986). *Elements of Vibration Analysis*. McGraw-Hill.
- Modelica Association. (2018). *modelica.org*. Retrieved 05 01, 2018, from <https://www.modelica.org/>
- Molland, A. (2008). *The Maritime Engineering Reference Book : A Guide to Ship Design, Construction and Operation*. Elsevier Science.
- NORSOK U-100. (2015). *Manned underwater operations - Edition 5*. Standard Norge.
- Norwegian Petroleum Directorate. (n.d.). *www.npd.no*. Retrieved 01 09, 2018, from <http://factpages.npd.no/factpages/default.aspx?culture=nb-no&nav1=field&nav2=PageView%7cAll&nav3=23395946>
- Omerdic, E., Roberts, G., & Ridao, P. (2003). Fault Detection and Accomodation for ROVs. *6th IFAC Conference on Maneuvring and Control of Marine Craft*, 127-132.
- Ong, M. C., Lee, S., Lim, A., Lo, E., & Tan, S. K. (2007). Simulating Ship Maneuvers in Deep and Coastal Waters. *Journal of Ship Research, Vol. 51*, 204-216.
- OpenModelica. (2018). *openmodelica.org*. Retrieved 01 15, 2018, from <https://openmodelica.org/?id=78:omconnectioneditoromedit&catid=10:main-category>
- Parsons, M. G., & Vorus, W. S. (1981). Added Mass and Damping Estimates for Vibrating Propellers. *Propellers '81 Symposium*, 273-302.
- Petzold, L. (1982). A description of DASSL : A differential/algebraic system solver. *Proc. 10th IMACS World Congress*. Montréal.
- Proakis, J., & Manolakis, D. (2007). *Digital Signal Processing*. Pearson Prentice Hall.
- Scheffer, C., & Girdhar, P. (2004). *Practical Machinery Vibration Analysis & Predictive Maintenance*. Elsevier.
- Schwanecke, H. (1963). *Gedanken wur Frage de Hydrodynamischen Erregungen des Propellers und der Wellenleitung*. JSTG.
- SKF Group. (2016). *Rolling Bearings*. Retrieved 04 29, 2018, from [www.skf.com/binary/77-121486/SKF-rolling-bearings-catalogue.pdf](http://www.skf.com/binary/77-121486/SKF-rolling-bearings-catalogue.pdf)

- Taneja, S. (2012). The Effect of Unbalance on Bearing Life. *IOSR Journal of Mechanical and Civil Engineering, Vol. 1, Issue 2*, 47-54.
- Thurman, H. V. (1994). *Introductory Oceanography (7th edition)*. Macmillan.
- Tong, V.-C., & Hong, S.-W. (2014). Characteristics of Tapered Roller Bearing Subjected to Combined Radial and Moment Loads. *International Journal of Precision Engineering and Manufacturing-Green Technology, Vol. 1*, 323-328.
- Veritec : Marine Technology Consultants. (1985). *Vibration Control in Ships*. Oslo: Veritec AS.
- Vizentin, G., Vukelić, G., & Srok, M. (2017). Common failures of ship propulsion shafts. *Scientific Journal of Maritime Research 31*, 85-90.
- Xing, Y., Pedersen, E., & Moan, T. (2011). An inertia-capacitance beam substructure formulation based on the bond graph method with application to rotating beams. *Journal of Sound and Vibration 330*, 5114-5130.



# Appendices

A.	Dynamic forces and moments.....	II
B.	Wageningen B-series – Open water diagrams .....	IV
C.	OpenModelica.....	VI
D.	Bearing life.....	IX
E.	Comparison of added mass and damping terms .....	XIV
F.	2D - Drawings .....	XXI
G.	Inputs for unbalanced propeller .....	XXV
H.	Digital appendices.....	XXVII

## A. Dynamic forces and moments

The first and second order dynamics forces for 4 to 6 bladed propellers for preliminary estimation purposes according to Carlton (2012) and Veritec (1985) are as follows:

Four blade propellers:

$$F_{x(1)} = 0.084T_0 \pm 0.031T_0, F_{x(2)} = 0.022T_0 \pm 0.004T_0 - \text{Thrust}$$

$$F_{z(1)} = 0.008T_0 \pm 0.004T_0, F_{z(2)} = 0.008T_0 \pm 0.004T_0 - \text{Vertical force} \quad (3.25)$$

$$F_{y(1)} = 0.012T_0 \pm 0.011T_0, F_{y(2)} = 0.00T_0 \pm 0.001T_0 - \text{Horizontal force}$$

$$M_{x(1)} = 0.062Q_0 \pm 0.025Q_0, M_{x(2)} = 0.016Q_0 \pm 0.010Q_0 - \text{Torque}$$

$$M_{z(1)} = 0.075Q_0 \pm 0.05Q_0, M_{z(2)} = 0.019Q_0 \pm 0.013Q_0 - \text{Vertical torque} \quad (3.26)$$

$$M_{y(1)} = 0.138Q_0 \pm 0.09Q_0, M_{y(2)} = 0.040Q_0 \pm 0.036Q_0 - \text{Horizontal torque}$$

Five blade propellers:

$$F_{x(1)} = 0.020T_0 \pm 0.006T_0, F_{x(2)} = 0.017T_0 \pm 0.003T_0 - \text{Thrust}$$

$$F_{z(1)} = 0.011T_0 \pm 0.009T_0, F_{z(2)} = 0.002T_0 \pm 0.002T_0 - \text{Vertical force} \quad (A.1)$$

$$F_{y(1)} = 0.021T_0 \pm 0.016T_0, F_{y(2)} = 0.006T_0 \pm 0.003T_0 - \text{Horizontal force}$$

$$M_{x(1)} = 0.0011Q_0 \pm 0.0008Q_0, M_{x(2)} = 0.014Q_0 \pm 0.008Q_0 - \text{Torque}$$

$$M_{z(1)} = 0.039Q_0 \pm 0.026Q_0, M_{z(2)} = 0.012Q_0 \pm 0.011Q_0 - \text{Vertical torque} \quad (\text{A.2})$$

$$M_{y(1)} = 0.125Q_0 \pm 0.085Q_0, M_{y(2)} = 0.080Q_0 \pm 0.040Q_0 - \text{Horizontal torque}$$

Six blade propellers:

$$F_{x(1)} = 0.036T_0 \pm 0.0024T_0, F_{x(2)} = 0.015T_0 \pm 0.002T_0 - \text{Thrust}$$

$$F_{z(1)} = 0.003T_0 \pm 0.002T_0, F_{z(2)} = 0.001T_0 \pm 0.001T_0 - \text{Vertical force} \quad (\text{A.3})$$

$$F_{y(1)} = 0.009T_0 \pm 0.004T_0, F_{y(2)} = 0.001T_0 \pm 0.001T_0 - \text{Horizontal force}$$

$$M_{x(1)} = 0.030Q_0 \pm 0.020Q_0, M_{x(2)} = 0.010Q_0 \pm 0.002Q_0 - \text{Torque}$$

$$M_{z(1)} = 0.040Q_0 \pm 0.015Q_0, M_{z(2)} = 0.007Q_0 \pm 0.002Q_0 - \text{Vertical torque} \quad (\text{A.4})$$

$$M_{y(1)} = 0.073Q_0 \pm 0.062Q_0, M_{y(2)} = 0.015Q_0 \pm 0.002Q_0 - \text{Horizontal torque}$$

## B. Wageningen B-series – Open water diagrams

Open water diagrams used in this study, from Bernitsas et al. (1981):

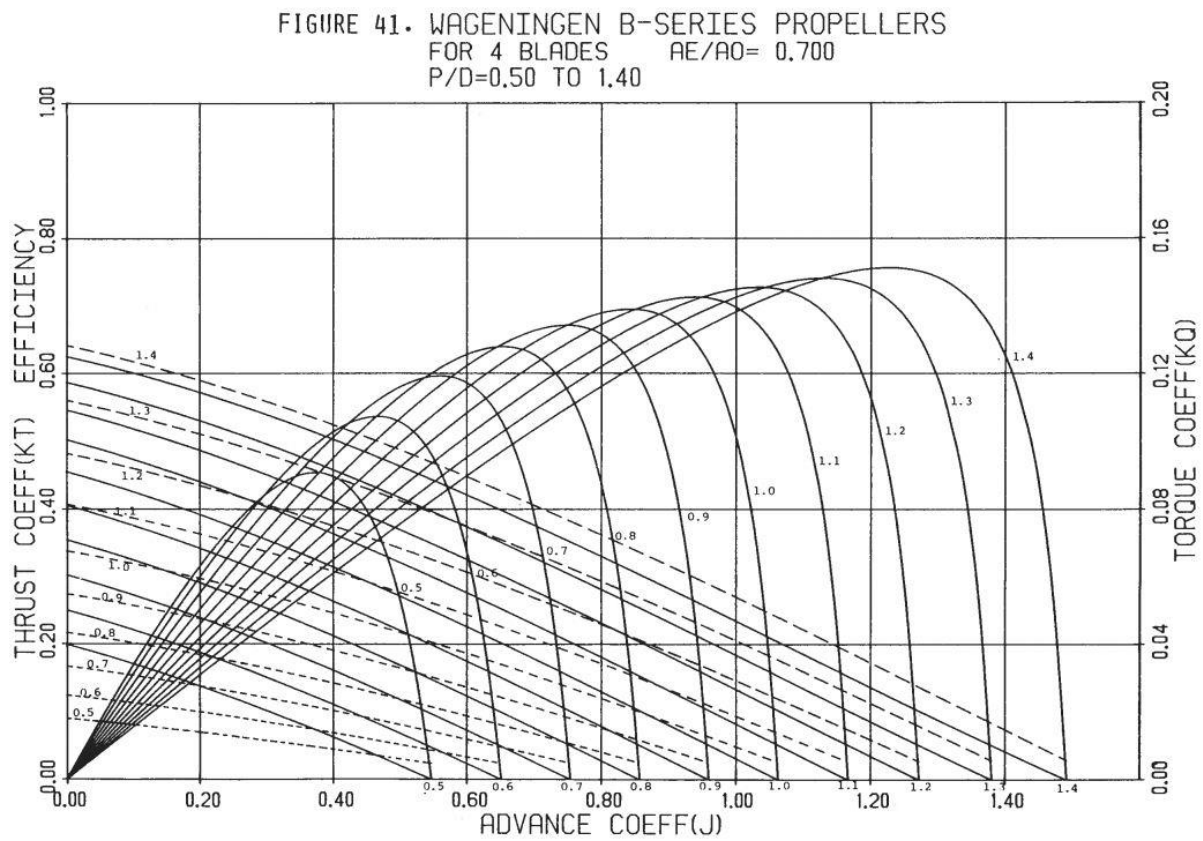


Figure 3.2:  $K_t$ ,  $K_q$  and efficiency curves for B4-70 propeller (Benitsas et al., 1981, p. 47).

FIGURE 61. WAGENINGEN B-SERIES PROPELLERS  
 FOR 5 BLADES  $AE/AO=0.900$   
 $P/D=0.50$  TO  $1.40$

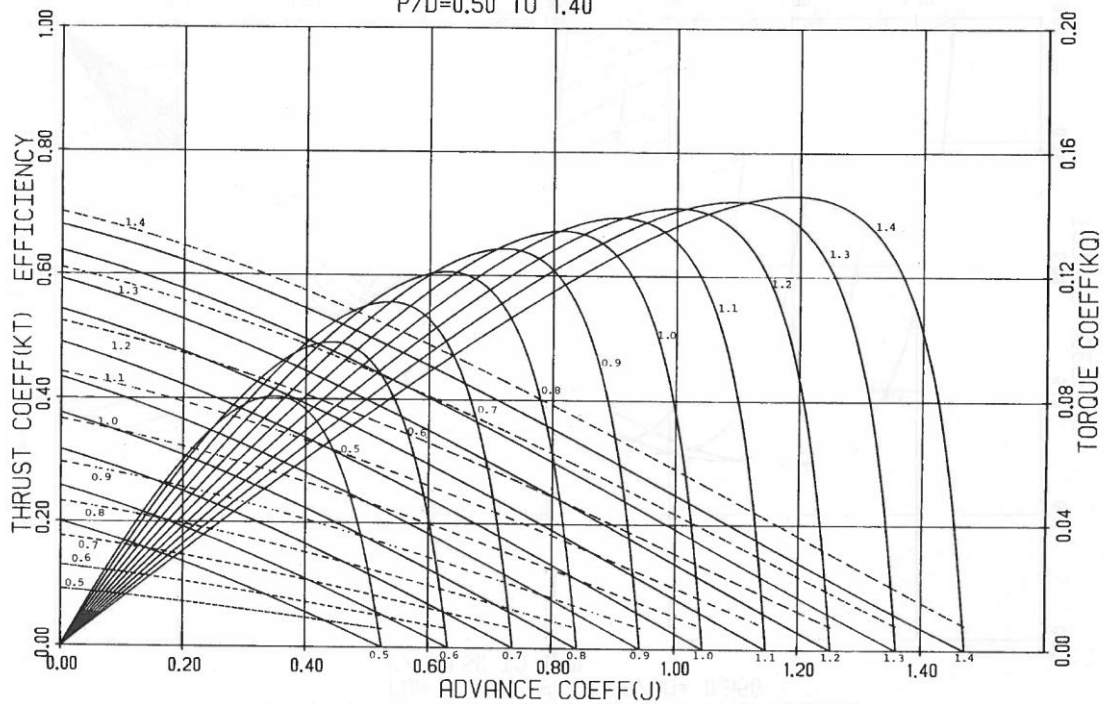


Figure B.1:  $K_t$ ,  $K_q$  and efficiency curves for B4-70 propeller (Bernitsas et al., 1981, p. 67).

FIGURE 80. WAGENINGEN B-SERIES PROPELLERS  
 FOR 6 BLADES  $AE/AO=1.050$   
 $P/D=0.50$  TO  $1.40$

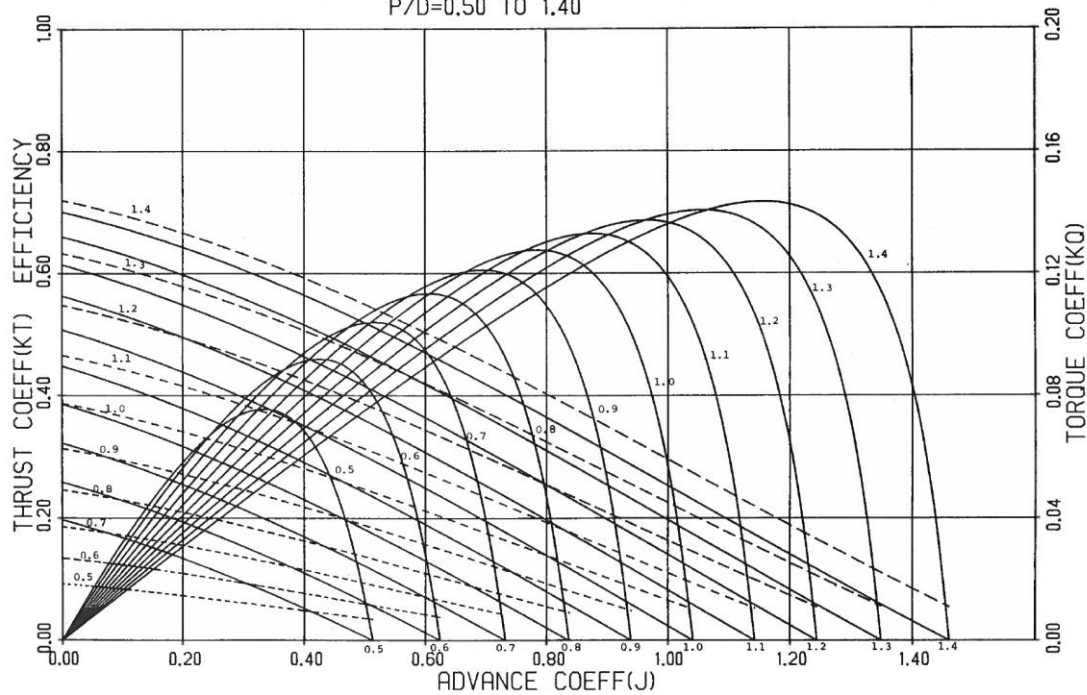
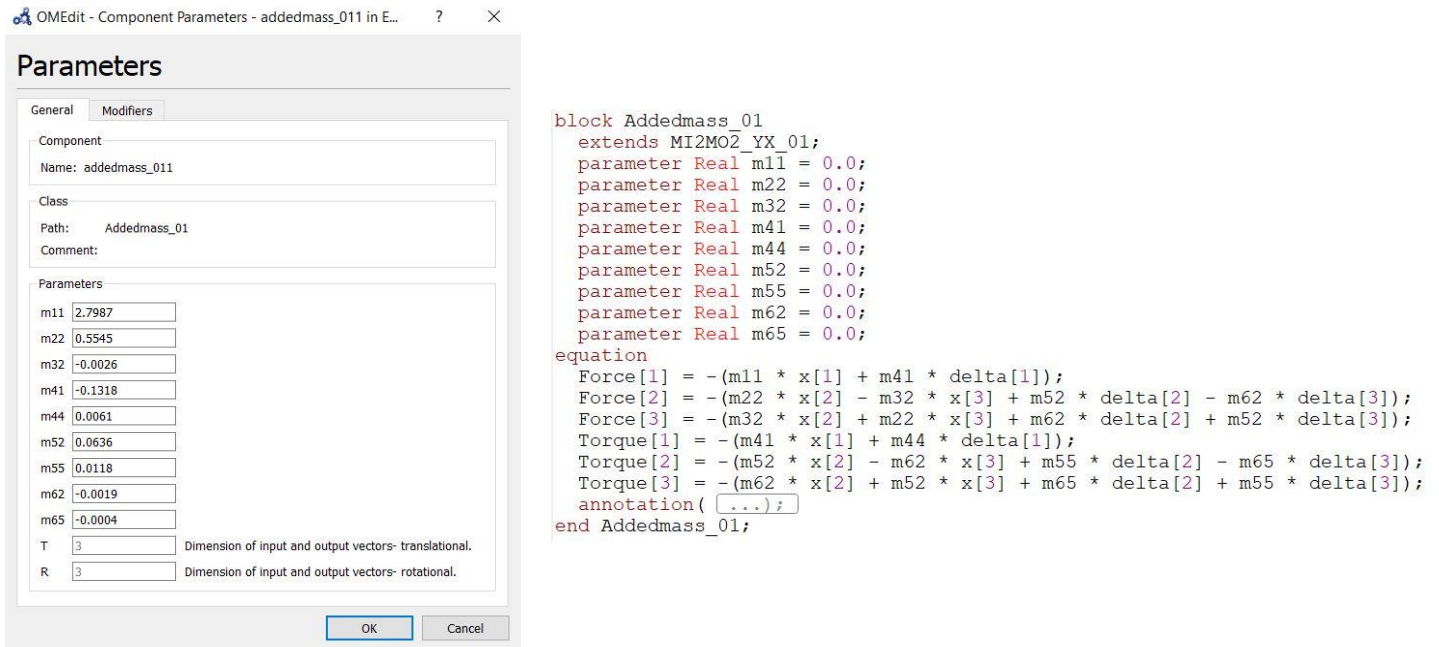


Figure B.2:  $K_t$ ,  $K_q$  and efficiency curves for B4-70 propeller (Bernitsas et al., 1981, p. 86).

## C. OpenModelica

The coding for the added mass, damping, bearing (stiffness), and the force-torque blocks are shown in the following figures. Moreover, are the inputs for the B4-70 propeller at 1655 RPM shown. Note that the bearing (stiffness) block is zero at the propeller for the 6 DOF model, as shown in Figure C.3. Moreover, an example for inputs to bearing one and bearing two is shown in Figure C.5.



The screenshot shows the 'Parameters' dialog for the component 'addedmass\_011'. The 'General' tab is active, showing the component name, class path, and a list of parameters. The parameters are:

Parameter	Value	Dimension
m11	2.7987	T
m22	0.5545	T
m32	-0.0026	T
m41	-0.1318	T
m44	0.0061	T
m52	0.0636	T
m55	0.0118	T
m62	-0.0019	T
m65	-0.0004	T
T	3	Dimension of input and output vectors- translational.
R	3	Dimension of input and output vectors- rotational.

The corresponding Modelica code for the 'Addedmass\_01' block is shown on the right:

```
block Addedmass_01
  extends MI2MO2_YX_01;
  parameter Real m11 = 0.0;
  parameter Real m22 = 0.0;
  parameter Real m32 = 0.0;
  parameter Real m41 = 0.0;
  parameter Real m44 = 0.0;
  parameter Real m52 = 0.0;
  parameter Real m55 = 0.0;
  parameter Real m62 = 0.0;
  parameter Real m65 = 0.0;
equation
  Force[1] = -(m11 * x[1] + m41 * delta[1]);
  Force[2] = -(m22 * x[2] - m32 * x[3] + m52 * delta[2] - m62 * delta[3]);
  Force[3] = -(m32 * x[2] + m22 * x[3] + m62 * delta[2] + m52 * delta[3]);
  Torque[1] = -(m41 * x[1] + m44 * delta[1]);
  Torque[2] = -(m52 * x[2] - m62 * x[3] + m55 * delta[2] - m65 * delta[3]);
  Torque[3] = -(m62 * x[2] + m52 * x[3] + m65 * delta[2] + m55 * delta[3]);
  annotation(
    ..
  );
end Addedmass_01;
```

Figure C.1: Added mass block inputs and coding.

OMEdit - Component Parameters - damping\_011 in EM\_... ? X

### Parameters

General Modifiers

Component  
Name: damping\_011

Class  
Path: Damping\_01  
Comment:

Parameters

c11

c22

c32

c41

c44

c52

c55

c62

c65

T  Dimension of input and output vectors- translational.

R  Dimension of input and output vectors- rotational.

OK Cancel

```

block Damping_01
  extends MI2MO2_YX_01;
  parameter Real c11 = 0.0;
  parameter Real c22 = 0.0;
  parameter Real c32 = 0.0;
  parameter Real c41 = 0.0;
  parameter Real c44 = 0.0;
  parameter Real c52 = 0.0;
  parameter Real c55 = 0.0;
  parameter Real c62 = 0.0;
  parameter Real c65 = 0.0;
equation
  Force[1] = -(c11 * x[1]+ c41 * delta[1]);
  Force[2] = -(c22 * x[2] - c32 * x[3] + c52 * delta[2] - c62 * delta[3]);
  Force[3] = -(c32 * x[2] + c22 * x[3] + c62 * delta[2] + c52 * delta[3]);
  Torque[1] = -(c41 * x[1]+c44 * delta[1]);
  Torque[2] = -(c52 * x[2] - c62 * x[3] + c55 * delta[2] - c65 * delta[3]);
  Torque[3] = -(c62 * x[2] + c52 * x[3] + c65 * delta[2] + c55 * delta[3]);
  annotation( ... );
end Damping_01;

```

Figure C.2: Damping block inputs and coding.

OMEdit - Component Parameters - bearing\_011 in EM\_B... ? X

### Parameters

General Modifiers

Component  
Name: bearing\_011

Class  
Path: Bearing\_01  
Comment:

Parameters

k11

k22

k33

k44

k55

k66

T  Dimension of input and output vectors- translational.

R  Dimension of input and output vectors- rotational.

OK Cancel

```

block Bearing_01
  extends MI2MO2_YX_01;
  parameter Real k11 = 0.0;
  parameter Real k22 = 0.0;
  parameter Real k33 = 0.0;

  parameter Real k44 = 0.0;
  parameter Real k55 = 0.0;
  parameter Real k66 = 0.0;

equation
  Force[1] = -(k11 * x[1]);
  Force[2] = -(k22 * x[2]);
  Force[3] = -(k33 * x[3]);
  Torque[1] = -(k44 * delta[1]);
  Torque[2] = -(k55 * delta[2]);
  Torque[3] = -(k66 * delta[3]);
  annotation( ... );
end Bearing_01;

```

Figure C.3: Bearing (stiffness) block inputs and coding.

### Parameters

General Modifiers

Component  
Name: forcetorque1

Class  
Path: forcetorque  
Comment:

Parameters

F1	143.44	
F2	13.6609	
F3	20.4914	
T1	5.05835	
T2	6.11897	
T3	11.2589	
F12	37.5676	
F22	13.6609	
F32	1.70762	
T12	1.30538	
T22	1.55014	
T32	3.26345	
Omega	173.3	
Z	4	
T	3	Dimension of input and output vectors- translational.
R	3	Dimension of input and output vectors- rotational.

OK Cancel

```

block forcetorque
  extends MI2M02_YX_01;
  parameter Real F1 = 0.0;
  parameter Real F2 = 0.0;
  parameter Real F3 = 0.0;
  parameter Real T1 = 0.0;
  parameter Real T2 = 0.0;
  parameter Real T3 = 0.0;
  parameter Real F12 = 0.0;
  parameter Real F22 = 0.0;
  parameter Real F32 = 0.0;
  parameter Real T12 = 0.0;
  parameter Real T22 = 0.0;
  parameter Real T32 = 0.0;
  parameter Real Omega = 0.0;
  parameter Real Z = 0.0;
  equation
    Force[1] = (F1 * Modelica.Math.cos(Z*Omega*time) + F12 * Modelica.Math.cos(2*Z*Omega*time));
    Force[2] = (F2 * Modelica.Math.cos(Z*Omega*time) + F22 * Modelica.Math.cos(2*Z*Omega*time));
    Force[3] = (F3 * Modelica.Math.cos(Z*Omega*time) + F32 * Modelica.Math.cos(2*Z*Omega*time));
    Torque[1] = (T1 * Modelica.Math.cos(Z*Omega*time) + T12 * Modelica.Math.cos(2*Z*Omega*time));
    Torque[2] = (T2 * Modelica.Math.cos(Z*Omega*time) + T22 * Modelica.Math.cos(2*Z*Omega*time));
    Torque[3] = (T3 * Modelica.Math.cos(Z*Omega*time) + T32 * Modelica.Math.cos(2*Z*Omega*time));
  annotation( ... );
end forcetorque;
    
```

Figure C.4: Force and torque block inputs and coding.

OMEdit - Component Parameters - bearing\_011 in EM\_B... ? X

### Parameters

General Modifiers

Component  
Name: bearing\_011

Class  
Path: Bearing\_01  
Comment:

Parameters

k11	1e8	
k22	1e8	
k33	1e8	
k44	2.4e4	
k55	4e4	
k66	4e4	
T	3	Dimension of input and output vectors- translational.
R	3	Dimension of input and output vectors- rotational.

OK Cancel

OMEdit - Component Parameters - bearing\_011 in EM\_B... ? X

### Parameters

General Modifiers

Component  
Name: bearing\_011

Class  
Path: Bearing\_01  
Comment:

Parameters

k11	0.0	
k22	1e8	
k33	1e8	
k44	0.0	
k55	4e4	
k66	4e4	
T	3	Dimension of input and output vectors- translational.
R	3	Dimension of input and output vectors- rotational.

OK Cancel

Figure C.5: Inputs bearing 1 and bearing 2 – Base case.



## D. Bearing life

Bearing life calculations for Section 7.3 bearing response:

Case 2:

$$0.4F_r = 0.4892 \times 10^{-6}m \times 2.5 \times 10^8 N/m = 122.30N.$$

$$1.7F_a = 6.86 \times 10^{-6}m \times 2.5 \times 10^8 N/m = 1715.00N.$$

$$L_{10h} = \frac{10^6}{60 \times 1655 RPM} \times \left( \frac{79700N}{0.4 \times 122.30 + 1.7 \times 1715.00} \right)^{10/3} = 58.63 \times 10^4 h.$$

Case 3:

$$0.4F_r = 5.7248 \times 10^{-6}m \times 5 \times 10^7 N/m = 286.24N.$$

$$1.7F_a = 34.26 \times 10^{-6}m \times 5 \times 10^7 N/m = 1713.00N.$$

$$L_{10h} = \frac{10^6}{60 \times 1655 RPM} \times \left( \frac{79700N}{0.4 \times 286.24 + 1.7 \times 1713.00} \right)^{10/3} = 54.71 \times 10^4 h.$$

Case 4:

$$0.4F_r = 1.3624 \times 10^{-6}m \times 10^8 N/m = 136.24N.$$

$$1.7F_a = 17.11 \times 10^{-6}m \times 10^8 N/m = 1711.00N.$$

$$L_{10h} = \frac{10^6}{60 \times 1655 RPM} \times \left( \frac{79700N}{0.4 \times 136.24 + 1.7 \times 1711.00} \right)^{10/3} = 58.71 \times 10^4 h.$$

Case 5:

$$0.4F_r = 1.0526 \times 10^{-6}m \times 10^8 N/m = 105.26N.$$

$$1.7F_a = 17.14 \times 10^{-6} m \times 10^8 N/m = 1714.00N.$$

$$L_{10h} = \frac{10^6}{60 \times 1655 RPM} \times \left( \frac{79700N}{0.4 \times 105.26 + 1.7 \times 1714.00} \right)^{10/3} = 59.19 \times 10^4 h.$$

Case 6:

$$0.4F_r = 3.2066 \times 10^{-6} m \times 10^8 N/m = 320.66N.$$

$$1.7F_a = 17.14 \times 10^{-6} m \times 10^8 N/m = 1714.00N.$$

$$L_{10h} = \frac{10^6}{60 \times 1655 RPM} \times \left( \frac{79700N}{0.4 \times 320.66 + 1.7 \times 1714.00} \right)^{10/3} = 53.79 \times 10^4 h.$$

Case 7:

$$0.4F_r = 15.2169 \times 10^{-6} m \times 10^8 N/m = 1521.69N.$$

$$1.7F_a = 17.14 \times 10^{-6} m \times 10^8 N/m = 1714.00N.$$

$$L_{10h} = \frac{10^6}{60 \times 1655 RPM} \times \left( \frac{79700N}{0.4 \times 1521.69 + 1.7 \times 1714.00} \right)^{10/3} = 32.99 \times 10^4 h.$$

Bearing life calculations for section 7.4:

Case A:

$$0.4F_r = 20.1916 \times 10^{-6} m \times 10^8 N/m = 2019.16N.$$

$$1.7F_a = 18.34 \times 10^{-6} m \times 10^8 N/m = 1834.00N.$$

$$L_{10h} = \frac{10^6}{60 \times 1655 RPM} \times \left( \frac{79700N}{0.4 \times 2019.16 + 1.7 \times 1834} \right)^{10/3} = 22.99 \times 10^4 h.$$

Case B:

X

$$0.4F_r = 1.3471 \times 10^{-6}m \times 10^8N/m = 134.71N.$$

$$1.7F_a = 19.05 \times 10^{-6}m \times 10^8N/m = 1905.00N.$$

$$L_{10h} = \frac{10^6}{60 \times 1655RPM} \times \left( \frac{79700N}{0.4 \times 134.71 + 1.7 \times 1905} \right)^{10/3} = 41.32 \times 10^4 h.$$

Case C:

$$0.4F_r = 8.1612 \times 10^{-6}m \times 10^8N/m = 816.12N.$$

$$1.7F_a = 54.90 \times 10^{-6}m \times 10^8N/m = 5490.00N.$$

$$L_{10h} = \frac{10^6}{60 \times 1655RPM} \times \left( \frac{79700N}{0.4 \times 816.12 + 1.7 \times 5490} \right)^{10/3} = 1.14 \times 10^4 h.$$

Case D:

$$0.4F_r = 18.5991 \times 10^{-6}m \times 10^8N/m = 1859.91N.$$

$$1.7F_a = 57.96 \times 10^{-6}m \times 10^8N/m = 5796.00N.$$

$$L_{10h} = \frac{10^6}{60 \times 1655RPM} \times \left( \frac{79700N}{0.4 \times 1859.91 + 1.7 \times 5796} \right)^{10/3} = 8.39 \times 10^3 h.$$

Case E:

$$0.4F_r = 3.0620 \times 10^{-6}m \times 10^8N/m = 306.20N.$$

$$1.7F_a = 59.96 \times 10^{-6}m \times 10^8N/m = 5996.00N.$$

$$L_{10h} = \frac{10^6}{60 \times 1655RPM} \times \left( \frac{79700N}{0.4 \times 306.20 + 1.7 \times 5996} \right)^{10/3} = 9.18 \times 10^3 h.$$

Case C.1:

$$0.4F_r = 5.1306 \times 10^{-6}m \times 10^8N/m = 513.06N.$$

$$1.7F_a = 54.08 \times 10^{-6}m \times 10^8N/m = 5408.00N.$$

$$L_{10h} = \frac{10^6}{60 \times 1655RPM} \times \left( \frac{128000N}{0.4 \times 513.06 + 1.7 \times 5408} \right)^{10/3} = 6.07 \times 10^4 h.$$

Case D.1:

$$0.4F_r = 7.8973 \times 10^{-6}m \times 10^8N/m = 789.73N.$$

$$1.7F_a = 57.97 \times 10^{-6}m \times 10^8N/m = 5797.00N.$$

$$L_{10h} = \frac{10^6}{60 \times 1655RPM} \times \left( \frac{128000N}{0.4 \times 789.73 + 1.7 \times 5797} \right)^{10/3} = 4.67 \times 10^4 h.$$

Case E.1:

$$0.4F_r = 3.3750 \times 10^{-6}m \times 10^8N/m = 337.50N.$$

$$1.7F_a = 60.08 \times 10^{-6}m \times 10^8N/m = 6008.00N.$$

$$L_{10h} = \frac{10^6}{60 \times 1655RPM} \times \left( \frac{128000N}{0.4 \times 337.50 + 1.7 \times 6008} \right)^{10/3} = 4.41 \times 10^4 h.$$

Unbalance Cases A2-E2:

Case A.2:

$$0.4F_r = 27.2041 \times 10^{-6}m \times 10^8N/m = 2720.41N.$$

$$1.7F_a = 18.34 \times 10^{-6}m \times 10^8N/m = 1834.00N.$$

$$L_{10h} = \frac{10^6}{60 \times 1655RPM} \times \left( \frac{79700N}{0.4 \times 2720.41 + 1.7 \times 1834} \right)^{10/3} = 18.27 \times 10^4 h.$$

Case B.2:

$$0.4F_r = 20.4778 \times 10^{-6}m \times 10^8N/m = 2047.78N.$$

$$1.7F_a = 19.05 \times 10^{-6}m \times 10^8N/m = 1905.00N.$$

$$L_{10h} = \frac{10^6}{60 \times 1655RPM} \times \left( \frac{79700N}{0.4 \times 2047.78 + 1.7 \times 1905} \right)^{10/3} = 20.59 \times 10^4 h.$$

Case C.2:

$$0.4F_r = 31.8694 \times 10^{-6}m \times 10^8N/m = 3186.94N.$$

$$1.7F_a = 54.08 \times 10^{-6}m \times 10^8N/m = 5408.00N.$$

$$L_{10h} = \frac{10^6}{60 \times 1655RPM} \times \left( \frac{2 \times 128000N}{0.4 \times 3186.94 + 1.7 \times 5408} \right)^{10/3} = 42.75 \times 10^4 h.$$

Case D.2:

$$0.4F_r = 37.6256 \times 10^{-6}m \times 10^8N/m = 3762.56N.$$

$$1.7F_a = 57.97 \times 10^{-6}m \times 10^8N/m = 5797.00N.$$

$$L_{10h} = \frac{10^6}{60 \times 1655RPM} \times \left( \frac{2 \times 128000N}{0.4 \times 3762.56 + 1.7 \times 5797} \right)^{10/3} = 32.55 \times 10^4 h.$$

Case E.2:

$$0.4F_r = 43.0841 \times 10^{-6}m \times 10^8N/m = 4308.41N.$$

$$1.7F_a = 60.08 \times 10^{-6}m \times 10^8N/m = 6008.00N.$$

$$L_{10h} = \frac{10^6}{60 \times 1655RPM} \times \left( \frac{2 \times 128000N}{0.4 \times 4308.41 + 1.7 \times 6008} \right)^{10/3} = 27.60 \times 10^4 h.$$

## E. Comparison of added mass and damping terms

The following figures show the difference in selected added mass and damping terms for  $\text{\O}300$  propellers with 4, 5, and 6 blades at 1655 RPM.

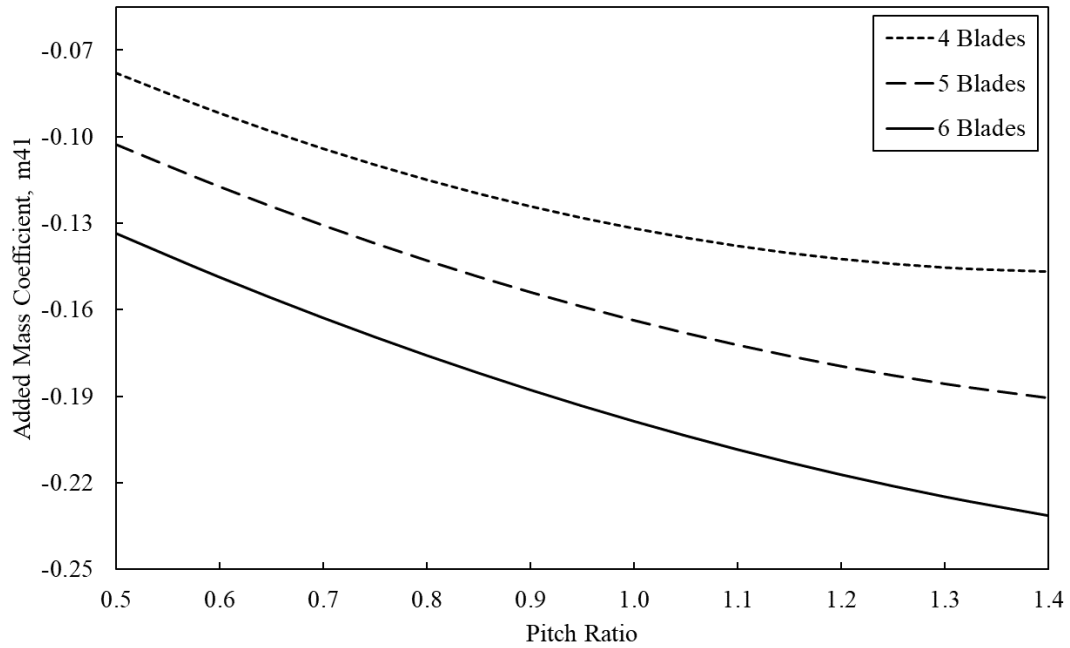


Figure E.1: Added mass, coefficient  $m_{41}$  – 1655 RPM.

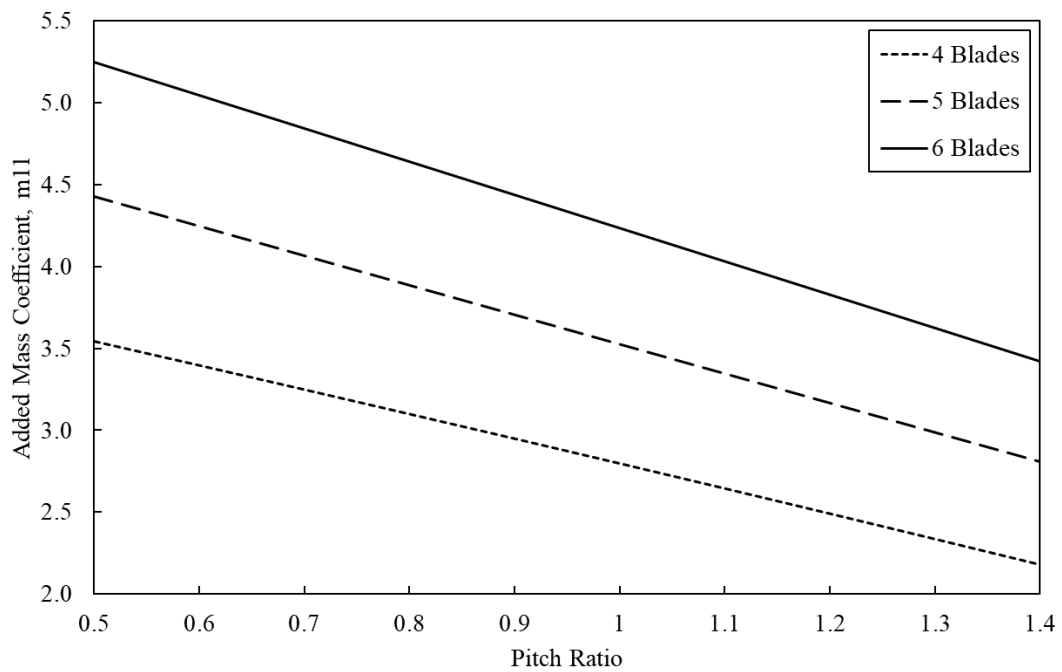


Figure E.2: Added mass, coefficient  $m_{11}$  – 1655 RPM.

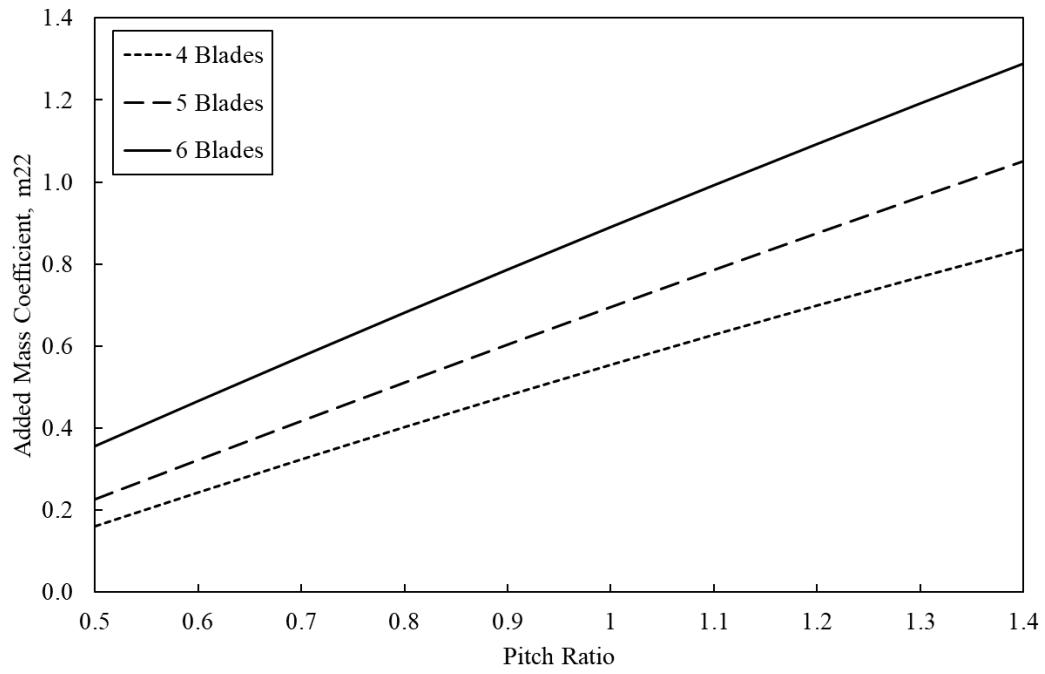


Figure E.3: Added mass, coefficient  $m_{22}$  – 1655 RPM.

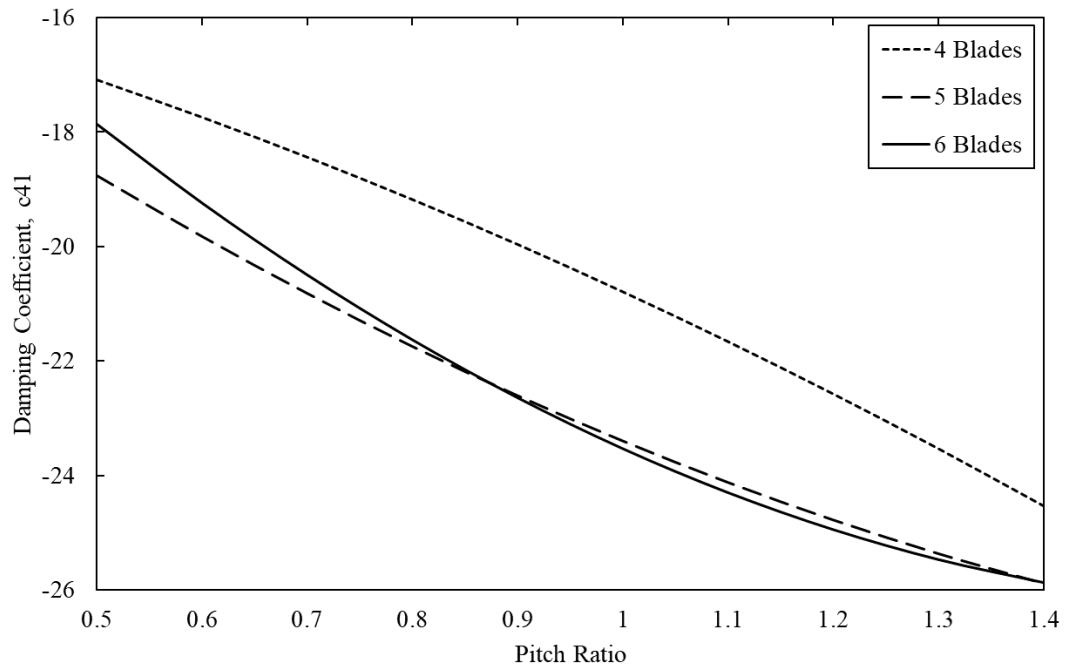


Figure E.4: Damping, coefficient  $c_{41}$  – 1655 RPM.

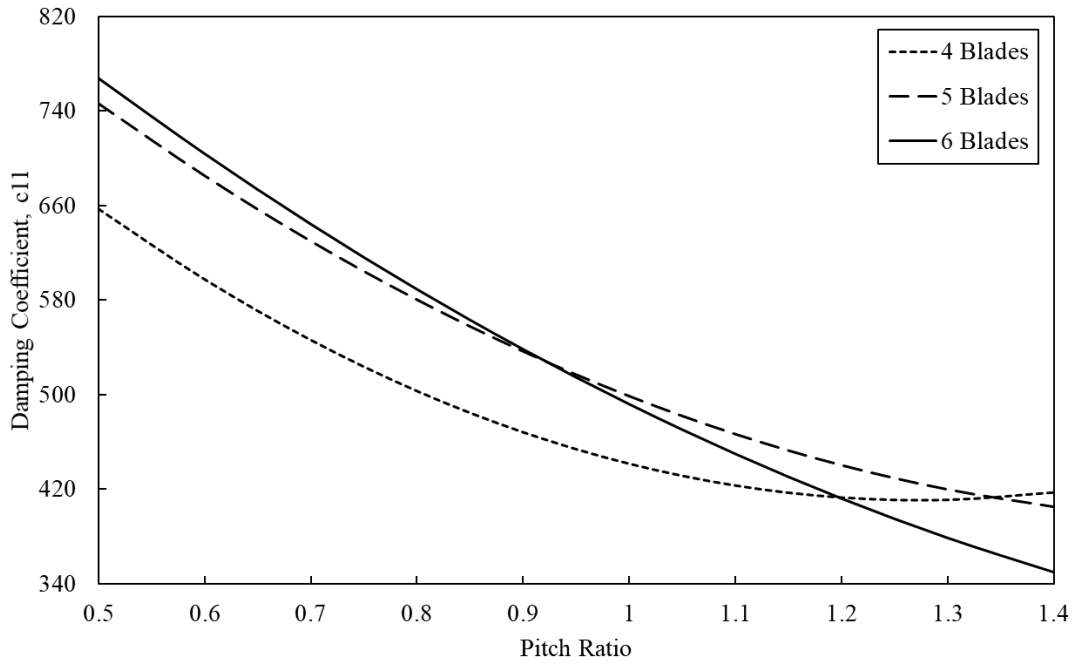


Figure E.5: Damping, coefficient c11 – 1655 RPM.

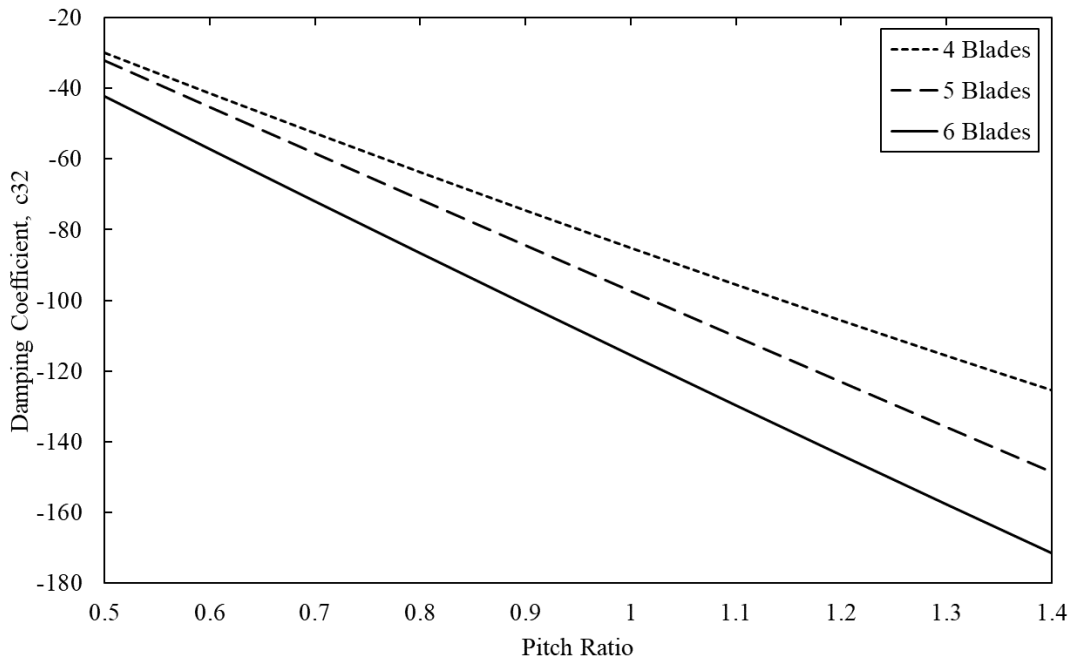


Figure E.6: Damping, coefficient c32 – 1655 RPM.



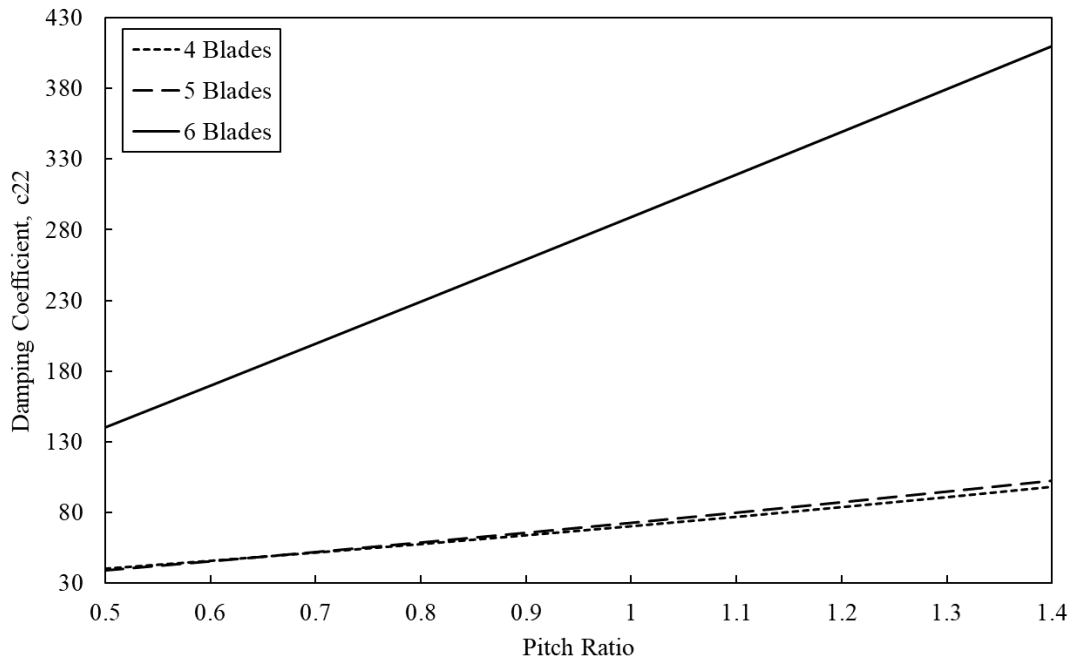


Figure E.7: Damping, coefficient  $c_{22}$  – 1655 RPM.

As seen from the figures of the added mass values, do the coefficients for the various propellers follow the same pattern. The only difference is in the magnitude of the coefficient, it increases with increased number of blades.

The results of the damping values are different, and there are no patterns except for the  $c_{32}$  coefficient which has similar behavior as the added mass coefficients. Especially for the added mass coefficients  $c_{41}$  and  $c_{11}$  it is seen that these values do not increase linearly with increased number of blades. This means that some of the damping coefficients have a different behavior as an effect of the number of blades on the propeller. However, the magnitude of the coefficients between the various propellers does not vary much, except for the 6-blade propeller for coefficient  $c_{22}$ .

The following figures show the difference between various speeds of the 4-blade propeller.

As seen in Figure E.8 are the added mass coefficients not affected by the rotational speed.

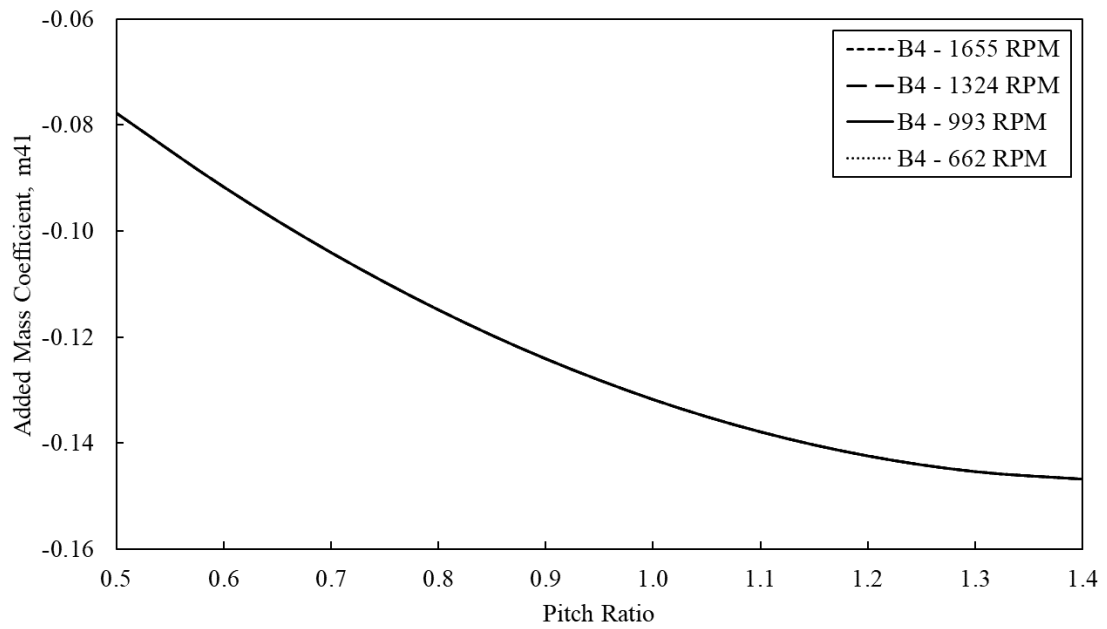


Figure E.8: Added mass, coefficient  $m_{41}$  – various speeds.

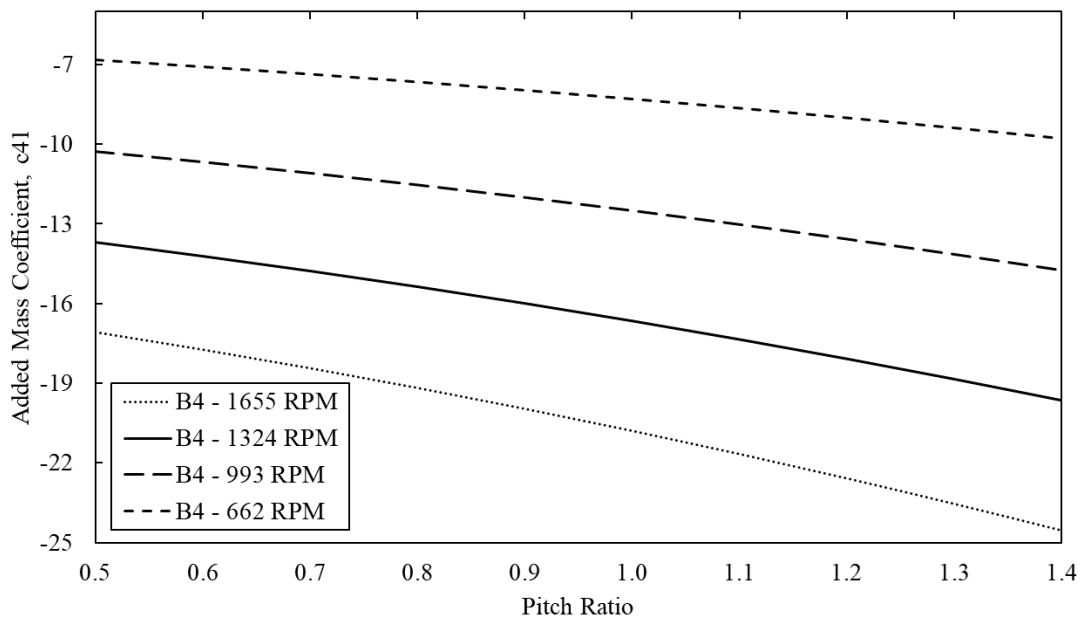


Figure E.9: Damping, coefficient  $c_{41}$  – various speeds.

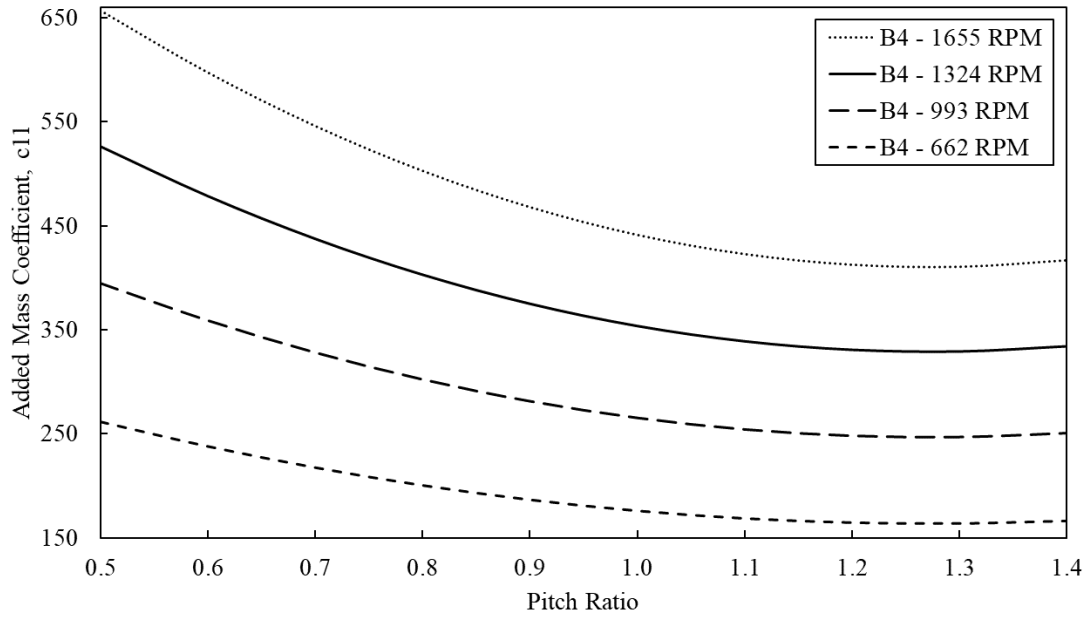


Figure E.10: Damping, coefficient  $c_{11}$  – various speeds.

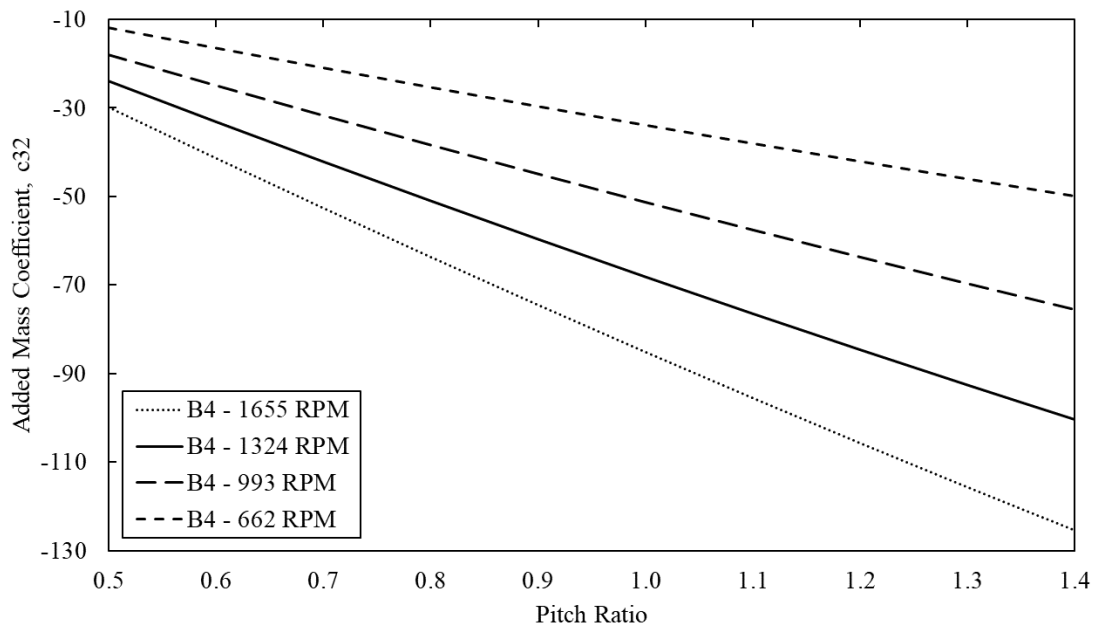


Figure E.11: Damping, coefficient  $c_{32}$  – various speeds.

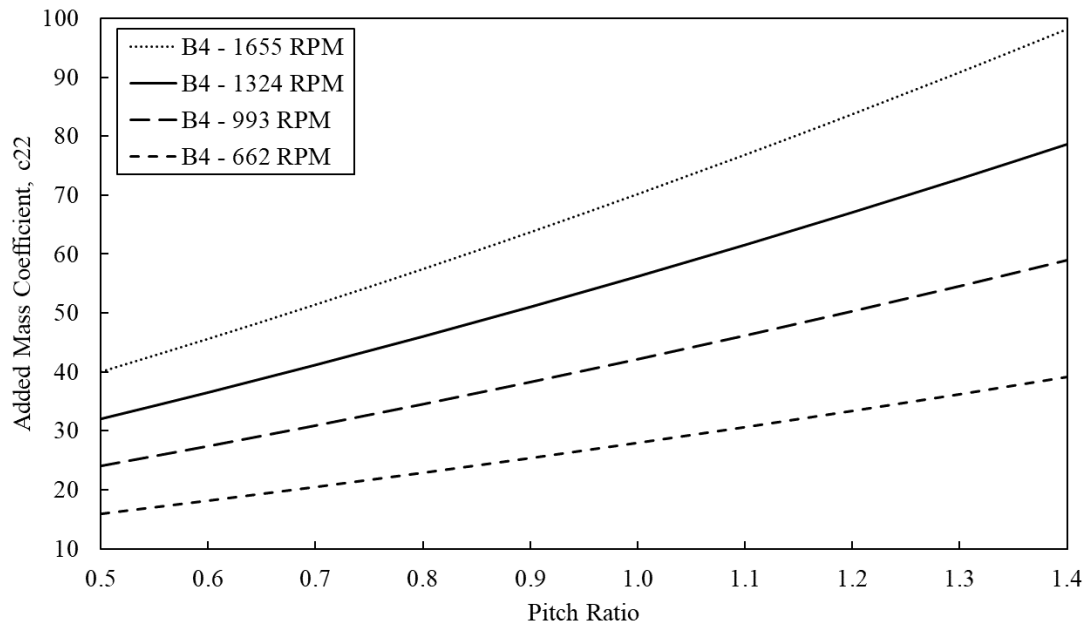


Figure E.12: Damping, coefficient  $c_{22}$  – various speeds.

As seen from the figures with damping coefficients do these follow the same pattern with the various speeds. However, the magnitude is higher with higher rotational speed.



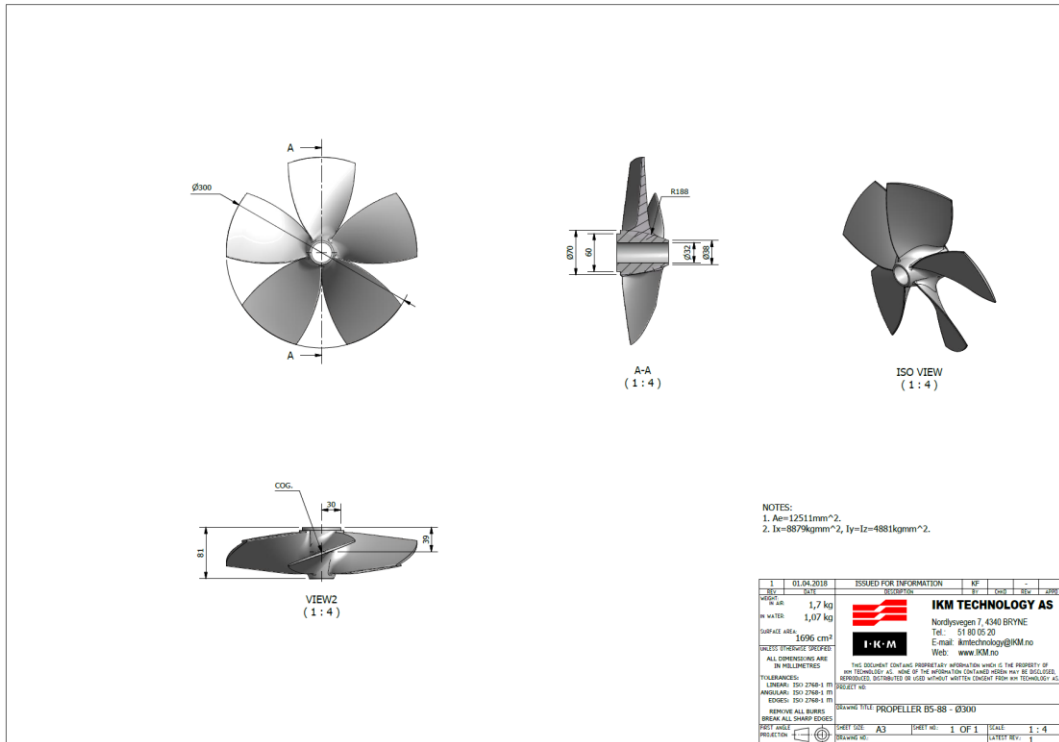


Figure F.3: B5-88 – Ø300.

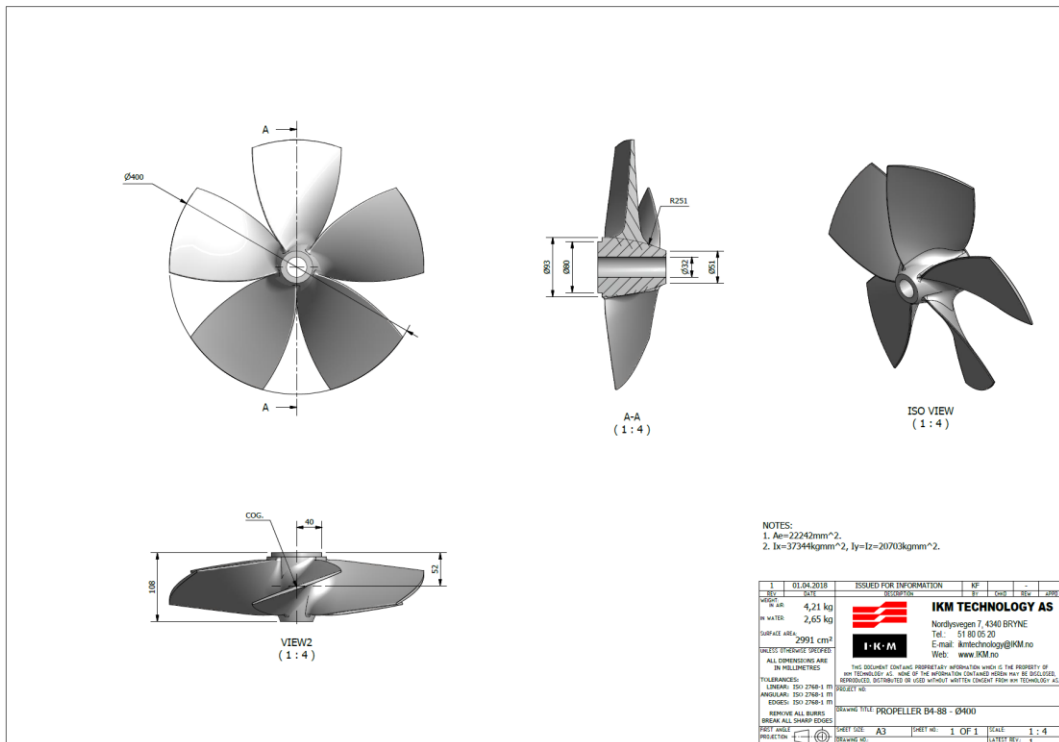


Figure F.4: B5-88 – Ø400.

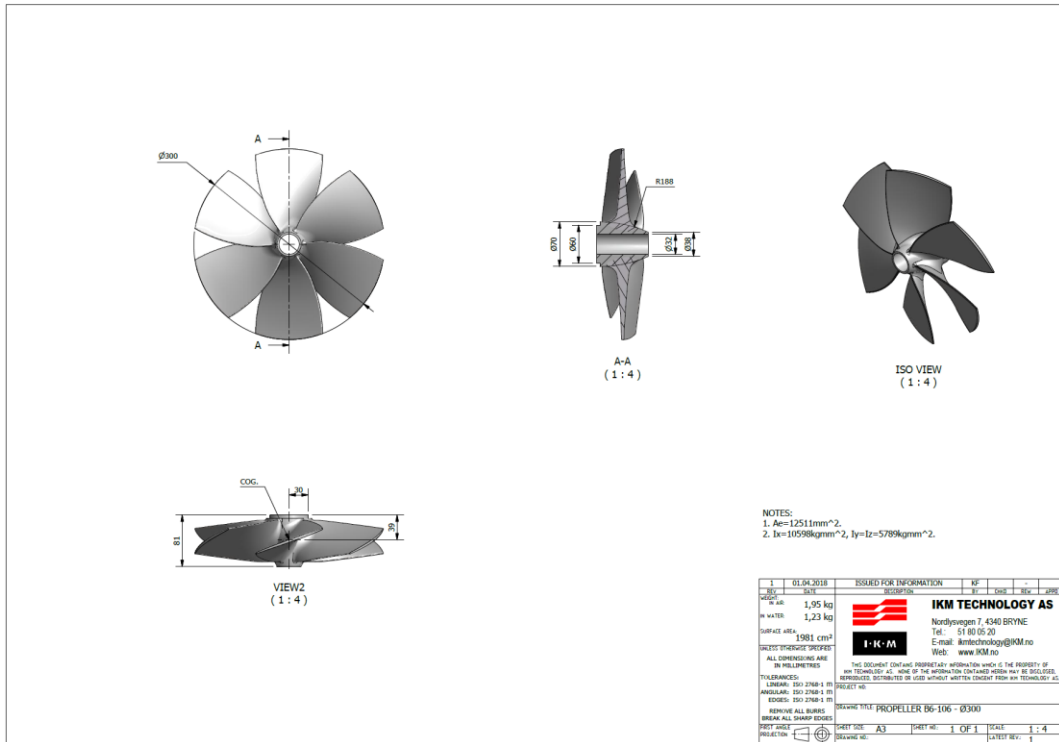


Figure F.5: B6-106 – Ø300.

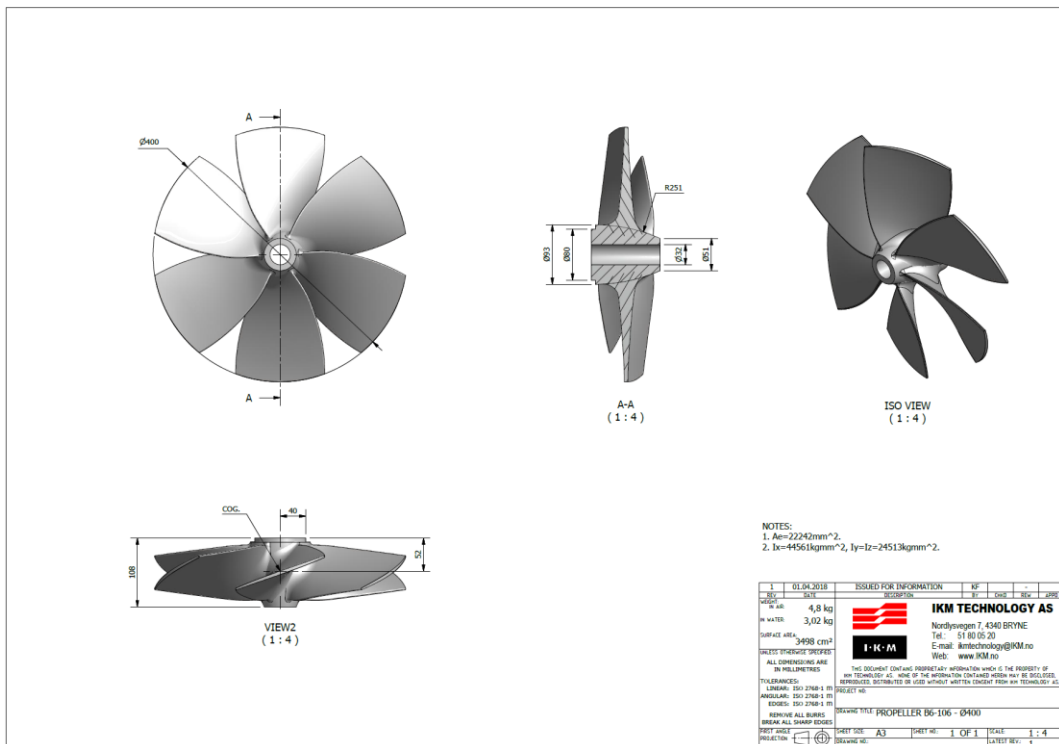


Figure F.6: B6-106 – Ø400.





## G. Inputs for unbalanced propeller

Inputs for the various unbalanced cases are shown in the following figures.

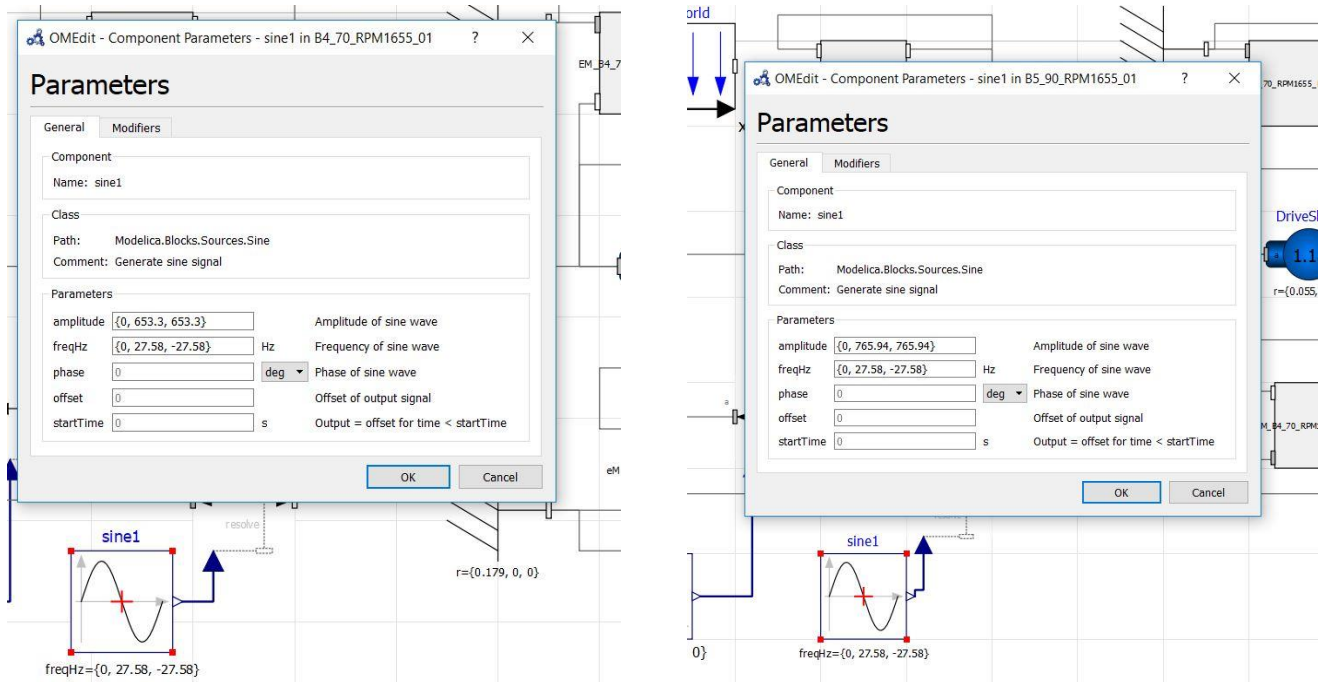


Figure G.1: Cases 7 and A.2.

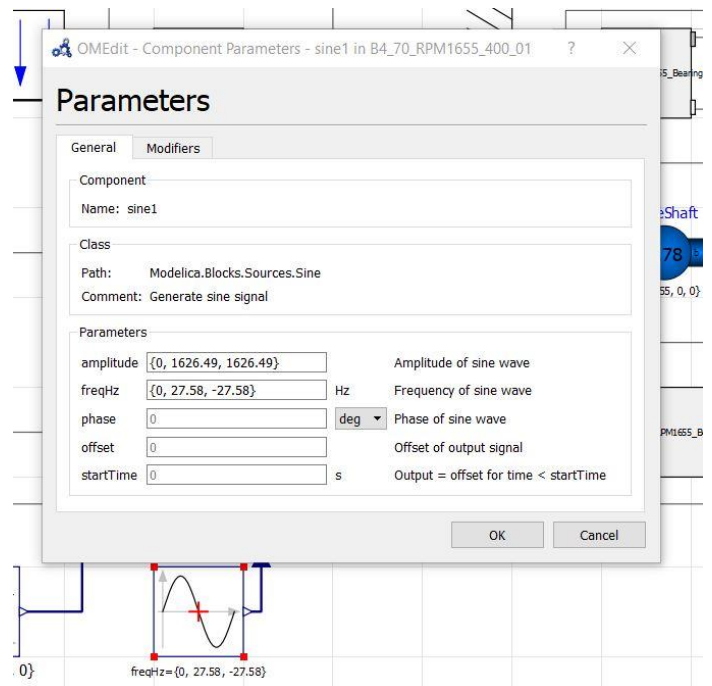
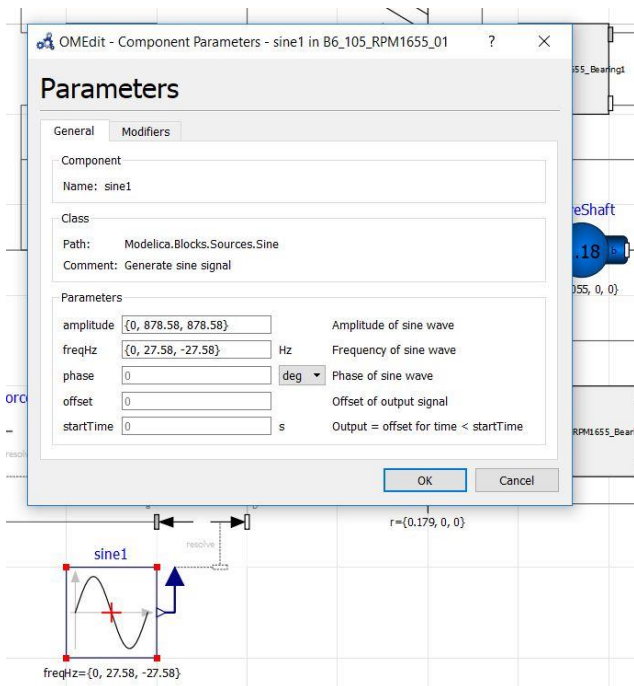


Figure G.2: Cases B.2 and C.2.

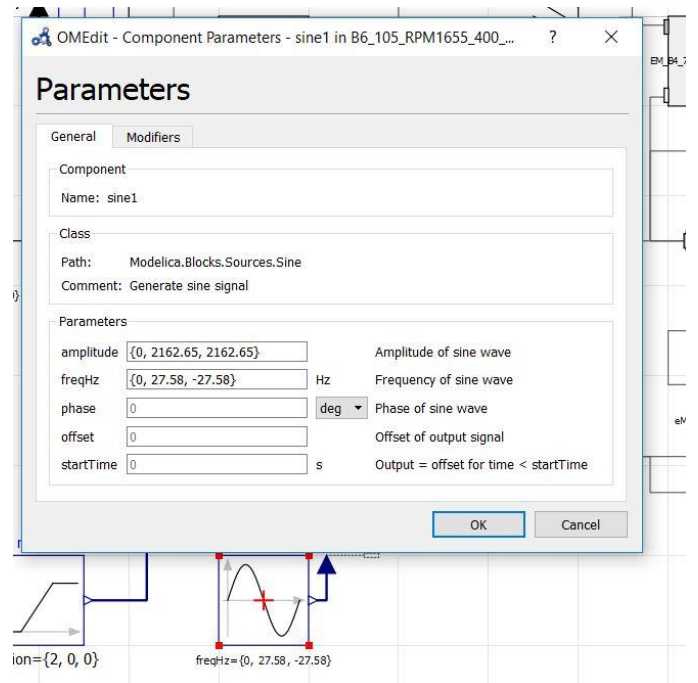
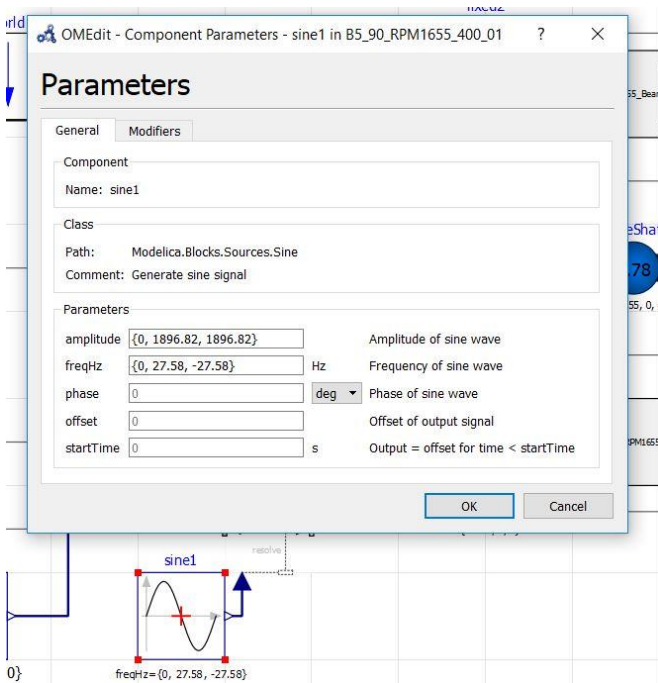


Figure G.3: Cases D.2 and E.2.

## **H. Digital appendices**

The digital appendix includes the following:

- Regression equations, excel file.
- Thrust and torque, excel file.
- Vibration amplitudes, excel file.
- OpenModelica files.
- Selection of OpenModelica simulation graphical results, png files.
- OpenModelica simulation results, excel files.
- Matlab files.